NOVEL COST-EFFECTIVE LIGHT EMITTERS BASED ON METAL HALIDE PEROVSKITES

- Tesis doctoral -

Doctorado en Nanociencia y Nanotecnología

VNIVERSITAT DE VALÈNCIA

Sang-Hyun Chin

October 2022

Directors:

Prof. Dr. Hendrik Jan Bolink

Dr. Michele Sessolo

Tutor:

Prof. Dr. Hendrik Jan Bolink

Prof. Hendrik Jan Bolink y Dr. Michele Sessolo, Investigadores de la Universidad de Valencia en el Instituto de Ciencia Molecular (ICMol), certifican que la memoria presentada por el estudiante de doctorado Sang-Hyun Chin, con el título "*Novel cost-effective light emitters based on metal halide perovskites*", corresponde a su Tesis Doctoral y ha sido realizada bajo su dirección y tutoría, autorizando mediante este escrito la presentación de la misma.

En Valencia, a 25 de octubre de 2022

Prof. Hendrik Jan Bolink
(Director y tutor)

Dr. Michele Sessolo
(Director)

여러 변덕스러운 우연이, 지쳐버린 타인이, 그리고 누구보다 자신이 자신에게 모질게 굴 수 있으니 마음 단단히 먹기 바랍니다. 나는 커서 어떻게 살까, 오래된 질문을 오늘부터의 매일이 대답해줍니다.

취업 준비, 결혼 준비, 육아, 교육, 승진, 은퇴, 노후 준비를 거쳐 어디 병원 그럴듯한 1인실에서 사망하기 위한 준비에 산만해지지 않기를 바랍니다. 무례와 혐오와 경쟁과 분열과 비교와 나태와 허무의 달콤함에 길들지 말길, 의미와 무의미의 온갖 폭력을 이겨내고 하루하루를 온전히 경험하길, 그 끝에서 오래 기다리고 있는 낯선 나를 아무 아쉬움 없이 맞이하길 바랍니다.

- 프린스턴 허준이 교수, 서울대학교 졸업식 축사 중

Index

Chapter 1.
Introduction

1.1. Overview

Modern society receives over 80 % of information by optical signals and with the rise of Internet of Things (IoT)-era, electronic devices will offer significant amount of information ubiquitously.[1] Since displays are indispensable to provide and process most of the information, the costs associated with materials and processes used in displays fabrication should be minimized. Light-emitting diodes (LEDs) are widely adopted as alternative light sources to incandescent light bulbs and fluorescent tubes. Electrical bias to LEDs results in light emission with photon energy equivalent to the band gap energy of the chosen semiconductor. LEDs' advantages over former light sources include higher efficiency, extended lifetime, and compact size.[2] Initially, LEDs were commercialized employing inorganic, direct band gap semiconductors, fabricated at high temperatures by complex epitaxial deposition methods. Importantly, these inorganic LEDs are rigid point light sources, which makes them difficult to implement in flexible displays or flat luminescent panel.

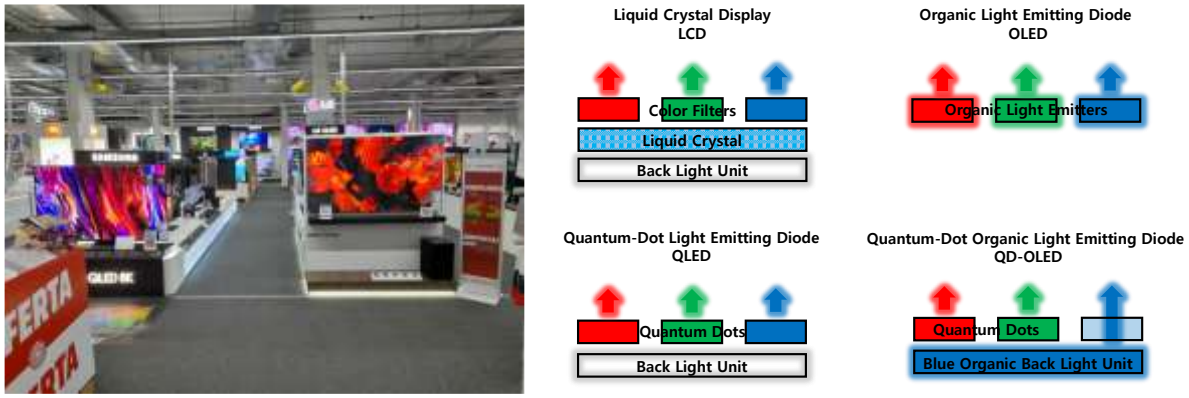

Figure 1.1. Commercial OLED and QLED displays (left), and schematics of the working mechanism for the main display technologies (right).

To solve this issue, organic LEDs (OLEDs) based on soft organic semiconductors, have emerged and are currently commercialized. Organic materials can be solution-processed into thin films at low temperature; however, current OLEDs are still thermally evaporated in vacuum, hence with high processing costs. Quantum dot LEDs (QLEDs)

are another option which can be realized with cost-effective solution processes, yet the quantum dots are not the electroluminescent component, as they are used as luminescent down-converted in combination with inorganic LEDs. Among the criteria of display performance, full width at half maximum (FWHM) is an important factor that dictates colour gamut. For instance, green OLEDs emit light with FWHM of 40 nm, while QLEDs have narrower spectra with FWHM of 30 nm. Researchers have recently found that lead halide perovskite-based LEDs can achieve FHWM as narrow as 20 nm.[3] After the first reports with room temperature-LEDs based on perovskite quantum dots and polycrystalline films in 2014, this material group has been intensively investigated.[4,5]

1.2 Rise of Metal Halide Perovskite Optoelectronics

In 1839, the mineral $CaTiO_3$ was discovered in the Ural Mountains of Russia by Gustav Rose and is named after Russian mineralogist Lev Perovski. Perovskite's notable crystal structure was first described by Victor Goldschmidt in 1926 and published in 1945 from X-ray diffraction data on $BaTiO_3$ by Helen Dick Megaw.[6,7] Perovskite oxides have a cubic or tetragonal crystal structure described by the simplified notation ABO_3, corresponding to a 3D framework of BO_6 octahedra with the smaller A cation occupying the centre of the unit cell and balancing the charge. The stability of the perovskite structure can be predicted by simple geometrical considerations using the tolerance factor *t,* defined by Goldschmidt as described below.

$$t = \frac{(R_A + R_O)}{\sqrt{2}(R_B + R_O)}$$

For instance, with $BaTiO_3$, the radius of Ba, Ti, and O could be noted as R_A, R_B, and R_O respectively (ABO_3). For stable perovskites, the Goldschmidt tolerance factor falls in the range $0.8 \leq t \leq 1$.[8] In metal halide perovskites, there are halide anions (X = Cl^-, Br^-, I^-) instead of oxygen, hence the structure is reported as ABX_3. The B site is occupied by a divalent metal (typically Pb^{2+} or Sn^{2+}), while A is either a small monovalent cation from the first or second group, or a small organic cation.[3]

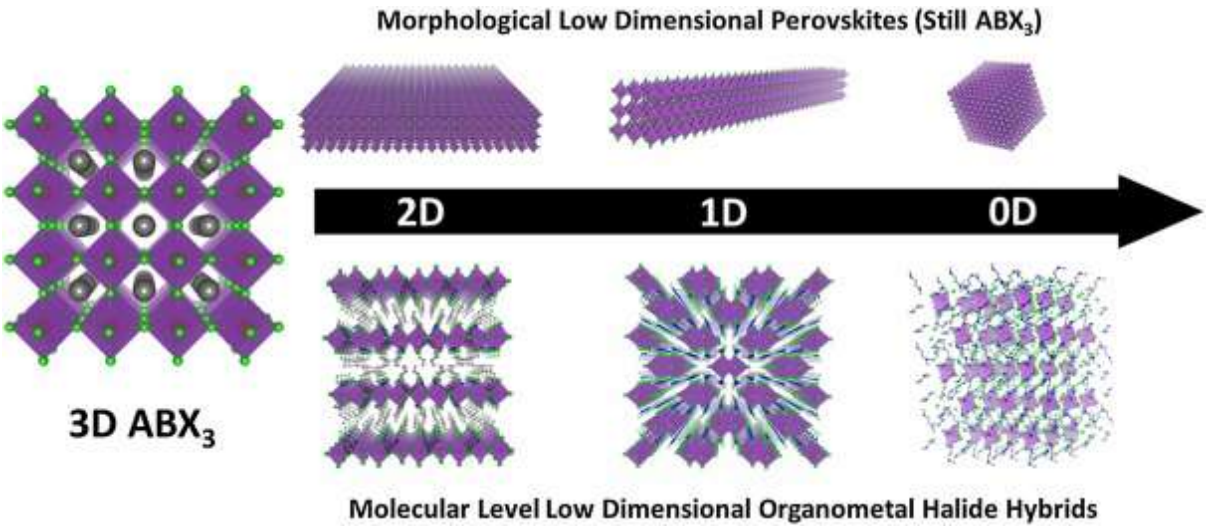

Figure 1.2. Metal halide perovskites and perovskite-related materials with different dimensionalities at morphological and molecular levels.[9]

In metal halide perovskites, there are several low dimensional structures depending on the size of the A cation and hence on the corresponding tolerance factor. Low dimensional halide perovskites could be divided in two categories: i) morphological low dimensional perovskites, ii) molecular low dimensional perovskites and related materials, as shown in **Figure 1.2.**[9] As 3D perovskites, morphological low dimensional perovskites have chemical formula ABX_3. Hence, the morphological low dimensional are defined by the shape and thickness of the three-dimensional network. Quantum dots with size close to the exciton Bohr radius are defined as 0D, while 1D and 2D low-dimensional perovskites are nanorods and nanoplatelets, respectively. Molecular low dimensional perovskite and perovskite-related materials still contain the BX_6^{4-} octahedral unit but depending on its arrangement in space it can also lead to 1D and 2D crystals.

In 1994, Shogo Saito group in Kyushu University (Japan) first applied a 2D metal halide perovskite of the type $(C_6H_5C_2H_4NH_3)_2PbI_4$ to an LED, which could deliver high luminance (over 10,000 cd/m^2) at liquid nitrogen temperature.[10] 5 years later, room-temperature operational PeLEDs based on $(H_3NC_2H_4C_{16}H_8S_4\text{-}C_2H_4NH_3)PbCl_4$ are realized in a report by Professor David B. Mitzi in IBM T. J. Watson Research Centre (United

States, currently Duke University).[11]

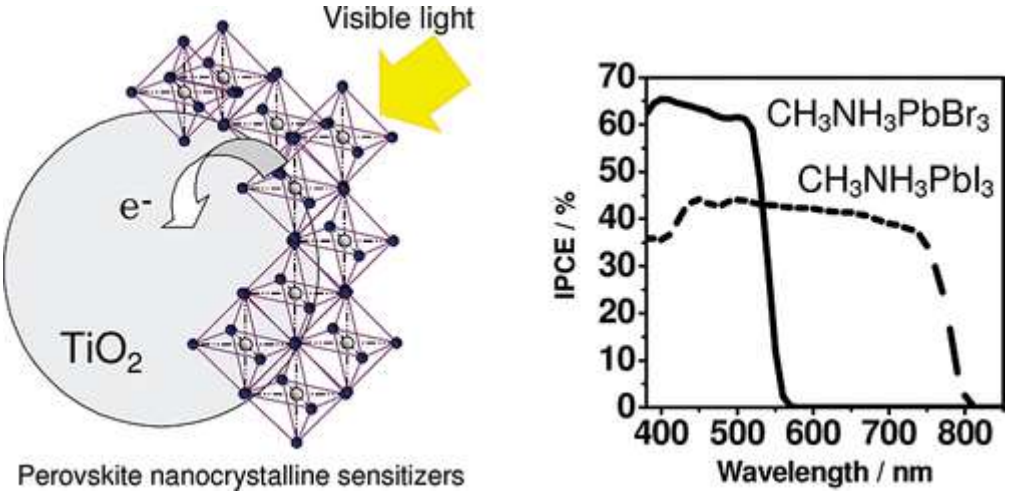

Figure 1.3. First perovskite solar cells exploiting $CH_3NH_3PbBr_3$ and $CH_3NH_3PbI_3$ sensitizers.[12]

In the first introduction of $CH_3NH_3PbI_3$ in dye-sensitized solar cells in 2009 by Tsutomu Miyasaka group in Toin University of Yokohama (Japan), perovskites have been re-examined by showing 3.8% power conversion efficiency (**Figure 1.3**).[12] After only 3 years, research groups in University of Oxford (United Kingdom) and Sungkyunkwan University (Republic of Korea) led by Henry Snaith and Nam Gyu Park developed all-solid state $CH_3NH_3PbI_3$ solar cells with high efficiency of approximately 10%.[13,14] Currently, solid-state perovskite solar cells are attracting huge attention from researchers all over the world owing to their unique properties, among which:[2,3,15]

a. The low-cost of precursors and simple synthetic processes

b. High absorption coefficient

c. Long charge carrier diffusion length

In only one decade of investigation, record power conversion efficiency exceeding 25 % have been demosntrated.[15,16]

This remarkable improvement of photovoltaics based on metal halide perovskite also led to the revival of perovskite light emitters. In two reports in 2014, perovskite light-emitting diodes (PeLEDs) with perovskite polycrystalline films and perovskite quantum dot had shown room-

temperature operation, for the first time.[4,5] For LED applications, the band gap (hence the emission color) can be easily modulated by the choice of the halide anion, and it is possible to achieve high photoluminescent quantum yield (PLQY) by chemical or structural defect passivation.[2,17,18] In accordance with the International Telecommunication Union (ITU) and the International Commission on Illumination (Commission Internationale de l'éclairage, CIE) recommendations, the three primary emission peaks for displays and for the wide-gamut colorimetry are centred at 630 nm (red), 532 nm (green), and 467 nm (blue). With lead halide perovskite, green emission can be obtained with pure bromide compositions. On the other hand, red and blue can be achieved by mixed iodide/bromide and bromide/chloride perovskites, respectively.[19]

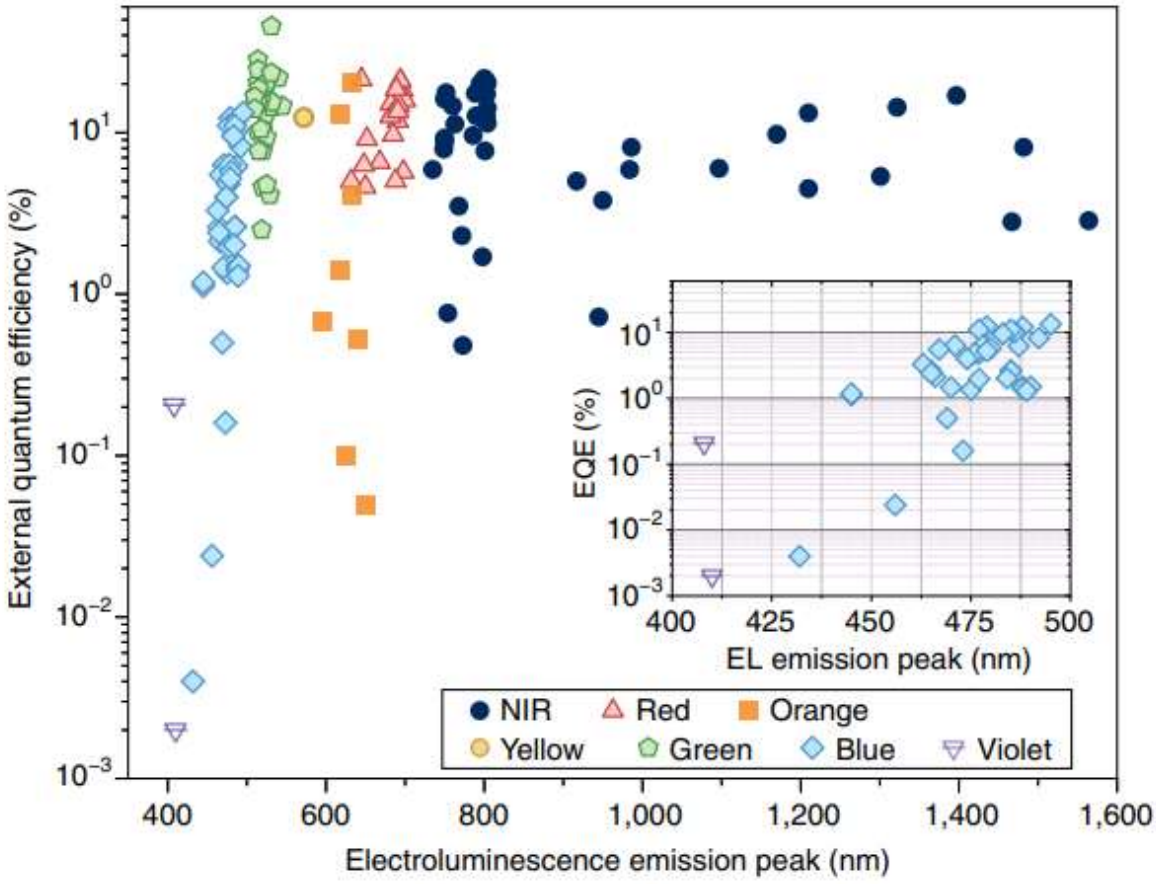

Figure 1.4. Peak EQE of recent state-of-the-art PeLEDs. Inset: the EQE trends of blue PeLEDs.[2]

PeLEDs have quickly evolved so that they are now as efficient as QLED, in terms of their EQE (External Quantum Efficiency), which can be described as follows.[3]

$$EQE\,(\%) = \frac{Photons\ emitted\ into\ free\ space}{Charges\ injected\ into\ the\ emitter\ film} = \eta_{inj} \cdot \eta_{rad} \cdot \eta_{out}$$

Where the injection efficiency (η_{inj}) describes the number of charge carriers passing the device electrodes that are injected into the light emissive layer. The radiative recombination efficiency (η_{rad}) refers to the ratio of the radiatively recombined charges to the total number of charges generated into the device. The last efficiency term, the light outcoupling efficiency (η_{out}), depends on the optical losses originating from the waveguide and substrate modes due to the mismatched refractive indices between the different layers, substrate, and air.

In order to quantify the performance of LEDs, there are several other representative figures of merit, such as luminance, current density, and current efficiency:

- Luminance (L): the intensity of emitted light in a given direction (expressed in candelas, cd) per unit area of the device, accounting for the human eye sensitivity curve. It is expressed in cd/m^2 in the International System of Units.
- Current density (J): the electrical current per unit area of the device. Its unit is A/m^2.
- Current efficiency (CE): the ratio between the luminance and the correspondent current density. It is expressed in cd/A.

In a report from Prof. Tae-Woo Lee and co-workers, PeLEDs employing guanidinium-incorporated formamidinium lead bromide nanocrystal PeLEDs allowed extremely high CE of 108 cd/A and EQE of 23.4%, owing to effective defect passivation with 1,3,5-tris(bromomethyl)-2,4,6-triethylbenzene. These efficiencies were subsequently risen to 205 cd/A and EQE of 45.5% with the use of hemispherical lenses which substantially improved light outcoupling. [18]

1.3 Thin Film Deposition Techniques for Metal Halide Perovskites

At the lab-scale, two main categories exist to deposit metal halide perovskite polycrystalline films, as described in **Figure 1.5**: solution and vacuum processes.

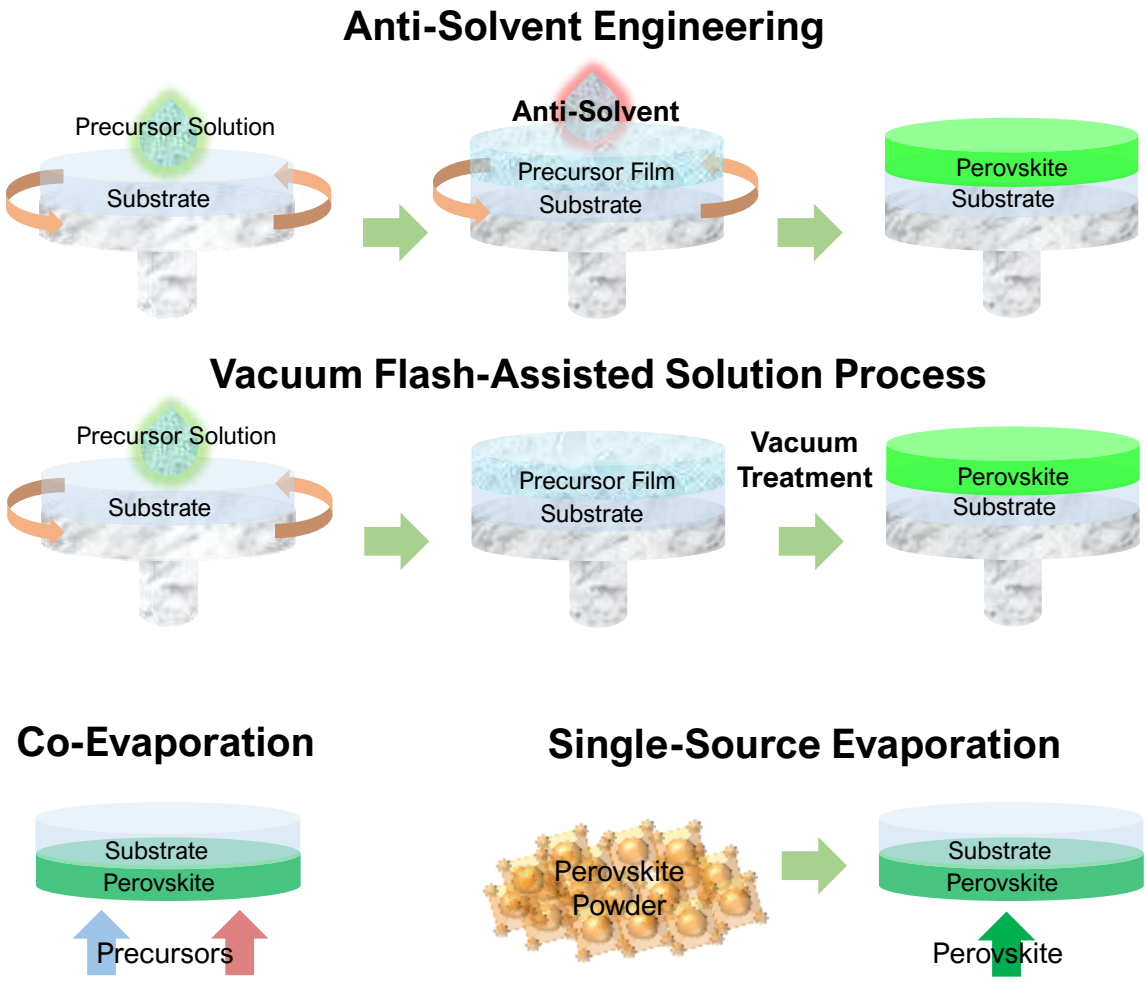

Figure 1.5. Schematic illustration of several perovskite thin film deposition processes

To date, the solution-based deposition is dominant in perovskite optoelectronics research due to the lower investment in comparison with vacuum deposition tools. Currently, record perovskite solar cells and LEDs are fabricated using solution processing and employing anti-solvent

engineering for the perovskite layer.[16,20] In the simplest approximation, the perovskite solution is prepared with two precursors (the halide salt of the monovalent cation and the salt of the divalent, heavy metal cation) in an organic polar solvent, such as dimethyl sulfoxide (DMSO), dimethyl formamide (DMF), and γ-butyrolactone (GBL). However, standard spin-coating does not lead to a compact morphology of the perovskite polycrystalline films. The first breakthrough, anti-solvent engineering, was shown by Sang-Il Seok group in Korea Research Institute of Chemical Technology (Currently placed in UNIST, Ulsan National Institute of Science and Technology, Republic of Korea).[21] They spin-coated $CH_3NH_3Pb(I_{1-x}Br_x)_3$ precursor in a DMSO-GBL mixture and then dropped an anti-solvent (in this case toluene, which does not dissolve the perovskite) onto the forming perovskite film during the spin coating process. Successful anti-solvent engineering induces fast nucleation and allows compact, and defect-less polycrystalline perovskite films. Anti-solvent engineering has been widely used to date, and the papers mentioned with record perovskite optoelectronic devices employed this process.

However, the process window of the antisolvent engineering is not wide enough. For instance, the height from where the antisolvent is dropped and the injection time severely affect the film morphology, making the process challenging to reproduce when performed manually. Michael Grätzel group in École Polytechnique Fédérale de Lausanne (EPFL, Switzerland) introduced an alternative process to anti-solvent injection which employs fast vacuum treatment of the as-coated perovskite film, so called vacuum flash assisted solution process.[22] In that report, $FA_xCs_{1-x}PbI_yBr_{3-y}$ perovskite is dissolved in DMSO which forms a complex with lead halides. After the vacuum treatment, a compact film of the lead halide-DMSO complex is formed on the substrate. By annealing, residual DMSO can evaporated leading to high quality perovskite films, which have been used to prepare high efficiency solar cells (power conversion efficiency over 20%). In addition, this process can be applied to deposit uniform pixels on active areas ok 1.2 x 1.2 cm^2, making it relatively scalable compared to the anti-solvent protocol.

Solution processes have been considered as cost-effective processes for metal halide perovskite film formation. However, since halide perovskites are ionic and relatively soft materials, they require a well-controlled

environment, with moderate temperature, low humidity limited solvent vapours (typically the deposition is carried out in nitrogen atmosphere). Vacuum evaporation can be an attractive alternative since the process is solvent-free and scalable to large area deposition.[23] Moreover, evaporated perovskite films can be grown conformally on textured silicon solar cells, to prepare efficient tandem devices.[24] The research group in Oxford led by Henry Snaith and Michael Johnston firstly reported efficient perovskite solar cell made by vacuum thermal evaporation in 2012.[25] In this report, methylammonium iodide and lead chloride were co-evaporated. With this simple process, they could obtain pinhole-free perovskite film and planar solar cell with PCE of 15%. After a decade, the champion efficiency of vacuum evaporated perovskite solar cell by Professor Chenyi Yi´s group in Tsinghua University (China) reached 24.4 %.[26] First, caesium iodide, lead iodide, and lead chloride were co-evaporated. Later, formamidinium iodide was evaporated on top and the chloride component was eliminated by thermal annealing. The integrated chloride anion could accelerate the solid-state diffusion of organic ammonium halide salt, facilitate perovskite phase transition from the optically non-active phase (δ-phase) to the semiconducting phase (α-phase), and increase the crystallinity of the resulting perovskite crystals, leading to a high-quality film with fewer defects.

Currently, among evaporation techniques, single-source evaporation of perovskites is being increasingly investigated. The required perovskite powder can be synthesized by dry mechanochemical method, for instance, ball-milling.[27–29] Also, solution-grown perovskite single crystals, precipitated powders, and solution-processed film on evaporation boat could be used as source materials.[30,31] Mostly, single-source deposition has been applied to inorganic perovskite such as caesium lead halides, since evaporating organic-inorganic halide perovskite causes an increase of vacuum chamber pressure due to the degradation of alkylammonium-based precursors. The flash-evaporation is being studied since the rapidly applied high current (over 30 A) causes a sudden temperature increase which evaporates hybrid perovskites before their degradation.[32] So far, only few reports with perovskite solar cell and photodetector have been using with this method, hence, there is more room for further improvments.[32,33]

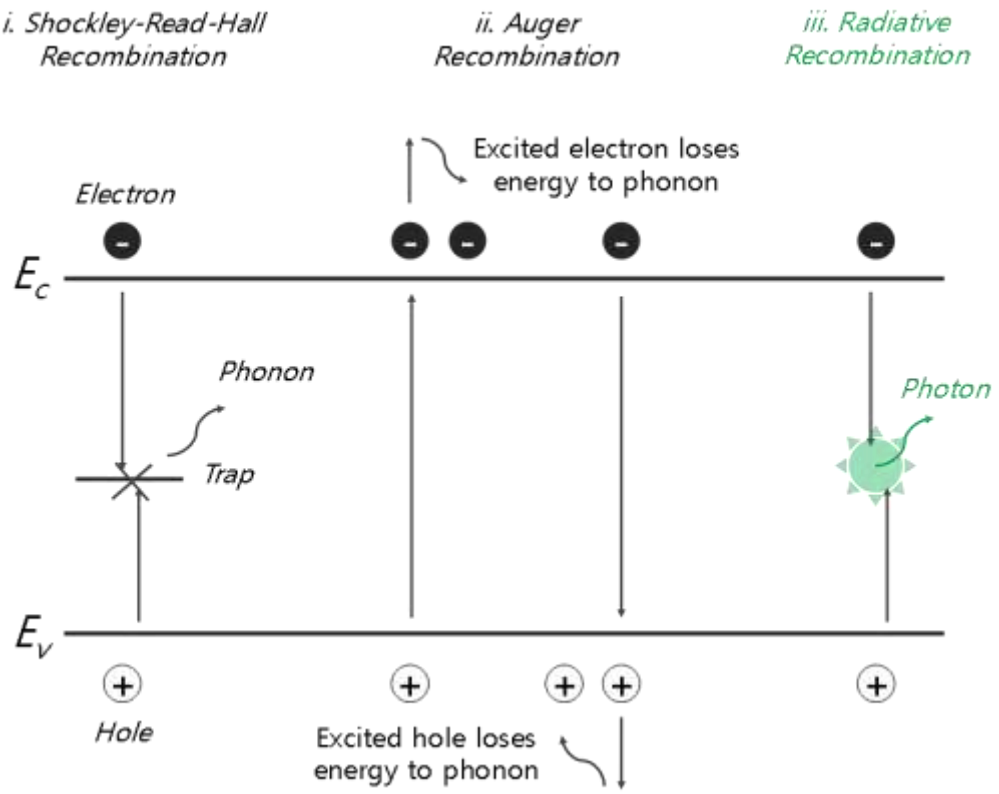

Figure 1.6. Schematic illustration of charge recombination processes in semiconductors

The generated electron-hole pairs tend to move back to its equilibrium via a recombination process, where an excited electron from the conduction band loses energy and decays into the valence band, *i.e.* recombining with a hole. There are several types of recombination processes important to the operation of optoelectronic devices, commonly referred to as the Shockley-Read-Hall (SRH) recombination, Auger recombination, and radiative recombination.[34,35]

i. Shockley-Read-Hall recombination

The SRH recombination is a non-radiative recombination and originates from electronic defects of the semiconductors which act as recombination centres. Impurities and structural defects in a

semiconducting material can give rise to allowed energy levels in the forbidden gap. These defects effectively trap an electron or hole (depending on their energy difference with respect to the conduction and valence band) in the bandgap. In case of an electron trap (electronic state deep in the bandgap but closer to the conduction band), an electron released from the conduction band is captured by the defect/trap level. From the trap level, it decays to the valence band, annihilating a hole and releasing the extra energy via lattice vibrations (phonons). A high defect density leads to a low lifetime of the carriers. The recombination trap centre can be imagined as a target presented to the traveling carrier with a certain velocity. For a given time, if the velocity is high, it will have a higher chance to be captured by the trap.

ii. Radiative recombination

Radiative recombination presents a phenomenon that an electron from the conduction band (higher energy state) recombines with the hole directly in the valence band (lower energy state) and releases the energy difference between the states in the form of a photon. This is the basic working principle of LEDs and solar cells.

iii. Auger recombination

The recombination process is the same as that of radiative recombination. However, instead of releasing the energy through a photon, the Auger recombination gives the energy to another carrier. This electron (or hole) relaxes the excess energy and momentum to the photon and is called thermal relaxation.

1.5 Basic Architecture of Light-Emitting Diodes

In semiconductors, electrons and holes leading to luminescence can be either photo-generated (photoluminescence, PL) or electrically injected (electroluminescence, EL). The process by which charge carriers recombine and emit photons is mentioned as radiative recombination. To achieve efficient luminescence, non-radiative recombination should be minimized by reducing the concentration of defects or charge accumulation. Although metal halide perovskites have high defect-

tolerance, trap states are still present in perovskite thin films.[36]

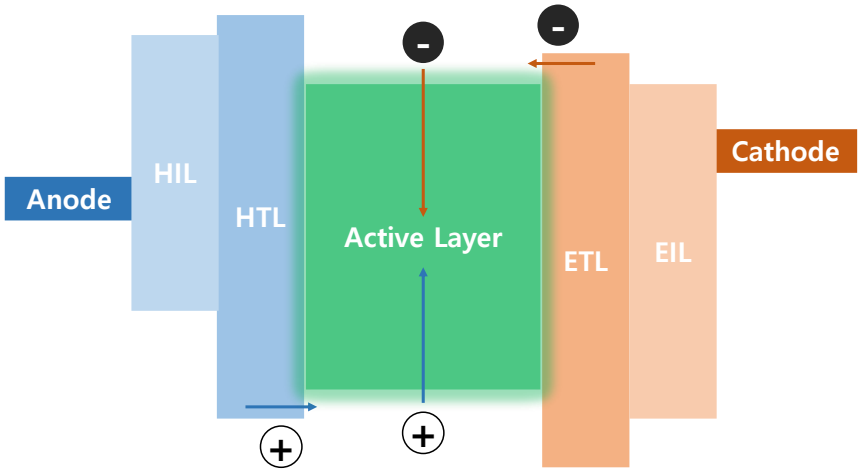

Figure 1.7. Working principle of LEDs. HIL: hole injection layer; HTL: hole transport layer; ETL: electron transport layer; EIL: electron injection layer.

In LEDs, the active layers are sandwiched between semiconducting films that selectively inject and transport electrons and holes from the electrodes into the luminescent material. Once the charge carriers (electrons and holes) meet in the active layer, they can either recombine as free carriers or via the formation of excitons, releasing photons in a process known as electroluminescence. Excitons are bounded electron-hole pairs quasiparticles with a characteristic binding energy. If the exciton binding energy is higher that the thermal energy at RT, their formation will be favoured, otherwise free charge carriers will dominate the recombination mechanism in the semiconductor. An approximate model to describe the working mechanism of a perovskite diode is the p-i-n junction, where the perovskite acts as the intrinsic material in between oppositely doped layers. When the external electrodes of a LED are short-circuited, the Fermi levels of the metal contacts align, and the potential (built-in potential, V_{bi}) drops over the intrinsic region. The current density vs. voltage (J-V) characteristics of LEDs are typically characterized by three regimes. The first is the ohmic regime, where the leakage current due to defects and shunts is observed. When a small positive voltage, lower than the V_{bi}, is applied to the diode, electrons and holes diffuse towards the intrinsic region, in the so-called diffusion current regime. If voltages higher than V_{bi} are applied, the electrons and holes move under

the effect of the applied voltage (drift current) and the current is either injection-limited or space-charged limited. The low mobility of the organic materials translates in an accumulation of charges that limits the current at high voltages. However, the mobility of the perovskite is higher compared to organic semiconductors, reducing the space-charge limitation.

1.6. Motivation and Thesis Overview

To contribute to the next generation display technology, simple preparation procedures with reduced economic cost are essential characteristics for LEDs. The results collected in this thesis aim to contribute to the progress in perovskite optoelectronics by the development of efficient and inexpensive light-emitting materials and devices which can be applied to current commercialized displays.

Chapter 2 focuses on obtaining stable and luminescent perovskite precursor solutions for down-conversion LED applications. The most common precursor for perovskite LEDs, $PbBr_2$, is soluble in liquid phase polyethylene glycol (PEG; also called polyethylene oxide with high molecular weight, PEO) and the PL is highly efficient. With these inexpensive materials, efficient light down-converting composite is realized with a one-pot synthesis. The emission can be shifted to green by introducing alkylammonium bromides, and with $PbCl_2$ reaches sky-blue emission.

In Chapter 3, solution processed $CsPbBr_3$ perovskite-PEO composite is introduced into light-emitting electrochemical cells (LECs, also called ¨Single layer LEDs¨), omitting charge transport layers and hence simplifying the device structure. In addition, CsCl and $PbCl_2$ are evaporated, forming 3D $CsPbCl_3$ perovskite and 0D Cs_4PbCl_6 non-perovskite material, to study halide anion diffusion at the interface with the perovskite emitter.

Finally, in Chapter 4, OLEDs are fabricated employing $CsPbCl_3$ hole transport layers. In this OLEDs, ultrathin (sub-nanometre thick) iridium complexes are evaporated without host-materials, greatly reducing material consumption and processing cost. I refer to these electroluminescent devices as PUE-LEDs (perovskite-ultrathin emitter

LEDs). This thin active layer reduces the distance between anode and cathode which results in shunting paths. The optimization of OLED with thick perovskite hole transport layer is mainly performed concerning the efficiency and leakage current which originates from the low thickness of these devices.

The context of all works from these chapters is briefly summarised in Chapter 5 and a resume of the thesis in Spanish (Castellano) is included in Chapter 6.

Chapter 2.
Luminescent Perovskite Solution Down-Converters

2.1. Introduction

As Dutta and Perkovic reported in 2002, $PbBr_2$ in acetonitrile (ACN) shows PL with a maximum at 610 nm, and a blue-shift upon the addition of tetrabutylammonium bromide (TBABr).[37] Despite the inefficient luminescence (PLQY of 0.5%), this compound has been applied to sensing, and the photophysical properties of lead halides in various solutions have been investigated.[38] However, so far there are only few reports on these materials and with very limited photoluminescence. Hence it is worth to investigate the luminescence properties of $PbBr_2$. In this chapter we specifically investigate the luminescence of $PbBr_2$ in liquid phase PEGs, which is a highly cost-effective and non-toxic polymer used in various application in industry.[39]

The PL properties of these composites make them interesting candidates for quantum dot-based display, where down-conversion quantum dots are coupled with a back lighting LED unit. In case of colloidal quantum dots, they typically synthesized, centrifuged, and re-dispersed in antisolvents. The process before deposition is complicated and inevitably increases the processing cost. In this chapter, precursors with low price are introduced to synthesize highly photoluminescent composite. In addition, several methods to shift emission wavelength are discussed.

2.2. Synthesis and Characterization

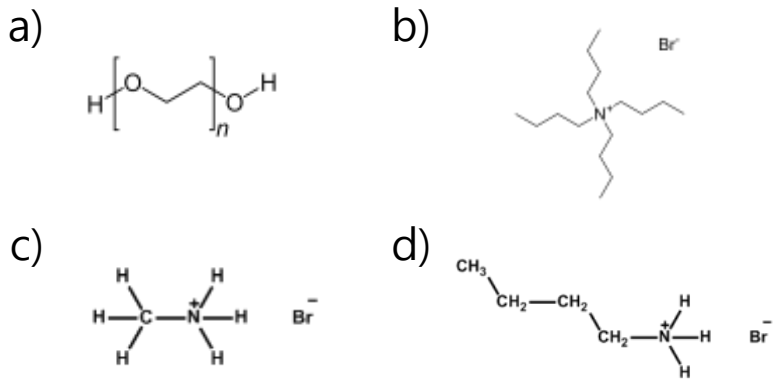

Figure 2.1. Molecular structures of a) PEG, b) TBABr, c) MABr, and d) BABr.

For the synthesis, polyethylene glycols (molecular structure is depicted in **Figure 2.1.a**) with different molecular weight are purchased and used to dissolve $PbBr_2$ with a 62.5 mM concentration. After overnight stirring at room-temperature, the samples already show intense luminescence. To control the PL property, tetrabutylammonium (TBABr), methylammonium bromide (MABr), and butylammonium bromide (BABr) (molecular structure is depicted in **Figure 2.1.b-d**), in DMSO are introduced. Addition of these compounds results in changes of the emission colour of the $PbBr_2$ solution.

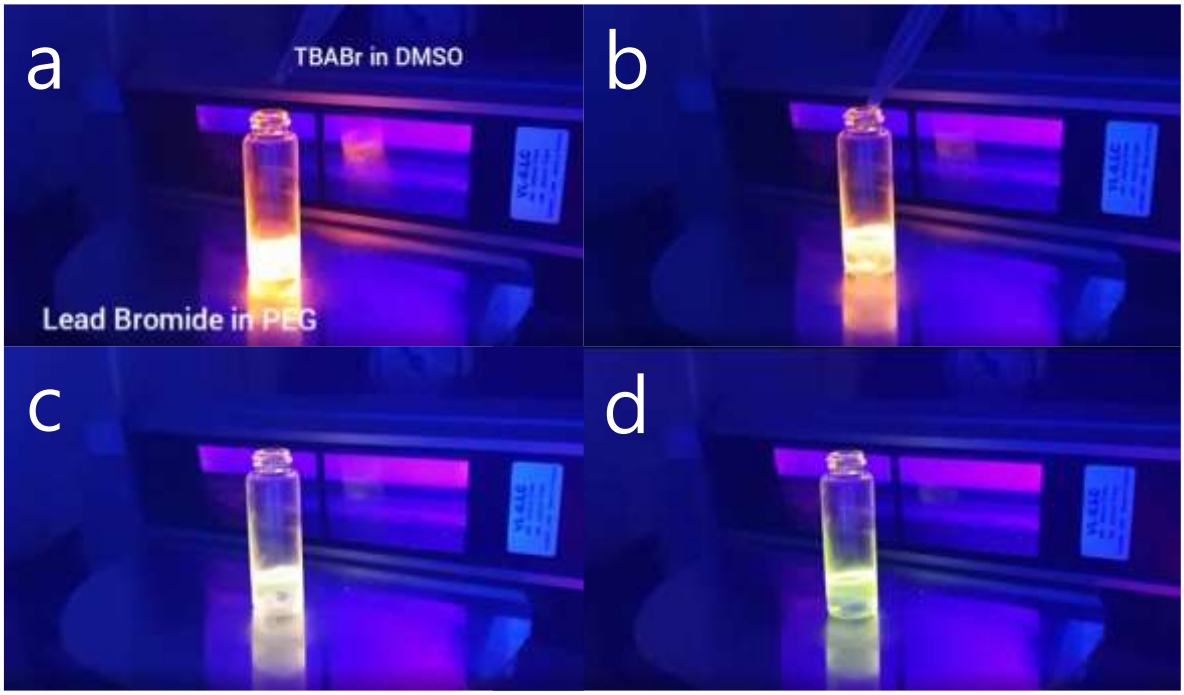

Figure 2.2. $PbBr_2$-PEG solutions under UV irradiation (excitation wavelength: 365 nm). (a) Pristine $PbBr_2$-PEG solution. (b) The moment of TBABr-DMSO solution injection and its evolution after (c) 3 and (d) 6 seconds.

This reaction occurs immediately as shown in **Figure 2.2.** To investigate the PL property of the solutions, several measurements are carried out. The instruments used for the characterization are illustrated in **Figure 2.3**. The solutions are transferred into quartz cuvettes to measure PL excitation property, static PL spectra and decay time, using Hamamatsu

fluorometer Quantaurus-Tau, Edinburgh FLS1000 using a μF2 Xe lamp and single-photon counting vis-PMT 980, respectively. In addition, the PLQY of solutions were estimated in an integrating sphere (Hamamatsu C9920-02 with a Hamamatsu PMA-11 optical detector) by excitation from a xenon lamp with monochromator. During the measurements with integrating sphere, CIE coordinates are also obtained.

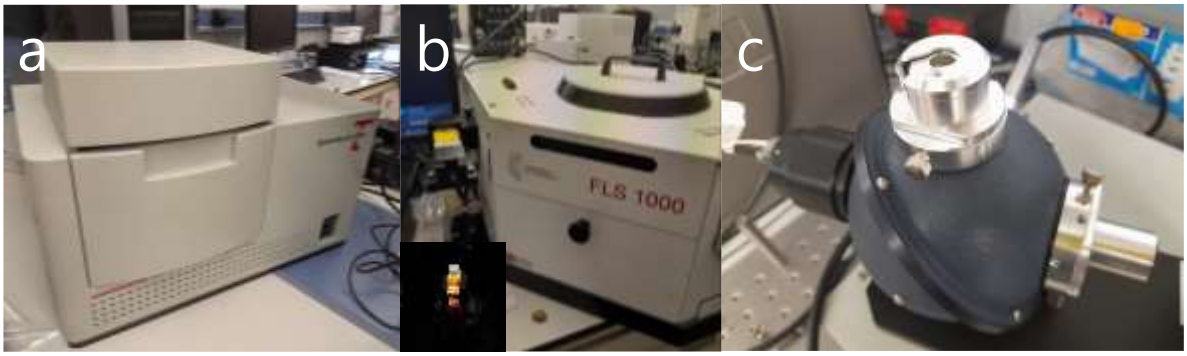

Figure 2.3. Measurement setups for (a) PL spectra and decay time measurement, (b) PLE spectra (inset: photograph of a luminescent sample inside the setup during measurement), and (c) integrating sphere for PLQY estimation.

2.3. Result and Discussion

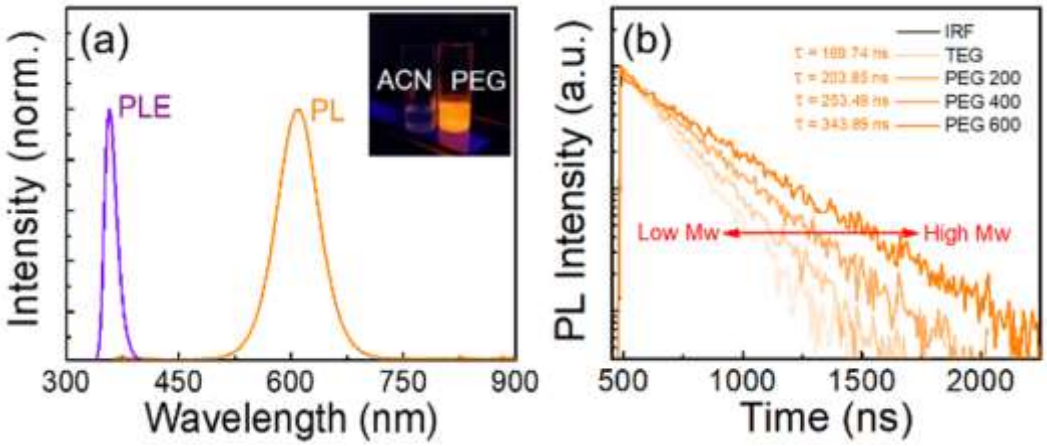

Figure 2.4. (a) Normalized PLE and PL spectra of lead bromide-PEG solution (inset: $PbBr_2$ dissolved in ACN and PEG on UV lamp with 365 nm excitation). (b) PEG-molecular weight dependency on PL decay time.

In **Figure 2.4.a**, the PLE and PL spectra of lead bromide-PEG 400 are introduced. The solution is characterized by a PL peak centred at 610 nm and a sharp PLE peak at 330 nm. According to a report from Oldenburg and Vogler, who first demonstrated lead bromide-ACN solutions for luminescence, this emission originates from $PbBr_3^-$.[40] As mentioned in the introduction, this luminescent lead bromide solution is mainly reported with ACN solvent, which results in inefficient PLQY of approximately 0.5 %, below the threshold of our setup (to visually compare, luminescent ACN and PEG based solutions are excited under a UV lamp, see inset of Figure 2.4a). In addition, PL decay time of PEG solutions with different molecular weight are investigated by time-correlated single photon counting (TCSPC) technique as shown in **Figure 2.4.b.** Tri-ethylene glycol (TEG) is the PEG with shortest chain among the PEGs which can dissolve $PbBr_2$. Ethylene glycol and Di-ethylene glycol could not dissolve $PbBr_2$. Also, PEG 200, PEG 400, and PEG 600 are included and compared in this series. As shown in **Table 2.1**, PLQY and PL decay time increase when the chain of PEGs becomes longer. PLQY and PL decay time increased from 9 % and 170 ns for TEG to 23 % and 344 ns for PEG 600 solutions.

Table 2.1. Photoluminescent characteristics of lead bromide in different polyethylene glycols

Solvent	PL peak (nm)	PLQY (%)	Average decay time (ns)
TEG	610	9	170
PEG 200	610	12	204
PEG 400	610	17	253
PEG 600	610	23	344

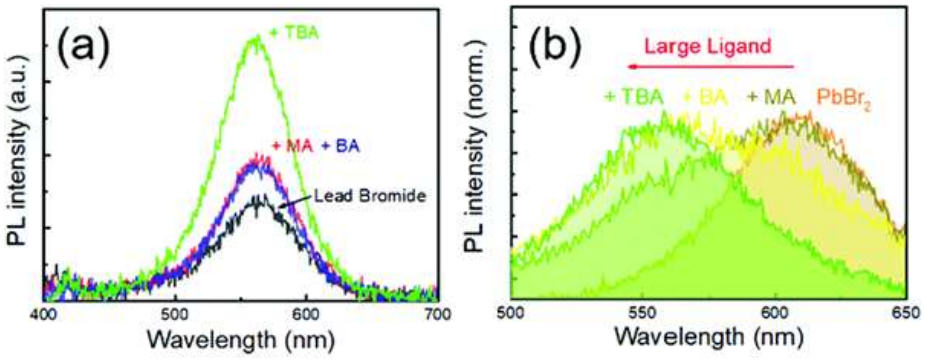

Figure 2.5. a) PL spectra of TBABr, MABr, and BABr added lead bromide solution and b) normalized spectra.

We further investigated the optical properties of the most luminescent system, lead bromide in PEG 600, by adding monovalent cations that are also frequently used in the preparation of lead halide perovskites. In order to introduce these additional cations, DMSO co-solvent (together with the PEG 600) was selected. This solvent is particularly interesting as DMSO also interacts with lead bromide, forming $PbBr_4^{2-}$, characterized by an excitation peak at 360 nm and a blue-shifted PL maximum at 560 nm.[41,42] The following salts were evaluated: methylammonium bromide (MABr), butylammonium bromide (BABr) and TBABr dissolved in DMSO (1.25 M). The ratio of alkylammonium bromide to $PbBr_2$ was kept constant at 2 : 1. The resulting PL spectra are depicted in **Fig. 2.5.a.** As expected, the emission peak for lead bromide in DMSO is not affected when adding the different alkylammonium salts and remains around 560 nm, while te PL intensity was found to increase. However, when mixing lead bromide and the alkylammonium bromides in the presence of PEG, the PL peak position changes. Prior to the addition of the alkylammonium bromides, the PL maximum is around 610 nm, while upon addition the PL maximum blue-shifts to 560 nm. The largest shift in the PL spectra was observed for the largest alkylammonium salt, TBABr. With TBABr, the PL maximum shifts to 560 nm, which is similar to what is observed for pure $PbBr_4^{2-}$ in DMSO. This suggests that there is a competition in the coordination of Pb^{2+} between PEG and DMSO, which is mediated by the alkylammonium bromide.

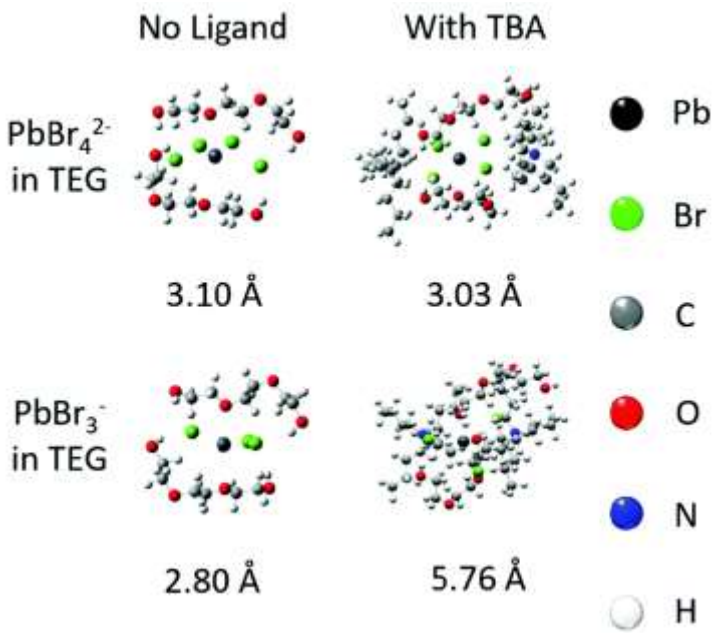

Figure 2.6. DFT simulation results on interaction distance in lead bromide complexes in solutions with alkylammonium bromide ligands.

In summary, DMSO-single solvent forms $PbBr_4^{2-}$ but co-solvent allows the co-existence of $PbBr_4^{2-}$ (from lead bromide-DMSO) and $PbBr_3^-$ (from lead bromide-PEG). To clarify the origin of this phenomenon, density functional theory (DFT) calculation was performed. In particular, we compared the average distance between Pb and O atoms as the most logical interaction sites in the presence of PEG (**Figure 2.6**). Note that TEG is employed as medium in this calculation to simplify the simulation. The initial Pb–O distances in the complexes of $PbBr_4^{2-}$ and $PbBr_3^-$ are 3.10 Å and 2.80 Å, respectively. After introducing the large TBABr salt, the Pb–O distance decreases to 3.03 Å for $PbBr_4^{2-}$ and increases to 5.76 Å in the case of $PbBr_3^-$.

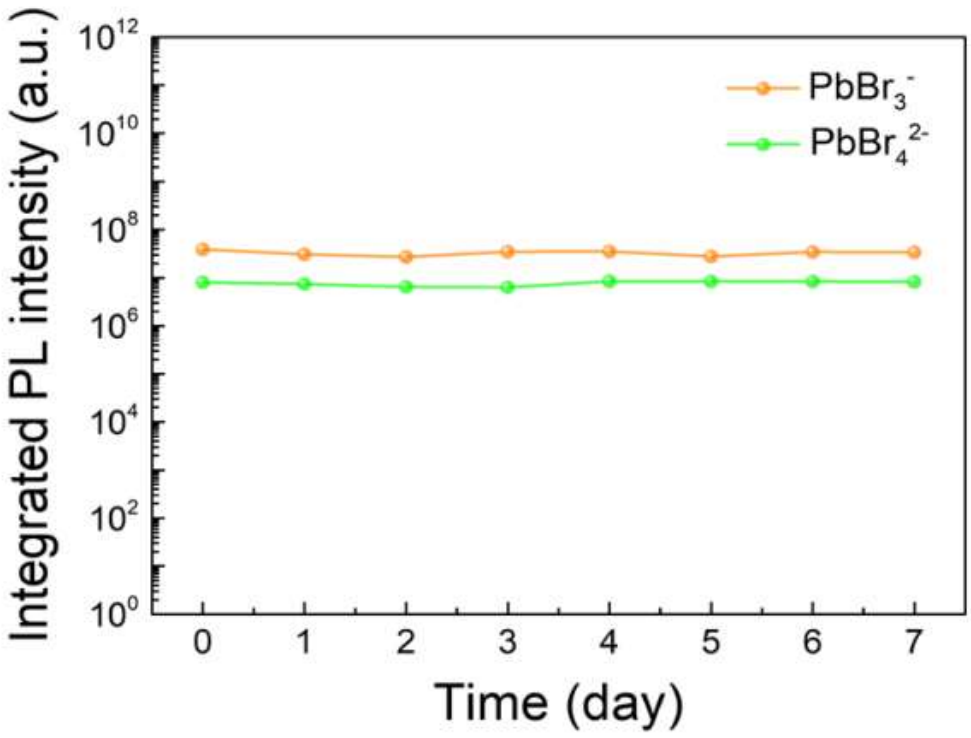

Figure 2.7. PL stability of $PbBr_3^-$ and $PbBr_4^{2-}$

In addition, the $PbBr_3^-$–TEG is unstable as the Br anions dissociate. This does not happen with $PbBr_4^{2-}$, which remains intact. This implies that $PbBr_3^-$ is the less favoured structure and transforms into $PbBr_4^{2-}$ in TEG in the presence of TBABr.[43] This is in line with the trend observed in the PL spectra: for instance, adding TBABr results in an effective blue-shift eventually coinciding with the PL of $PbBr_4^{2-}$ in pure DMSO. The introduction of TBABr leads to a large increase in the Pb–O distance and hence the DMSO to Pb^{2+} interaction becomes the dominant one. This leads to an increase of the green emission from the $PbBr_4^{2-}$ species. The stronger interaction between DMSO and Pb^{2+} also explains the dramatic decrease of PLQY after injecting DMSO in lead bromide–PEG solutions, from 23% to only 2%.

Also, a stability test was performed to evaluate the luminescent solutions, as shown in **Figure 2.7.** The PL intensity of $PbBr_3^-$ (lead bromide in PEG solvent) and $PbBr_4^{2-}$ (lead bromide in DMSO-PEG co-solvent with TBABr additive) are stable for 1 week at room temperature and in air with no appreciable variations.

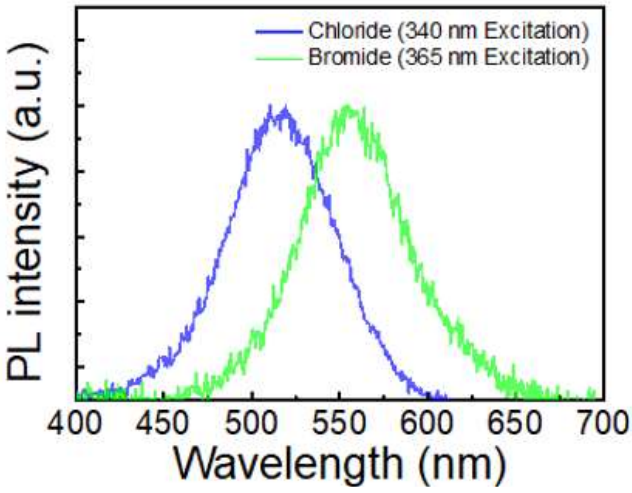

Figure 2.8. Photoluminescent spectra of lead chloride + TBACl and lead bromide + TBABr (TBAX is 2-fold to lead halide).

Finally, the bromide ions in the TBABr+$PbBr_2$ solution in PEG-DMSO were completely replaced by chlorides (using TBACl+$PbCl_2$), to investigate the influence of the halide anion. Interestingly, the peak blue-shifted from 560 nm to 510 nm in **Figure 2.8**, similar to what observed in solid-state metal halide perovskites when bromide is exchanged by chloride.[2,19]

White emission is highly sought after for lighting applications. For this, an organic blue dye, 4,4'-Bis(9-ethyl-3-carbazovinylene)-1,1'-biphenyl (BCzVBi), was injected into the lead bromide solution with equimolecular and 0.5-fold TBABr. Also, the materials were prepared in the form of a metallogel-like solution (transition temperature: 15°C), as shown in **Figure 2.9**.[44]

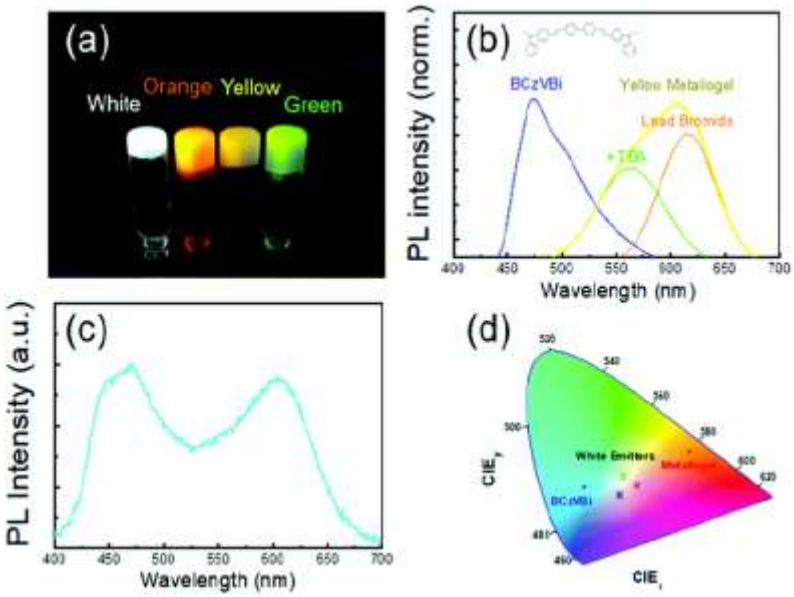

Figure 2.9. a) Luminescent metallogels under UV irradiation (365 nm). b) PL spectra of blue-emitting BCzVBi dye and yellow-emissive solution. c) PL spectrum and d) CIE-coordinates of white and yellow-emissive solution and BCzVBi.

At low TBABr content, the lead bromide metallogel was found to be yellow-emissive, due to co-existing orange emissive (610 nm) $PbBr_3^-$ and green emissive (560 nm) $PbBr_4^{2-}$. After BCzVBi injection in solution and phase transition in an ice bath, white emissive metallogels could be obtained. In **Figure 2.9.a-c**, white, orange, yellow, and green emissive metallogels are shown under UV irradiation. The four different emitters can be readily obtained using the following reagents:

White: BCzVBi + TBABr + $PbBr_3^-$ + $PbBr_4^{2-}$ in DMSO-PEG

Orange: $PbBr_3^-$ in PEG

Yellow: TBABr + $PbBr_3^-$ + $PbBr_4^{2-}$ in DMSO-PEG

Green: TBABr + $PbBr_4^{2-}$ in DMSO-PEG

Depending on the ratio between BCzVBi:TBABr:$PbBr_3^-$:$PbBr_4^{2-}$, the white emission can be fine-tuned as shown in **Figure 2.9.d**, where three different types of white emitters are realized with the protocols discussed

in the following.

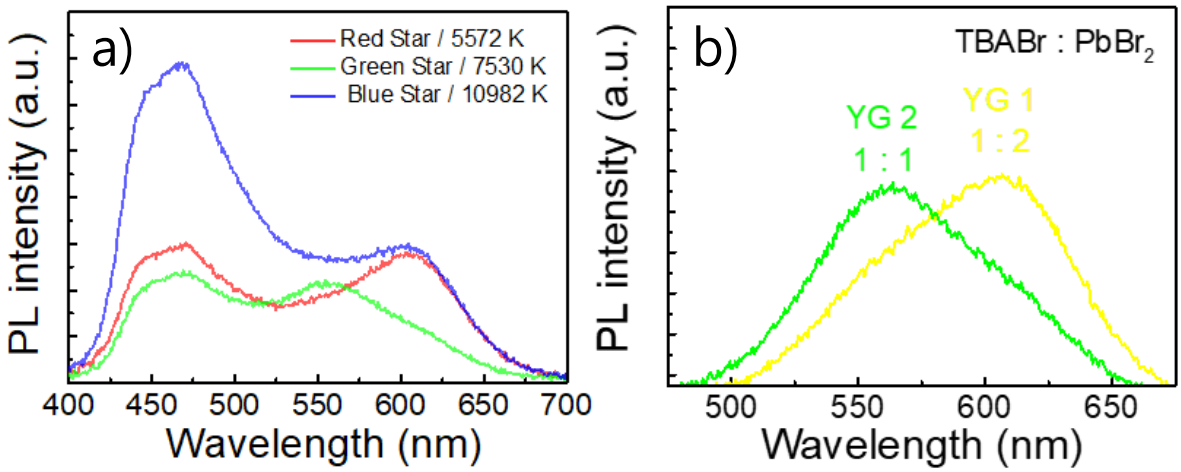

Figure 2.10. (a) PL spectra of 3 different white emitters and (b) PL spectra of 2 yellow emitters.

To obtain the 3 different white emitters, named W1 (red star), W2 (green star), and W3 (blue star) in **Figure 2.10.a**, 2 types of yellow emitters and different concentrations of BCzVBi were used. As shown in **Figure 2.10.b**, the yellow emission is controlled by the ratio between TBABr and $PbBr_2$ precursors. As noted in **Table 2.2**, the W1 to W3 exhibit different color on CIE coordinates and color temperature. The correlated color temperature (CCT, T_c) set is calculated by McCamy's approximation which is shown below.[45]

$$n = \frac{(CIE_x - 0.3320)}{(0.1858 - CIE_y)}, \quad T_c\,(K) = -437\,n^3 + 3601\,n^2 - 6861\,n + 5514$$

Table 2.2. Color of White emitters

	Concentration of BCzVBi	**CIE coordinate (CIE_x, CIE_y)**	**Color temperature (T_c)**
W1 (Red Star)	0.125 mg/ml in YG 1	0.331, 0.311	5572 K
W2 (Green Star)	0.625 mg/ml in YG 2	0.291, 0.345	7530 K
W3 (Blue Star)	1.250 mg/ml in YG 1	0.280, 0.273	10982 K

The CCT of W1 and W2 satisfies CIE D55 (5503K, mid-morning / mid-

afternoon daylight) and CIE D75 (7504K, north sky daylight), respectively. These CCTs are proper values in the desktop monitor's color temperature. However, when the blue dye is introduced in higher concentration, such as the case of W3, the CCT leaves the regime of practical use.

When the cost is approximately calculated, the work so far seems highly promising. 5 L of PEG 600 costs approximately 190 euros (38 euros per litre) and the cost of precursors, TBABr and $PbBr_2$, are less than 1 euro per gram. So, for the orange to green emitters, the approximated cost is less than 40 euros per litre. This price can be even lower in mass production. The blue dye introduction is the most expensive part in this work; however, the concentration is extremely low since the PLQY of this material is near unity (98%) leaving the synthesis cost-effective. In addition to this overview on the cost, all the PLQY values of lead halide solutions in this chapter are noted in **Table 2.3**, for a clear demonstration of the potential of our approach.

Table 2.3. PLQY Table

Solute	**Solvent**	**PLQY (%)**	**Note**
$PbBr_2$	GBL	10	
$PbBr_2$	DMF	2	
$PbBr_2$	DMSO	1	
$PbBr_2$ + 2MABr	DMSO	1	
$PbBr_2$ + 2BABr	DMSO	1	
$PbBr_2$ + 2TBABr	DMSO	2	
$PbBr_2$	TEG	9	
$PbBr_2$	PEG 200	12	
$PbBr_2$	PEG 400	17	
$PbBr_2$	PEG 600	23	- Due to the phase transition of PEG 600 on 15℃, measurements are conducted over 20℃. - The volume ratio between DMSO and PEG 600 in co-solvent is 1:10. - DMSO decreases PLQY of PEG-based solution (refer to $PbBr_2$ in DMSO and DMSO + PEG 600). - Pure $PbCl_2$ is unable to be dissolved in PEG. - The PLQY of white-emissive metallogel (W1-3) is highly dependent on the concentration of BCzVBi dye.
$PbBr_2$	DMSO + PEG 600	2	
$PbBr_2$ + 1.5MABr	DMSO + PEG 600	3	
$PbBr_2$ + 2MABr	DMSO + PEG 600	3	
$PbBr_2$ + 3MABr	DMSO + PEG 600	2	
$PbBr_2$ + 2BABr	DMSO + PEG 600	2	
$PbBr_2$ + 2TBABr	DMSO + PEG 600	3	
$PbCl_2$ + 2TBACl	DMSO + PEG 600	7	
YG1	DMSO + PEG 600	4	
YG2	DMSO + PEG 600	4	
W1	DMSO + PEG 600	7	
W2	DMSO + PEG 600	5	
W3	DMSO + PEG 600	9	

2.4. Conclusion

By dissolving $PbBr_2$ in PEG, it was possible to obtain simple and inexpensive orange luminescent down-converting material. Since the concentration of this solution is as low as 62.5 mM, the total materials cost is close to the price of PEG, making this luminescent system a cost-effective candidate. The emission property was tuned successfully by injecting alkylammonium halide solutions. The PL peak shifted from 610 nm to 560 nm and this process was more effective with larger alkylammonium ligands. Tetrabutylammonium based ligands are the best candidate in this work since it induced full PL shift only with 2-folds molar ratio with respect to lead. When the ligands are introduced in lower concentration, the solution emits yellow light with wide PL spectra. Hence, white emitter could be successfully realized by introducing small amount of blue emitting organic dye, BCzVBi. The work which is introduced in this chapter offers a method to obtain highly cost-effective down-converting light emitter.[43] In addition, this system can be introduced in many other applications such as multi-stimuli metallogel and neutron imaging scintillator with high spatial resolution.[44,46]

Chapter 3.

Light-Emitting Electrochemical Cells based on Perovskites and Perovskite Heterojunctions

3.1. Introduction

In 1995, light-emitting electrochemical cells (LECs) also known as Single-layer LEDs were first reported by Prof. Alan J. Heeger and co-workers in University of California Santa Barbara.[47] In that first report, a conjugated polymer, poly[2-methoxy-5-(2-ethylhexyloxy)-1,4-phenylenevinylene] (MEH-PPV) was blended with polyethyleneoxide (PEO) serving as an electrolyte and a salt lithium tri-fluoro-methane sulfonate ($LiCF_3SO_3$). This blend was sandwiched in between two electrodes, one of which was semi-transparent such that light can escape. Compared to most organic light-emitting diodes (OLEDs) this is a rather simple structure. Moreover, the electrodes employed are both air-stable. The turn on voltage for light-emission was 2.1 V which is low and implies that charge injection is very efficient.

The operational mechanism of LECs has been generally described by the electrodynamical (ED) and the electrochemical doping (ECD) models (**Figure 3.1**).

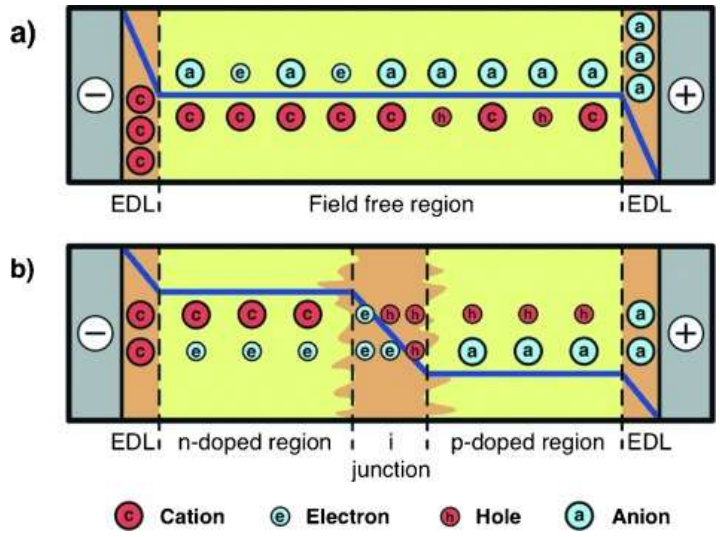

Figure 3.1. Illustration of the potential profile as well as the electronic and ionic charge distribution in a LEC during steady-state operation. Potential profiles and charge distributions as predicted by the a) ED and the b) ECD models. The thick blue line represents the potential profile; the electronic and ionic charge carriers are illustrated by the cyan (negatively charged) and red (positively charged) symbols, respectively.[48,49]

Both models agree in that the injection barrier for electrons and holes is reduced by the separation of the ions in the light-emitting layer upon application of a bias. The ED model assumes that the accumulation of ions leads to the formation of electric double layers (EDLs) at the electrodes, which causes a sharp drop of the electric potential near the electrode interfaces and promotes charge injection from the electrodes. In the bulk of the material the anions and cations are still bound, and light emission occurs from the so-called field-free region in the bulk of the device. The ECD model, on the other hand, assumes that the accumulation of ions at the anode and cathode leads to the formation of highly conductive p- and n-doped regions, respectively. The doped regions widen over time, until a p–i–n junction (i = intrinsic, undoped) between the electrodes is formed. Across the intrinsic region formed, the applied potential drops substantially and favours charge recombination and light emission.

Until recently, the active materials in LECs were based on either conjugated polymers or ionic transition metal complexes.[49] In addition to these materials, since 2015, the use of metal halide perovskites has been reported. Prof. Zhibin Yu from Florida State University reported a perovskite:PEO composite-based light emitter that was sandwiched in between two electrodes.[50–52] Even though no specific salts were added to the light-emitting composite, the device did show electroluminescence and resembles a LEC. The lack of a salt may be compensated by the ionic chemical nature of metal halide perovskite. Hence, this would reduce the blend complexity and improve its phase stability. As perovskites are prepared from low-cost components, it may also lead to very low cost electroluminescence devices.

Prof. Jason D. Slinker and Prof. Anvar A. Zakhidov from the University of Texas Dallas also developed LECs comprising perovskites. They used the inorganic perovskite, $CsPbBr_3$, which was blended with $LiPF_6$ and PEO.[53] To prepare the LECs, they relied on the use of InGa eutectic composites as the top-electrode. The salt, $LiPF_6$ was mentioned to passivate defects in the $CsPbBr_3$ and support charge injection, improving the overall device performance. However, this InGa top electrode is a liquid which makes it difficult to operate the device and define the active area. In following works, the same team deposited poly(3,4-ethylenedioxythiophene) polystyrene sulfonate (PEDOT:PSS) on ITO to obtain a more flat film morphology such

that air-stable Al electrodes could be used, albeit with a very thin LiF charge injection layer in between the light-emitting film and the Al electrode.[54] These devices reached a high luminance over 2000 cd/m^2 which was improved to over 3000 cd/m^2 when a salt was added to the light-emitting layer.

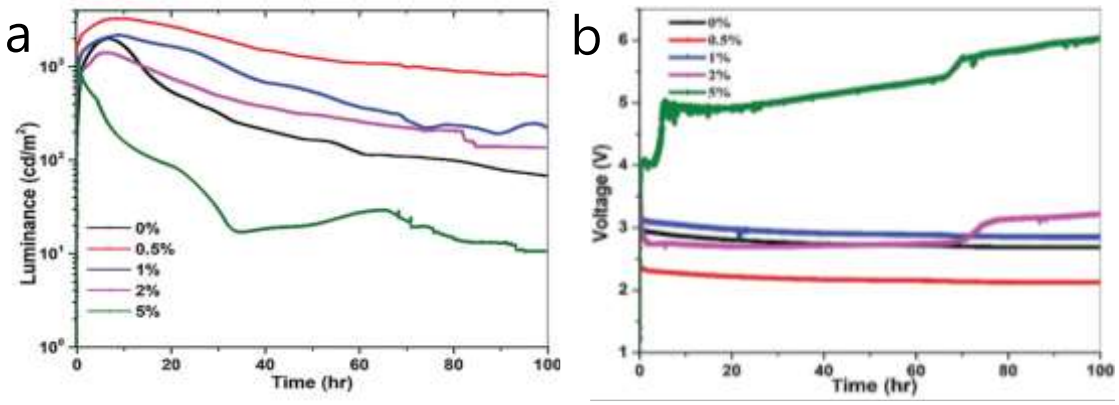

Figure 3.2. a) Luminance and b) voltage under constant current operation for the devices with different $LiPF_6$ concentrations (depicted in the legend).[54]

However, these devices also had significant shortcomings. The main one is the time it takes to reach the maximum luminance, more than 10 hours. Additionally, the exact device performance depends strongly concentration of $LiPF_6$ salt as shown in **Figure 3.2**.

The topic of this chapter is to develop LECs based on metal halide perovskite that have a much faster time response then those reported in the literature. Additionally, the interdiffusion of ions in a bilayer heterojunction consisting of two different types of perovskite films will be investigated. Finally, the device performance of the developed single perovskite LECs and the LECs employing the perovskite heterojunction will be discussed.

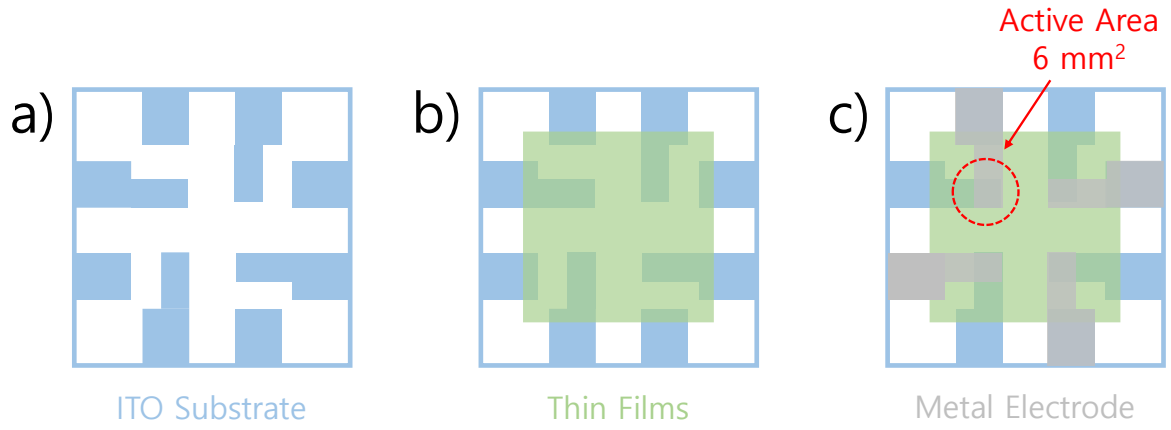

Figure 3.3. Schematic of the ITO coated substrate (panel a), the deposited perovskite blend on top it (panel b) and the finished devices, having the Al top electrodes deposited (panel c). Dimensions of the substrate is 3 cm x 3 cm.

Figure 3.3 depicts the layout of the substrate in the different phases of the device fabrication process. In the first step the commercial ITO substrate with 3 cm x 3 cm size is cleaned. Afterwards, the charge transport layers, and light-emitting layers are deposited in a square shape that extends over the central part of the ITO electrodes. Such a squared shape is easy to obtain via shadow masks in a vacuum process, whereas for the solution process, the material deposited outside the targeted area is removed by solvent cleaning. Finally, the entire device is finished by the deposition of a top metal electrode, Ag or Ba/Ag via different shadow mask. The overlap area between the ITO and top metal electrode is the active cell area and is 6 mm^2.

In the following section a more detailed description is given for the different processing steps. First, the ITO substrate is cleaned by emerging the plates in a detergent containing beaker under the influence of ultrasonic vibrations. The next step is a rinsing de-ionized water to remove the detergent and finally by isopropyl alcohol (IPA). The as such cleaned substrate is treated by ozone, which is generated by a strong UV light source. The Ozone removes remaining organic residues and renders the

ITO substrate hydrophilic. This is required to allow for a good contact with the transport layers but also to have a proper wetting during coating with charge transport materials.

Figure 3.4. Spin-coater

A commercial aqueous PEDOT:PSS (Clevios™ P VP AI 4083; filtered with 0.45 µm pore size PVDF filters) is used as a hole injection layer. It is spin-coated using a spin-coater from Chemat Technology KW-4A on the UV-treated substrate (**Figure 3.4**). This is done in cleanroom conditions in ambient air. After the coating process the substrates are heated to 70 °C to remove residual solvent. After this the substrate is transferred to a N_2 filled glovebox to proceed with the following process steps. Prior to depositing the perovskite, the perovskite:PEO solution has to be prepared and stirred overnight at 70 °C. This solution is cooled down right before spin-coating for 30 minutes. The perovskite:PEO films are vacuum-flash annealed as previously reported by Prof. Jason D. Slinker.[53,54] This vacuum-flash annealing is performed in the anti-chamber of the glovebox

on the as-deposited perovskite precursor film before its crystallization. The 90 seconds vacuum treatment accelerates the crystallization caused by the rapid evaporation of the solvent. This leads to the formation of compact perovskite:PEO films. In our experiments the weight ratio of perovskite to PEO is 1.5:1 and no salt, such as $LiPF_6$ was added. This is different from most conventional LECs based on organic semiconductors that do require the addition of a salt. For the halide anion interdiffusion experiments, caesium lead chloride is deposited by thermal co-evaporation in a vacuum chamber (**Figure 3.5.** a custom made by Thermal Vacuum Projects and controller from Cressington Vacuum System) with a base pressure under 2×10^{-6} mbar. And to evaluate the device performance, every sample is finished with Ag or Ba/Ag electrodes in another high vacuum thermal evaporator.

To characterize the optical properties, such as absorption and PL, of the perovskite thin films, a spectrometer setup is prepared as shown briefly in **Figure 3.6.** A light source arrives on the film through waveguide and collected signal goes to the spectrometer (Avantes, Avaspec2048). With the same spectrometer, the PL characterization is performed. A coherent Laser light source (375 nm) is used to excite the perovskite film, and the reflected light signal is collected. To prevent saturation of the sensor a long pass filter (cut-off under 400 nm) is used. After full device fabrication, the samples are introduced into a setup for a current density and luminance versus voltage (J-V-L) scan. For this we employ a Keithley 2400 Source-Meter and a photodiode coupled to a Keithley 6485 pico-ammeter. A Minolta LS100 camera is used to determine the luminance in cd/m^2 and to calibrate the photocurrent to luminance values. A LabVIEW program is used to control the Keithleys and obtain the data.

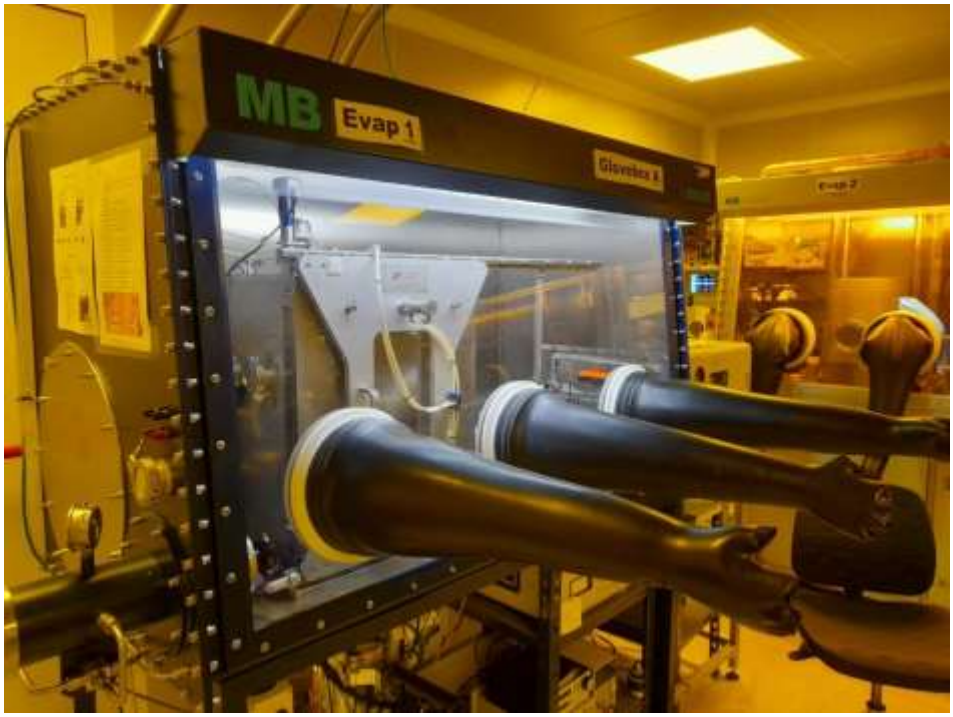

Figure 3.5. Thermal evaporator integrated in a N_2 glovebox inside a Class 10000 cleanroom

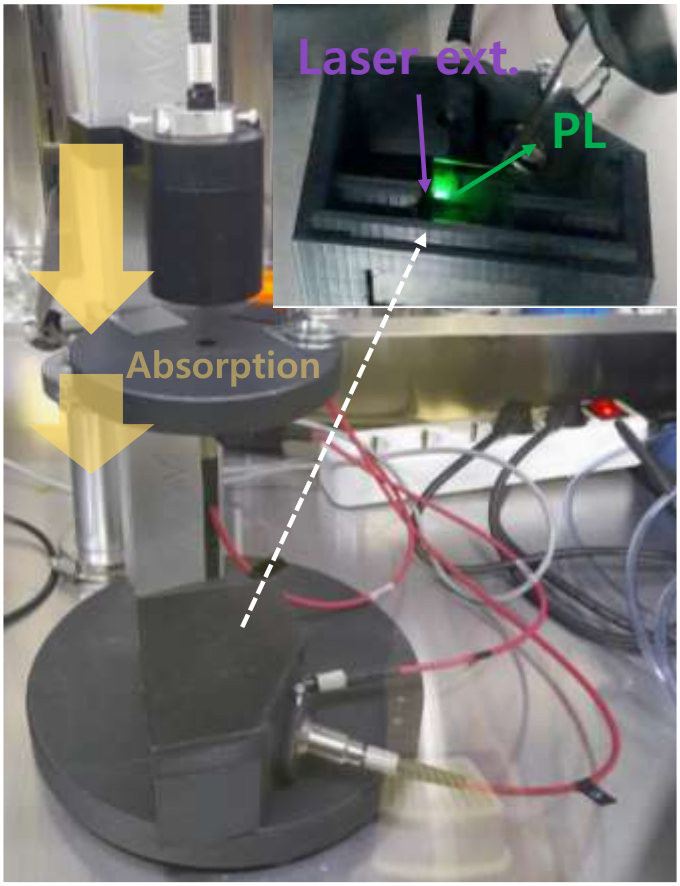

Figure 3.6. Spectrometer setup to characterize thin films (inset: PL measurement inside of setup)

Figure 3.7. a. Keithley setup for device characterization. b. Measurement configuration employing photodiode to evaluate luminance.

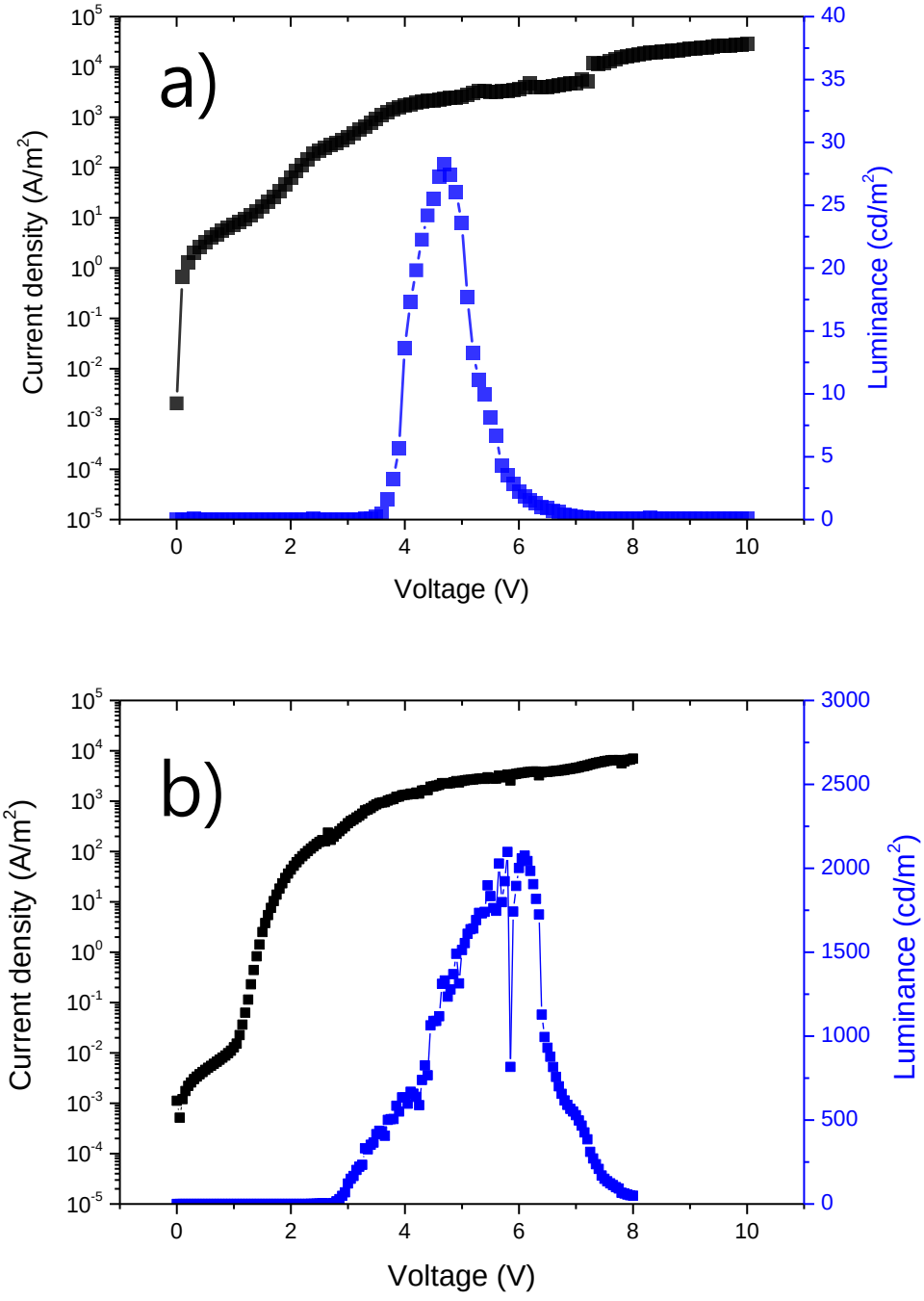

Figure 3.8. J-V-L results of a) $FAPbBr_3$ and b) $CsPbBr_3$ LECs

The first perovskite LECs have the following configuration: ITO/PEDOT:PSS (30 nm)/Perovskite:PEO (300 nm)/Ba (5 nm)/Ag (70 nm).

For the perovskite emitter, formamidinium lead bromide (hybrid) and caesium lead bromide (inorganic) are employed due to their electrochemical stability.[55] The implementation of inorganic perovskite instead of hybrid perovskite increased the luminescence values from 30 cd/m^2 to 2200 cd/m^2 for $FAPbBr_3$ and $CsPbBr_3$, respectively. The improved operation could be attributed to higher conductivity of $CsPbBr_3$:PEO composite, according to recent works led by Pablo Docampo and Rubén D. Costa.[56,57] Also, inorganic perovskites show a high luminance over 2000 cd/m^2 and fast response (total time for J-V-L scan was less than 1 minute). In this regard, $CsPbBr_3$ is benchmarked as a material for reference LECs for further study in this chapter.

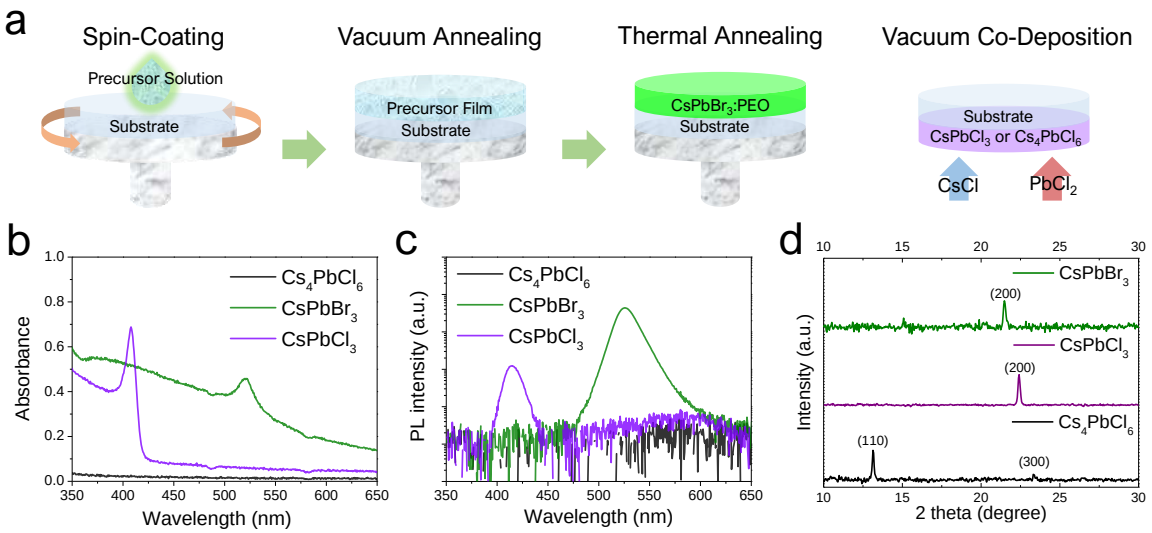

Figure 3.9. a) Fabrication process of solution processed caesium lead bromide:PEO and sublimation of caesium lead chloride films. b) Absorbance, c) PL spectra (excitation wavelength: 375 nm), and d) XRD pattern of $CsPbBr_3$:PEO, $CsPbCl_3$, and Cs_4PbCl_6.

The general deposition method is briefly summarized in **Figure 3.9.a.** The perovskite precursor solution is spin-coated on the ITO/PEDOT:PSS anode followed by annealing in vacuum to promote nucleation and formation of compact films. After this process, the samples are thermally annealed at 70 °C for 3 min to eliminate the residual solvent. The chloride-based films are deposited by vacuum co-sublimation of caesium chloride and lead chloride. The dimensionality of the caesium lead chloride

compounds is controlled via the relative deposition rates of the two precursors. In one case we form caesium lead chloride, $CsPbCl_3$, which is a 3D perovskite. However, with excess CsCl, a 0D non-perovskite phase of the type Cs_4PbCl_6 is formed. This Cs_4PbX_6 structure contains lead halide octahedra with Cs cation surrounding it, which results in a higher exciton binding energy and lower electric conductivity than the 3D perovskite counterpart.[58]

The absorption spectra for our solution-processed $CsPbBr_3$ and vacuum-deposited $CsPbCl_3$ and Cs_4PbCl_6 films are presented in **Figure 3.9.b.** $CsPbBr_3$ and $CsPbCl_3$ show the characteristic excitonic peaks at 520 and 400 nm, respectively. Cs_4PbCl_6 does not show any absorption in the entire visible region, which is expected in view of its band gap of 4.37 eV. [59] Upon excitation with a 375 nm laser, $CsPbBr_3$ and $CsPbCl_3$ show photoluminescence (PL) peaks centred at 528 and 405 nm, respectively (**Figure 3.9.c.**), with a small Stokes shift characteristic of direct band gap 3D perovskites. [19] In the case of Cs_4PbCl_6, we did not observe any PL signal because its band gap is larger than the excitation photon energy at 375 nm. **Figure 3.9.d** shows the XRD patterns for these three films. The diffractograms of the 3D perovskites show a main peak at $2\theta = 21.5°$ for $CsPbBr_3$ and $2\theta = 22.5°$ for $CsPbCl_3$, which can be ascribed to the (200) plane, which is expected to be the main diffraction signal for non-oriented crystals (according to the Inorganic Crystal Structure Database, ICSD, references 243734 and 243735). Two characteristic reflections for the 0D Cs_4PbCl_6 are observed at $2\theta = 13.1$ and $2\theta = 23.3°$ (according to ICSD, references 35703).

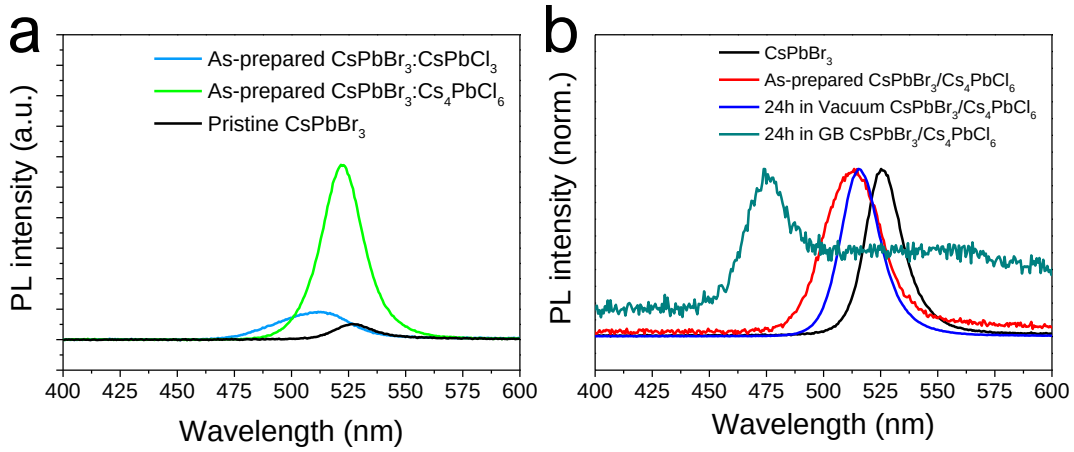

Figure 3.10. a) PL spectra of as-prepared $CsPbBr_3$ layer, $CsPbBr_3/CsPbCl_3$, and $CsPbBr_3/Cs_4PbCl_6$ bilayers. b) Normalized PL spectra of $CsPbBr_3$ films and $CsPbBr_3/Cs_4PbCl_6$ heterostructures that were stored in a vacuum chamber ($2 \cdot 10^{-6}$ mbar) and N_2 glovebox for 24 hours (excitation wavelength: 375 nm).

With these three films, heterojunction stacks are fabricated by combining spin-coating and vacuum co-evaporation to investigate the ion-diffusion property at the interface of these materials. Initially, the study focused on the PL of a 3D/3D heterojunction of the type $CsPbBr_3$ (300 nm)/$CsPbCl_3$ (50 nm) using a 375 nm laser excitation source (**Figure 3.10.b**). The as-prepared $CsPbBr_3/CsPbCl_3$ bilayers show a blue-shifted and asymmetric PL signal with respect to that of the pure $CsPbBr_3$, corresponding to a cyan colour emission. This observation is indicative of spontaneous anion exchange between the two materials, even at room temperature. In contrast, the 3D/0D $CsPbBr_3/Cs_4PbCl_6$ heterojunction shows a negligible PL shift and a PL with higher intensity as compared to the reference $CsPbBr_3$. This measurement is in good agreement with a report by Shen *et al.* who showed hindered anion diffusion and mixing in 0D Cs_4PbX_6 (X = Cl^-, Br^-). [60] The PL of 3D/0D $CsPbBr_3/Cs_4PbCl_6$ bilayers was further studied as a function of the storage condition (**Figure 3.10.b**). A blue shift of the PL signal is observed after storing the bilayer for 24 h in a N_2 atmosphere. It is worth to note that this glovebox for storage experiment is a different one from that for the spin-coating, hence the atmosphere is also free of any solvent vapor. On the contrary, when stored in a vacuum chamber (base pressure: $2 \cdot 10^{-6}$ mbar) for the same time, the

$CsPbBr_3/Cs_4PbCl_6$ maintained the initial PL peak position. Also, the PL peak was found to be sharper after storing the material in vacuum. This interesting observation agrees with a previous report by Karlsson *et al.,* who showed that in vacuum the material can reorganize and achieve a superior compositional homogeneity, in turn leading to a narrower PL peak.[61] With these three films, heterojunction stacks are fabricated by combining spin-coating and vacuum co-evaporation to investigate the ion-diffusion property at the interface of these materials.

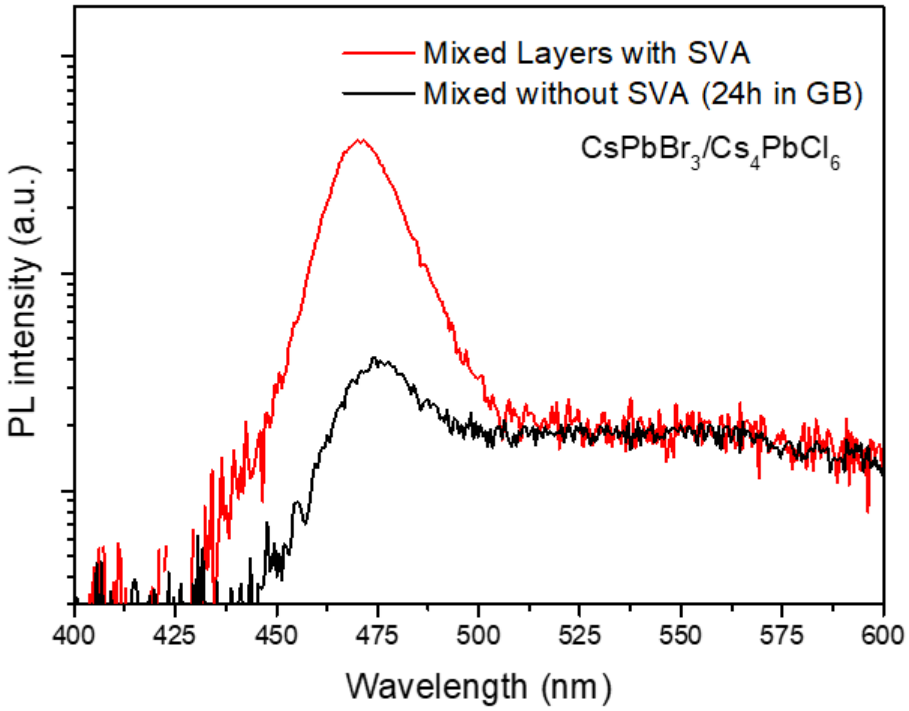

Figure 3.11. PL spectra of mixed $CsPbBr_3$ 300 nm / Cs_4PbCl_6 50 nm, with and without SVA

In addition, when these bilayers were treated via solvent vapour annealing (SVA) based on de-ionized water in a petri-dish using a modified condition from a previous report, as SVA induces a higher PL intensity compared to slow and spontaneous mixing in nitrogen (**Figure 3.11**).[62]

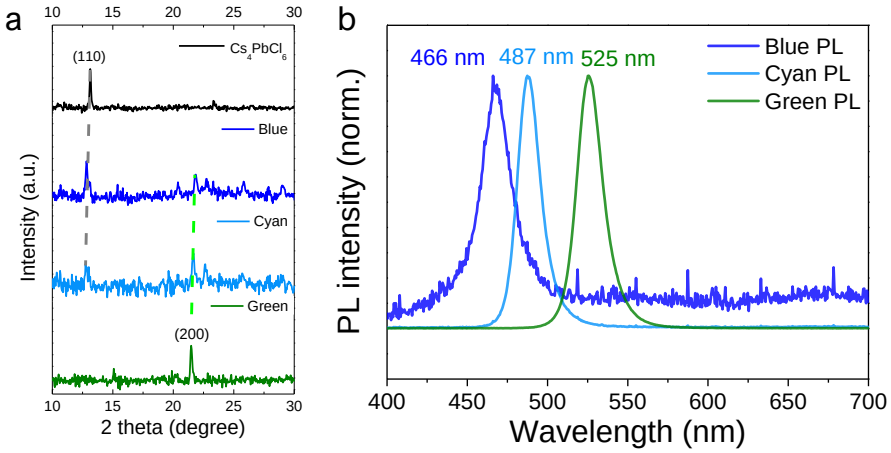

Figure 3.12. (a) XRD patterns of $CsPbBr_3$ (Green), Cs_4PbCl_6, and mixed-halide films (Cyan and Blue) obtained by mixing with SVA. (b) PL spectra of green-emissive $CsPbBr_3$, mixed cyan, and blue-emitting films.

Hence, we prepared a series of $CsPbBr_3/Cs_4PbCl_6$ 3D/0D bilayers with constant $CsPbBr_3$ thickness (300 nm) and with different Cs_4PbCl_6 top-layer thicknesses (0, 25, and 50 nm) and mixed these using the process of SVA. From the XRD patterns (**Figure 3.12.a**), the main (200) diffraction peak, characteristic of the orthorhombic $CsPbBr_3$ phase, shifts to higher angles after anion intermixing with the top layers, although the diffraction intensity is strongly reduced. This is due to partial bromide substitution with chloride, resulting in a smaller unit cell for mixed-halide $CsPbBr_{3-x}Cl_x$. Importantly, the (110) reflection at $2\theta = 12.7°$, corresponding to the 0D Cs_4PbCl_6 phase, is observed even after SVA treatment. This implies that the 3D/0D crystal structure is preserved even after halide mixing. The PL spectra of the $CsPbBr_3$, $CsPbBr_3/Cs_4PbCl_6$ (25 nm), and $CsPbBr_3/Cs_4PbCl_6$ (50 nm) films show sharp and symmetric peaks centred at 525 (green), 487 (cyan), and 466 nm (blue), respectively (**Figure 3.12.b**). Thus, by controlling anion intermixing through the material dimensionality (3D/0D) and the thickness of the 0D film, it is possible to fine tune the emission of the perovskite heterojunction. Interestingly, the PL quantum yield (PLQY) of the three materials do not follow a monotonic trend, with the cyan emitter having more efficient PL (14.0%) as compared to the green (9.5%) and blue (3.6%) materials.

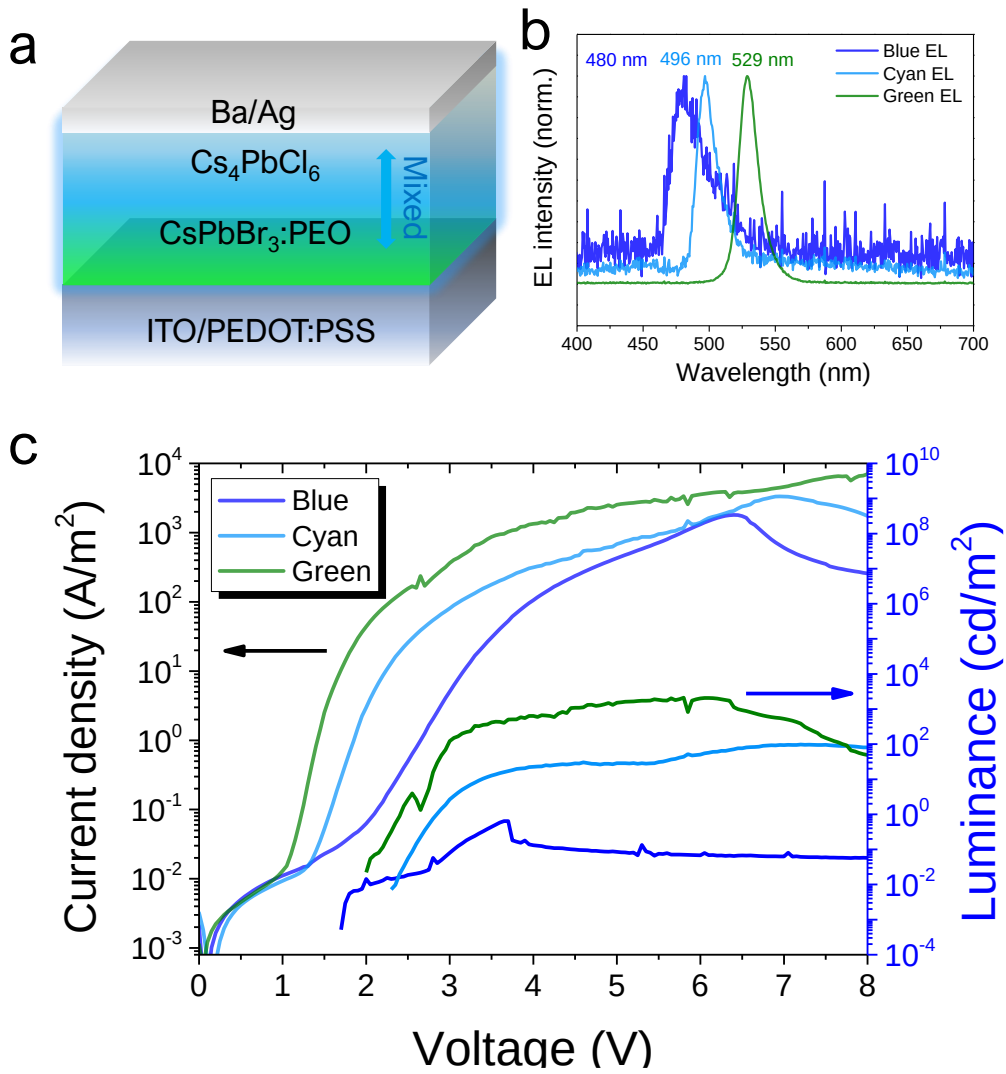

Figure 3.13. a) Schematic illustration of the EL devices, b) EL spectra, and c) J–V–L data of the light emitters based on the pristine and mixed perovskites.

The same set of materials were incorporated in thin-film LEDs with the structure depicted in **Figure 3.13.a**, where the perovskites are sandwiched between an ITO/PEDOT:PSS anode and a Ba/Ag cathode. The Ba layer with low work function is employed to ensure ohmic electron injection, like in previous reports where LiF interlayers were used. As shown in **Figure 3.13.b**, the EL spectra for the three materials are only slightly red-shifted as compared to their PL spectra. The JVL curves for three representative devices are reported in **Figure 3.13.c**. The maximum

measured luminance values were 2000 and 100 cd/m^2 for green and cyan emitters, respectively, which is comparable to other recent reports on similar $CsPbX_3$:PEO perovskite emitters.[54,63] A low current density and luminance for the blue emitter is observed, which might be related with the thicker insulating Cs_4PbX_6 0D top layer.

For the last part of this chapter, planar devices combining 0D and 3D metal halide films are prepared, to study their electroluminescent behaviour, in view of the absence of halide mixing in the 3D/0D heterojunctions ($CsPbBr_3$/Cs_4PbCl_6). In addition, this device type did not require Ba or LiF but only used Cs_4PbCl_6 instead, making it a very simple device with structure (anode/active layer/cathode) similar to what can be found in LECs. In particular, we used $CsPbBr_3$:PEO as the light emitters and studied the effect of the 0D Cs_4PbCl_6 layer below (at the anode, 0D/3D), on top (at the cathode, 3D/0D), and on both sides of the 3D $CsPbBr_3$ emitter (0D/3D/0D triple layers). The structure of the devices is illustrated in **Figure 3.14.a**, and they are named following the order and dimensionality of the corresponding heterojunctions.

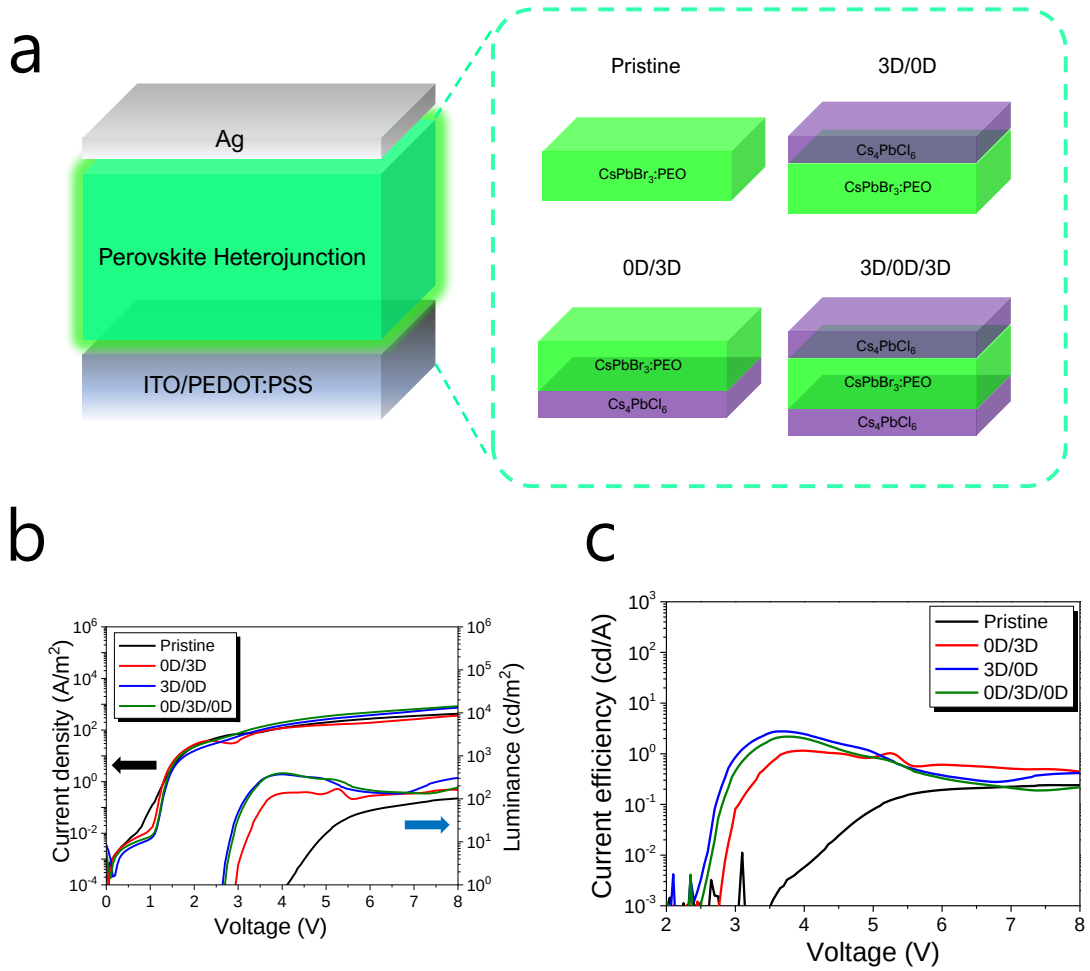

Figure 3.14. a) Schematic illustration of the perovskite heterojunction-based light emitters. b) Current density and luminance vs applied voltage for the same devices. The corresponding current efficiency is shown in c).

The J-V-L curves for this device set is presented in **Figure 3.14.b.** The heterojunction-based devices show a slightly reduced leakage current below 1 V, as compared to the reference single-layer 3D light emitter. More importantly, all heterojunction devices exhibited lower turn-on voltage and more intense electroluminescence as compared to the reference 3D device. In the perovskite heterojunctions, 25 nm thick Cs_4PbCl_6 films are deposited. After deposition, the main PL peak is slightly blue shifted, suggesting halide intermixing at the 3D/0D interface. Hence, the actual Cs_4PbCl_6 layer is even thinner compared to the nominal deposited thickness.

The 3D/0D and 0D/3D/0D devices reached luminance level of about 400

cd/m^2, at an applied bias of approximately 3.5 V. At the same voltage, 0D /3D device showed a lower EL intensity, about one third as compared to the others. As the current density is very similar for these three types of devices, their current efficiency (**Figure 3.14.c**) follows the trend of the lu minance. The reference 3D device shows a low current efficiency with a maximum of 0.1 cd/A at 5 V. With the 0D layer at the anode (0D/3D devi ce), the efficiency maximum was improved to 1 cd/A at 4 V, which is furth er improved when the Cs_4PbCl_6 0D film is placed in between the $CsPbBr_3$ 3D perovskite emitter and the cathode. 3D/0D and 0D/3D/0D device sh owed superior efficiency (>3 cd/A), indicating that non-radiative recombination at the $CsPbBr_3$/Ag interface is strongly reduced upon insertion of the 0D layer (as the current density is unvaried betwee n the different device configuration).

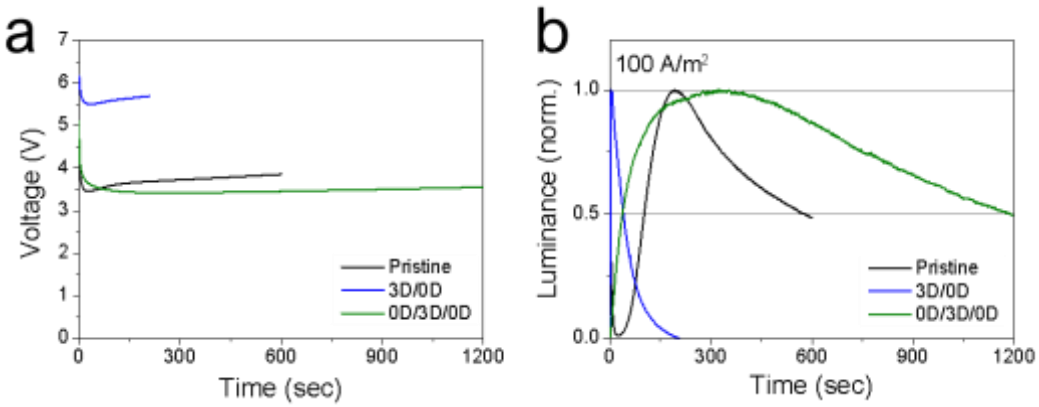

Figure 3.15. a) Time-dependent voltage and b) luminance for the same devices driven with a constant current density of 100 A/m^2.

To test the stability, the devices were driven with a constant current density of 100 A/m^2, while monitoring the evolution of the luminance and voltage. 3D/0D device was found to be unstable, while the pristine $CsPbBr_3$-based device shows a half lifetime ($t_{1/2}$, time to reach half of the maximum luminance) of approximately 10 min (**Figure 3.15**). Interestingly, the triple-layer heterojunction, 0D/3D/0D device, demonstrated a further improved operational stability: with $t_{1/2}$ = 20 min. The time to reach 100 cd/m^2 in this 0D/3D/0D device was only 25 s. In addition, this device shows negligible voltage variation (<0.1 V), indicating stable electrical properties, which might arise from the limited and balanced ion movement of the Cs_4PbCl_6 buffer layers. The mechanism responsible for the enhanced stability of the

0D/3D/0D heterojunctions is hard to identify precisely. However, it is possible that unbalanced charge injection and subsequent charge accumulation in bilayers might favour non-radiative recombination and trigger the degradation of the perovskite films. Correspondingly, the operational lifetime will be decreased significantly. [64,65]

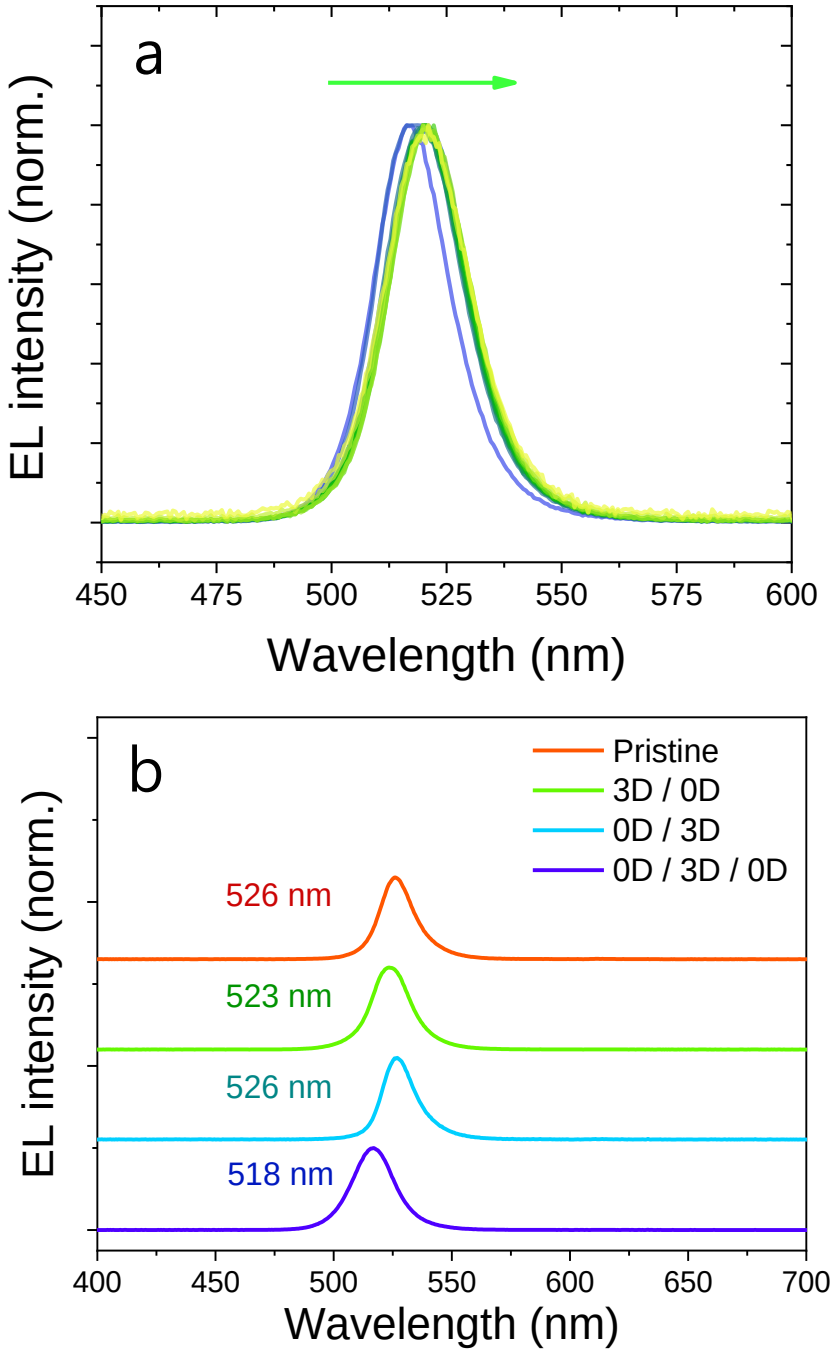

Figure 3.16 a) EL spectra of 0D/3D/0D device during operation b) original EL spectra of as-fabricated perovskite heterojunction LECs.

Most of all, this limitation on the ion movement by Cs_4PbCl_6 allows for a stable electroluminescence. Even after 20 min of the device operation with

100 A/m^2, devices based on the 0D/3D/0D active layer do not show a blue shift, due to the absence of halide intermixing. On the contrary, there is a small red shift happening at about 0.2 nm/min (**Figure 3.16a**) and a recovery of the green emission from $CsPbBr_3$ (from 518 nm to 522 nm). It is possible that EL recovery in this 0D/3D/0D device originates from the Cl anion diffusing out the radiative recombination zone. After 20 min of device operation, the EL peak (522 nm) becomes like that of the pristine device, 526 nm. This phenomenon supports our point that the heterojunction based on 0D caesium lead halide has less chance to donate a halide anion, which causes an emission peak shift.

3.4. Conclusion

In this chapter, a simple electroluminescent device employing air-stable electrodes is realized without adding salts to the light-emitting layer. This is possible by exploiting the ionic conductivity of metal halide perovskite emitters. We have prepared hetero-structures consisting of bi-layers of different 3D perovskites and a 0D metal halide structure. It is clearly confirmed that the 0D structure is only marginally donating halides to the adjacent 3D structure, whereas a 3D perovskite-perovskite bi-layer does lead to halide interchange. We have also shown that 0D-intercalation can stabilize the electroluminescence of the devices.

Chapter 4.

Phosphorescent Organic Light Emitting Diodes with Inorganic Perovskite Hole Transport Layers

4.1. Introduction

OLED technology is one of the most popular for the display market. OLEDs are used as an electroluminescent element in many applications as a stand-alone light source, but they are also used as a white or blue backlight in OLED TV screens and in quantum dot-based displays.

The first electroluminescent phenomenon was observed in 1965 from single crystals of anthracene in the National Research Council of Canada.[66]

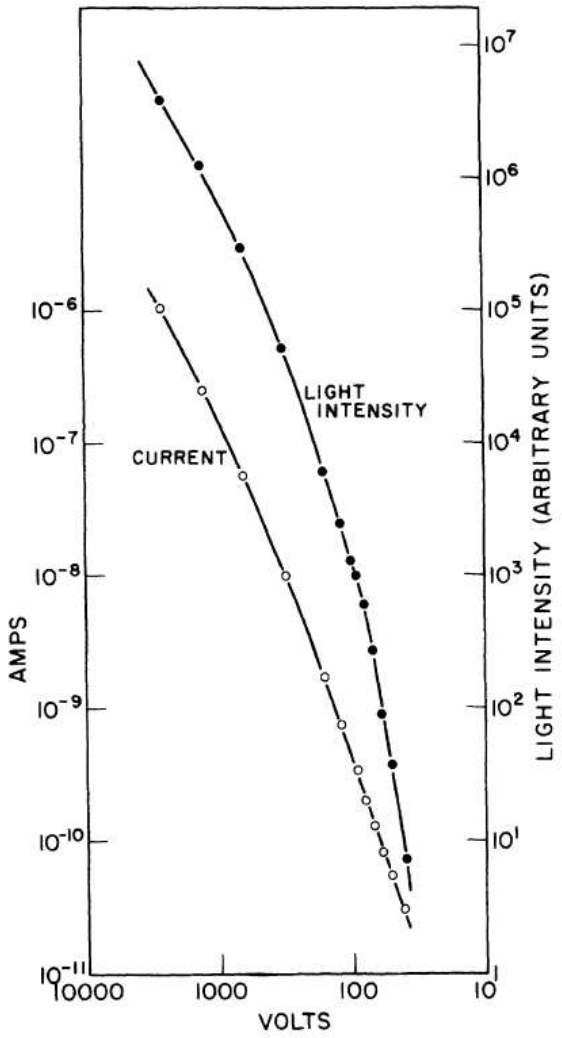

Figure 4.1. The first electroluminescence from anthracene single crystal.[66]

Helfrich and Schneider refined millimetre-thick single crystals with 1 cm diameter. Then, glass tubes cemented to the crystal surface containing the liquid electrodes with 0.2 cm^2 of contact area made this single crystalline anthracene luminescent. Despite this discovery, no application has been made after several decades due to the extremely high operational voltage, owing to thickness of the crystal and the poor electrical contact.

After 22 years, a huge breakthrough was made by Tang and Van Slyke from Kodak. They reported a p-n junction OLEDs using evaporated organic molecules.[67]

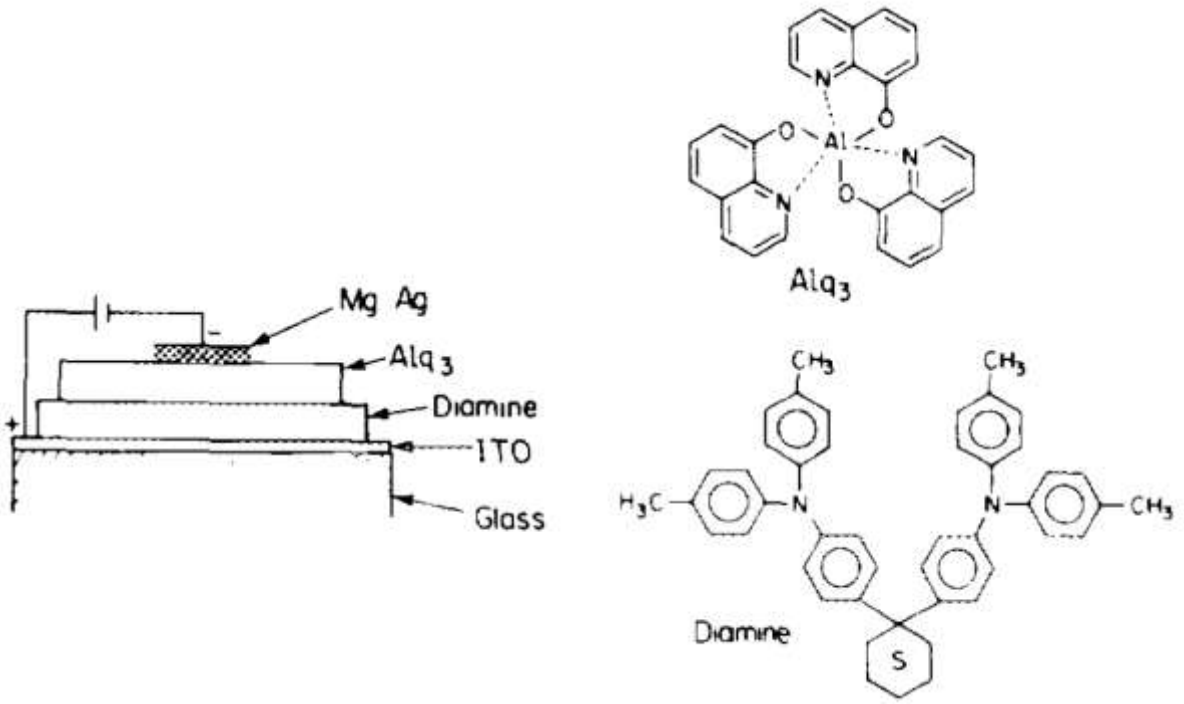

Figure 4.2. p-n junction OLED comprising Alq_3 (n-type, emitter)and diamine (p-type).[67]

They deposited 75 nm of an arylamine and 60 nm of Tris(8-hydroxyquinolinato) aluminium (Alq_3) on ITO and finished the devices with a Mg:Ag alloy. The efficient hole transport with the arylamine and electron injection with low work function of Mg-incorporated cathode made it

favourable for the electroluminescence of Alq_3, achieving 1000 cd/m^2 with a voltage less than 10 V.

In addition to this achievement with small molecules, another major finding was reported by Prof. Richard H. Friend and co-workers, producing the first conjugated polymer LED using a soluble version of poly (p-phenylene vinylene) (PPV, **Figure 4.3**).[68] The conjugated polymer is spin-coated between ITO and Al The advantage of this polymer OLED reside in the possibility of solution processing with low-cost on a large area.

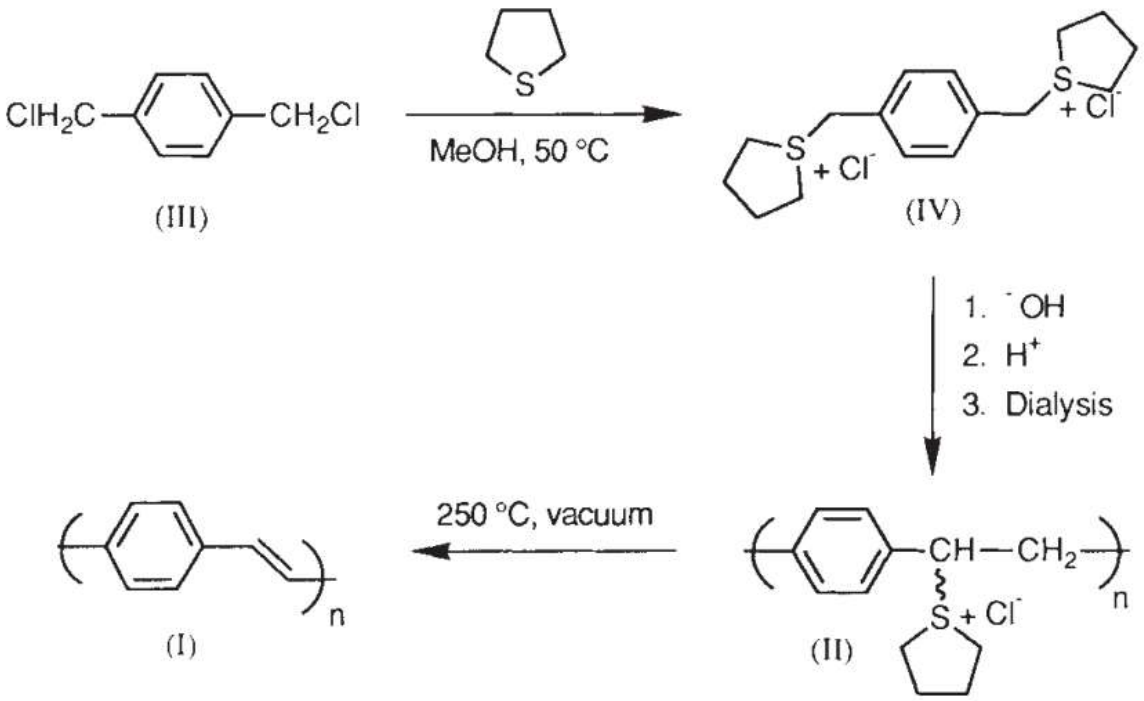

Figure 4.3. Synthesis of PPV.[68]

The efficiency of these fluorescent OLEDs is limited since only the singlet spin states induce fluorescent emission; these represent a small fraction (about 25 %, according to spin selection rule) of the total excited-state population (the rest are triplet states, 75 % that cannot be harvested at room temperature by most organic emitters). Phosphorescent dyes, however, offer a means of achieving improved light-emission efficiencies, as emission may result from both singlet and triplet states. As illustrated in **Figure 4.4**, fluorescent emissions occur during the transition from the first excited state to the ground state (S_1 to S_0). Meanwhile, the triplet

states T_1 are also formed when electrons and holes recombine in electroluminescent devices. Due to the low radiative rate in T_1 to S_0 transition, the de-activation of the T_1 state occurs non-radiatively at room temperature. In this regard, 75 % of the excitons are lost. However, phosphorescent emitters possess a central heavy metal ion which induces strong spin-orbital coupling. Due to that the S_1 state is transferred to the lower energy T_1 state via efficient intersystem crossing (ISC). Additionally, the spin-orbit coupling also leads to an increase in rate of the radiative T_1 to S_0 transition so that efficient phosphorescence can be realized even at room temperature.

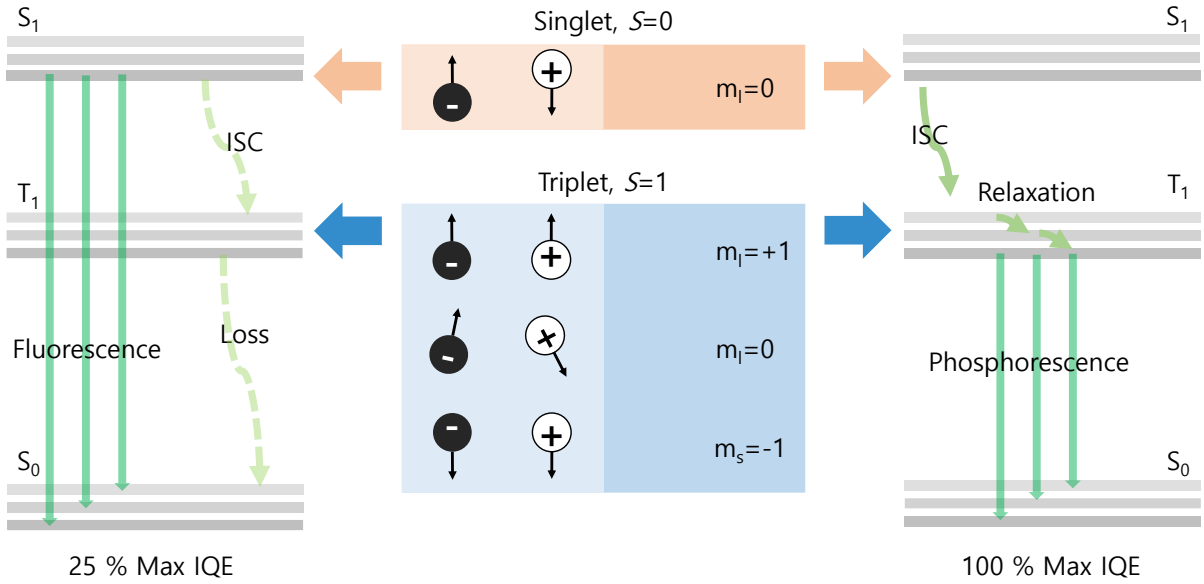

Figure 4.4. Schematic illustration of recombination process in fluorescent and phosphorescent emissions.

Prof. Stephen R. Forrest and co-workers in Princeton University reported high-efficiency energy transfer from both singlet and triplet states, in a host material doped with the phosphorescent dye, 2,3,7,8,12,13,17,18-octaethyl-21H,23H-porphine platinum (II) (PtOEP), resulting in efficient peak internal quantum efficiency (IQE) of 23 %.[69] In addition, the same research team carried the IQE to nearly 100 % using bis(2-phenylpyridine)iridium(III) acetylacetonate, $Ir(ppy)_2acac$, doped into 3-phenyl-4(1′-naphthyl)-5-phenyl-1,2,4-triazole (TAZ) to prevent triplet-triplet annihilation (TTA).[70] 18 years after that first paper, the first author in

that paper, Prof. Chihaya Adachi, developed a novel efficient OLED using an iridium complex comprising an extraordinarily thick layer of a metal halide perovskite, $CH_3NH_3PbCl_3$, that functions as both the hole and electron transport material.

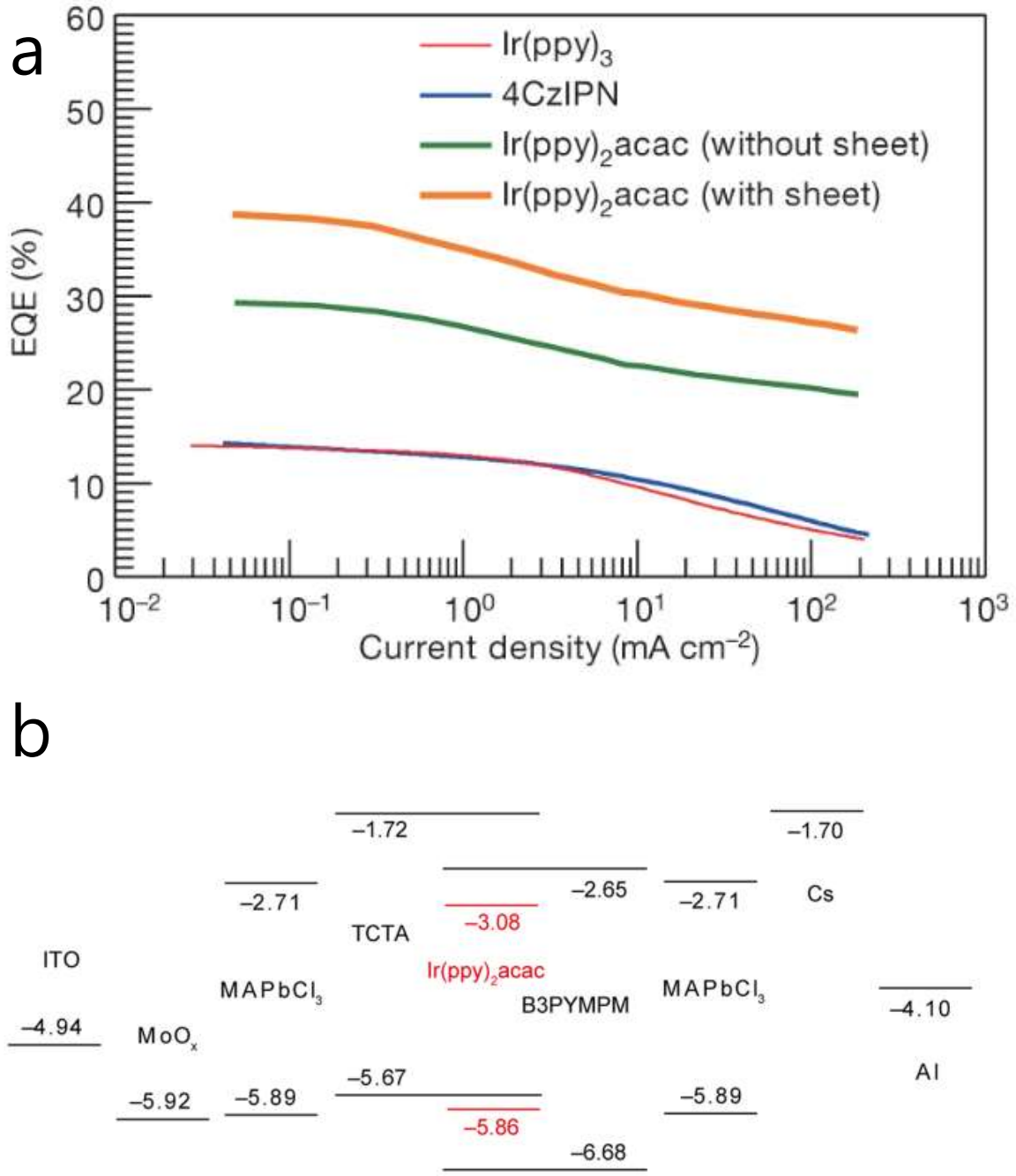

Figure 4.5. a) Efficiency of phosphorescent OLEDs with perovskite transport layers as a function of current density. b) flat band diagram of the energy levels (either valence, or conduction bands, work functions or highest occupied and lowest unoccupied molecular orbitals, HOMO and LUMO, respectively) of the materials employed in the device.[71]

The authors investigated OLEDs with a fluorescent Alq_3 emissive layer and $CH_3NH_3PbCl_3$ perovskite transport layers as well as more efficient phosphorescent emitting OLEDs that employed a complex emitting layer in which the emitter is dispersed in an organic host material with hole and electron transporting capabilities. The thick perovskite based transport layers prevent the formation of shunting paths between electrodes and even device failure.[72,73] In their report, a high EQE over 20 % was achieved which could be enhance with the use of light out-coupling foils. However, this fabrication process using vacuum co-evaporation of 3 sources for the light-emitting layer requires complex optimization and control during deposition, increasing the processing cost. In addition, the phosphorescent emitting materials such as iridium complex costs thousands of euros per gram.

Recently, more simple OLEDs were reported in which the phosphorescent emitters are no longer used in a suitable host matrix but as an ultrathin emissive layer (UEMLs). As this may lead to simpler devices employing lower amount of costly materials it has aroused much attention in the field.[74]

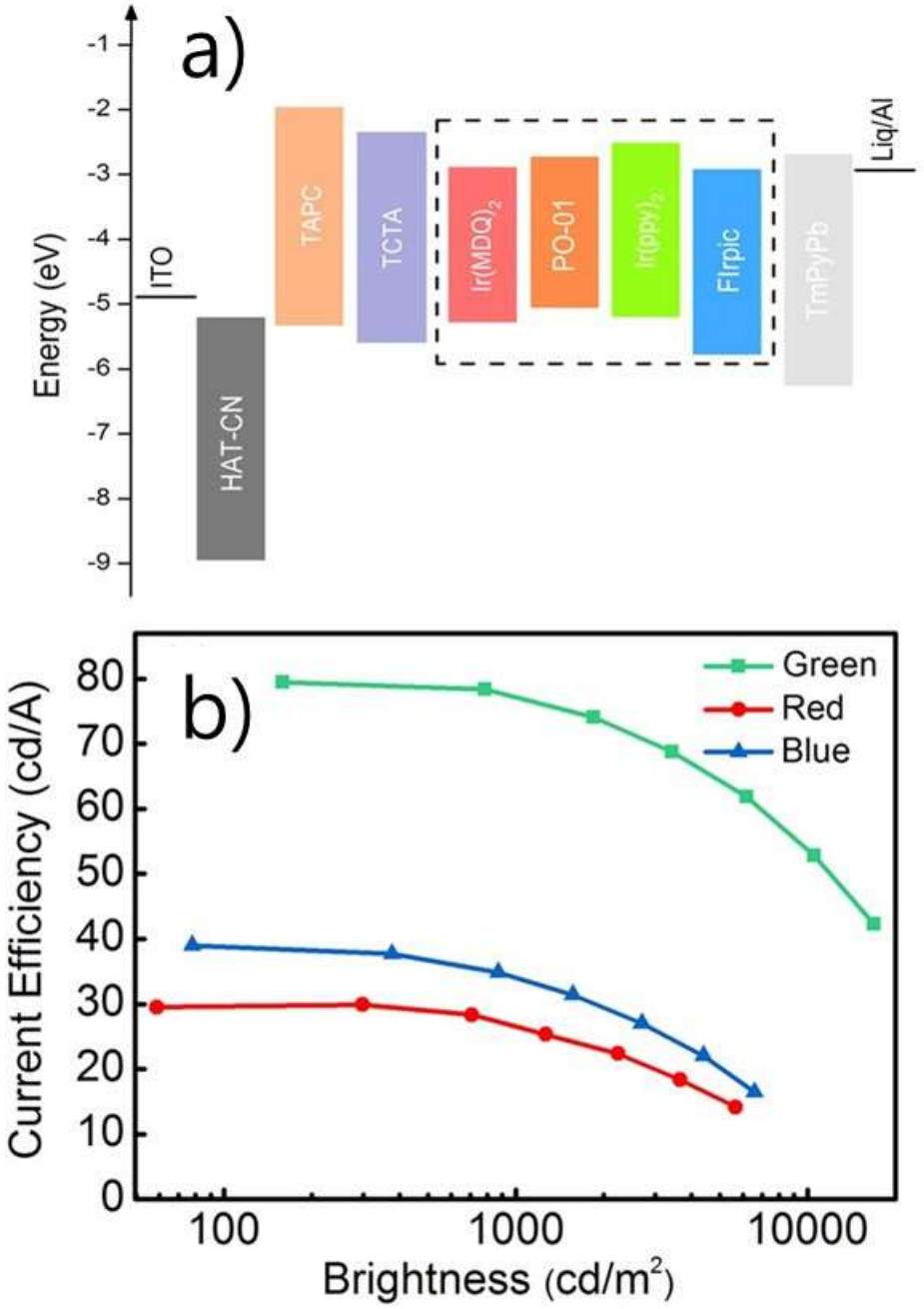

Figure 4.6. a) Flat band diagram and b) current efficiency as a function luminance of OLEDs comprising UEMLs.[75]

For example, Prof. Man-Keung Fung in Soochow University developed OLEDs with 0.3 nm thick UEMLs.[75] The phosphorescent emissive materials are intercalated between hole transporting tris(4-carbazoyl-9-ylphenyl) amine (TCTA) and electron transporting 1,3,5-Tri(m-pyridin-3-ylphenyl) benzene (TmPyPb) layers as shown in **Figure 4.6**. Their work

proves that this UEML is able to possess reasonable efficiency even with 0.3 nm. The authors claim that using 0.3 nm of UEML saves 70 % of material cost.

In this chapter the objective is to combine perovskite based charge transport layers with ultrathin phosphorescent emitters, here referred to as PUE-LEDs (perovskite-ultrathin emitter LEDs). Such a device structure would be economical due to low materials costs (perovskite precursor materials are very cheap, whereas organic semiconductors are not) and a more robust device structure allowing for higher throughput processes.

4.2. Results and discussion

The $CsPbCl_3$ charge transport layer is vacuum co-evaporated in the same manner as described in Chapter 3. The only addition is that we introduced a thin layer of CsCl to passivate potential defects at interfaces. This is introduced here because lead chloride perovskites can have defect states that have an energy level that lies within the band gap. And states in the bandgap can act as quenchers whereas if the states have energy levels outside the bandgap they are more benign. This is a direct result from the fact that the chloride perovskite has a much larger bandgap compared to the iodide and bromide counterparts.[76] In a recent report with an evaporated $CsPbI_2Br$ perovskite solar cell, intercalating a 6 nm thick CsBr buffer layer between the perovskite and the transport layer improved the device performance due to passivating defect.[77] To prove this technique is useful for defect passivation, a PL study is conducted with 30 nm co-evaporated $CsPbCl_3$ and ¨CsCl-Modified $CsPbCl_3$ (m-$CsPbCl_3$) ¨ in **Figure 4.7.**

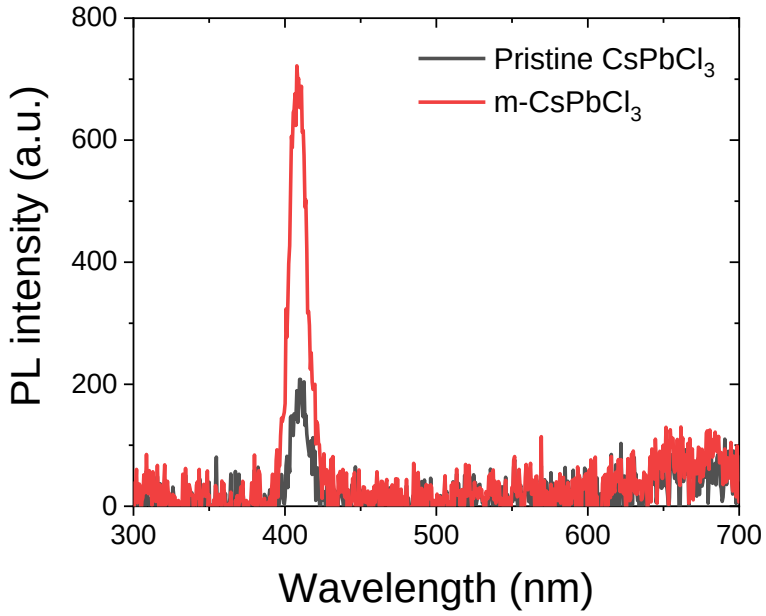

Figure 4.7. PL spectra of 30 nm $CsPbCl_3$ with (red line) and without (black line) CsCl passivation. (Excitation wavelength: 375 nm, a neutral density filter deletes signals before 400 nm)

In **Figure 4.7**, the peak PL intensity of $CsPbCl_3$ is more than 3.5 times higher than that of $CsPbCl_3$, without shifting the peak which remains at 410 nm. This improved PL implies that the CsCl-passivation is also effective in passivating some defects in the $CsPbCl_3$ as well. With this modified perovskite layer, we prepare and investigate the OLEDs with the very thin emitters.

The fabrication process is depicted in **Figure 4.8.** First, 150 nm thick ITO is cleaned and treated by UV-ozone and PEDOT:PSS is spin-coated to flatten ITO substrates as explained in previous chapter with details. To transport holes, $CsPbCl_3$ or m-$CsPbCl_3$ layer is evaporated in a vacuum chamber and thermally annealed at 120 °C during 10 minutes before used as the substrate for further depositions. After the perovskite layer, TCTA (20 nm), various thickness of $Ir(ppy)_2acac$, and 2,2',2''-(1,3,5-Benzinetriyl)-tris(1-phenyl-1-H-benzimidazole) (TPBi) (40 nm) is evaporated. All the devices are finished with Ba (5 nm) / Ag (70 nm).

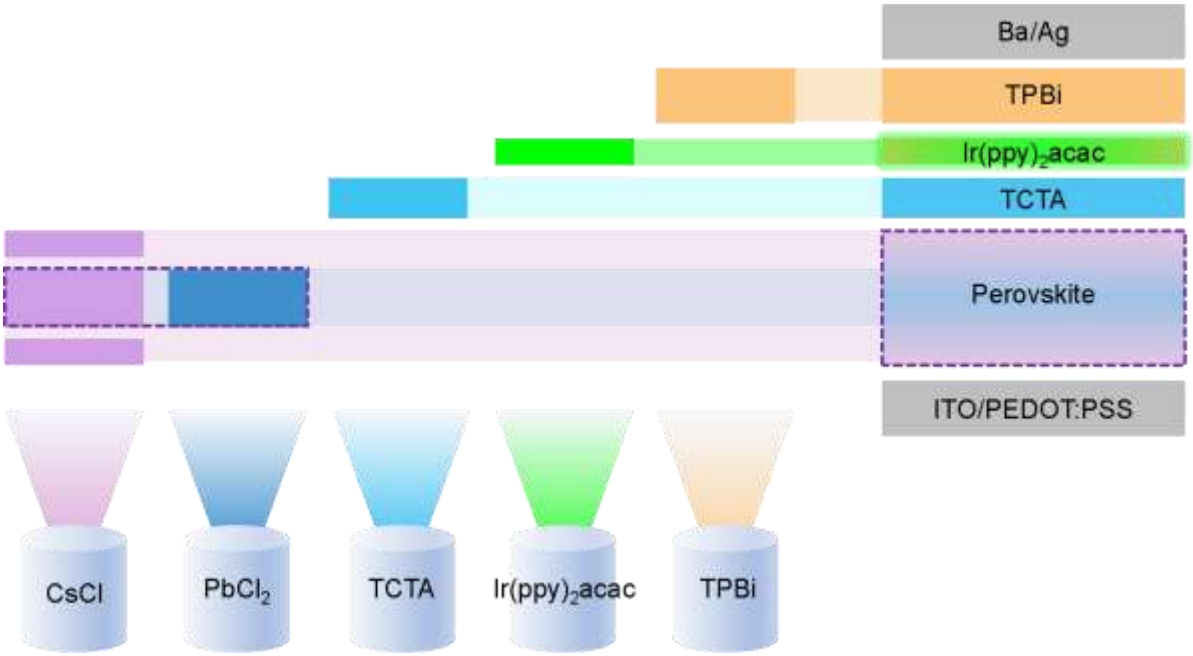

Figure 4.8. Fabrication process of PUE-LEDs.

Even though in this device stack we have eliminated the optimization of the emitter in the host layer, there are still a number of variations possible, primarily in the different layer thicknesses used. We first investigate the effect of the perovskite layer thickness on PUE-LEDs performance. For that we prepare OLEDs in which 30 nm $CsPbCl_3$ and m-$CsPbCl_3$ is investigated.

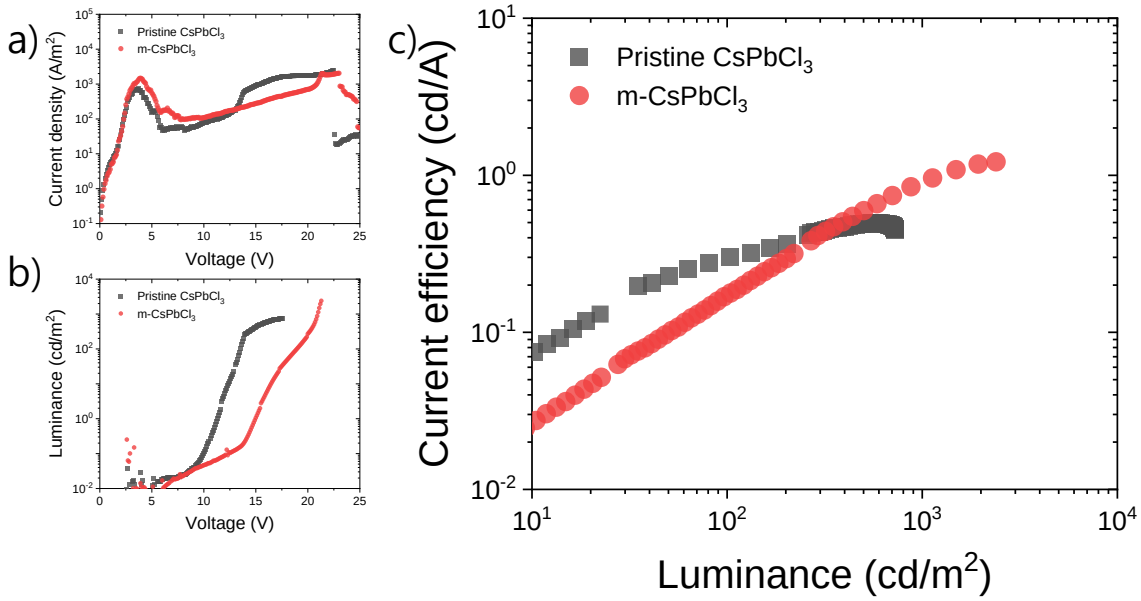

Figure 4.9. Performance parameters of the PUE-LEDs with perovskite layer thickness of 30 nm. a) J-V curves and b) L-V curves. c) Current efficiency as a function of Luminance.

The PUE-LEDs with thin perovskite layers had rather large leakage currents (below 5 V) regardless of CsCl passivation as shown in **Figure 4.9.**[71] The devices with CsCl-passivation show improvement in maximum luminance and efficiency, possibly owing to suppressed defect at interfaces. Therefore, a second batch of PUE-LEDs was prepared in which the thickness of the m-CsPbCl$_3$ layer is increased, from 30 nm to 200 nm, and the device performance is shown below in **Figure 4.10.**

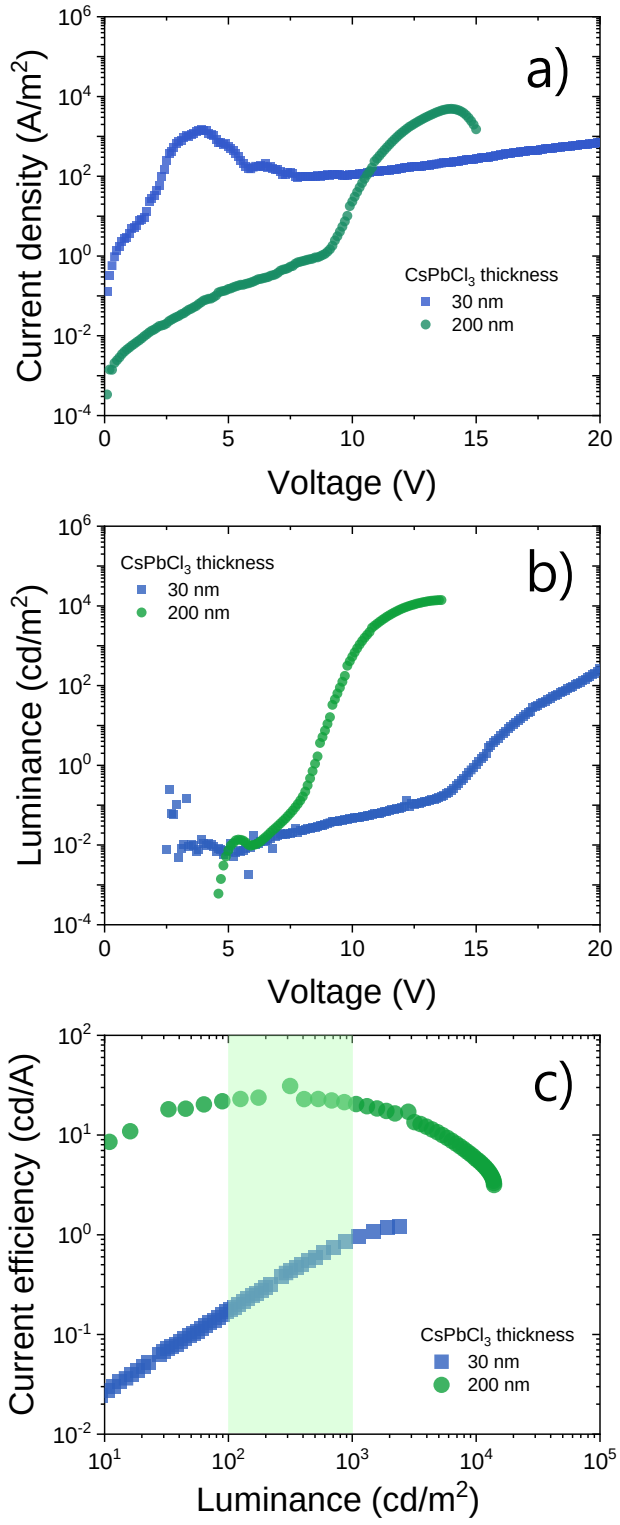

Figure 4.10. Performance parameters of the PUE-LEDs with m-$CsPbCl_3$ layer thickness of 30 and 200 nm a) J-V and b) L-V curves. c) Current efficiency as a function of Luminance.

In **Figure 4.10.a**, the current density at low driving voltages is strongly supressed for the PUE-LEDs employing the 200 nm thick perovskite layer, which is indicative of the much-reduced leakage current. In addition, the PUE-LEDs with 200 nm thick perovskite layer shows strong increase of the luminance near 8 V, resulting in a maximum luminance over 10000 cd/m^2 (**Figure 4.10.b**). As a result of the reduction in leakage current and increase in luminance the PUE-LEDs efficiency is enhanced from near 1 cd/A to over 31 cd/A as shown in **Figure 4.10.c.** Besides, the luminance with maximum efficiency is in display-relevant regime (100 to 1000 cd/m^2), making this device more attractive for display application. As the leakage current in the PUE-LEDs is already very low it is not necessary to further increase the perovskite layer thickness in this stack.

Another parameter that can affect the PUE-LEDs performance is the thickness of the thin film of light-emitter. We, therefore, prepared a series of PUE-LEDs in which the thickness of the iridium complex is varied from 0.05 to 0.5 nm. These are nominal thicknesses as read by the microbalance crystal sensors. It is unlikely that such thin films are homogeneous over the full area of the emitting layer. The results of the device analysis are shown below (**Figure 4.11**).

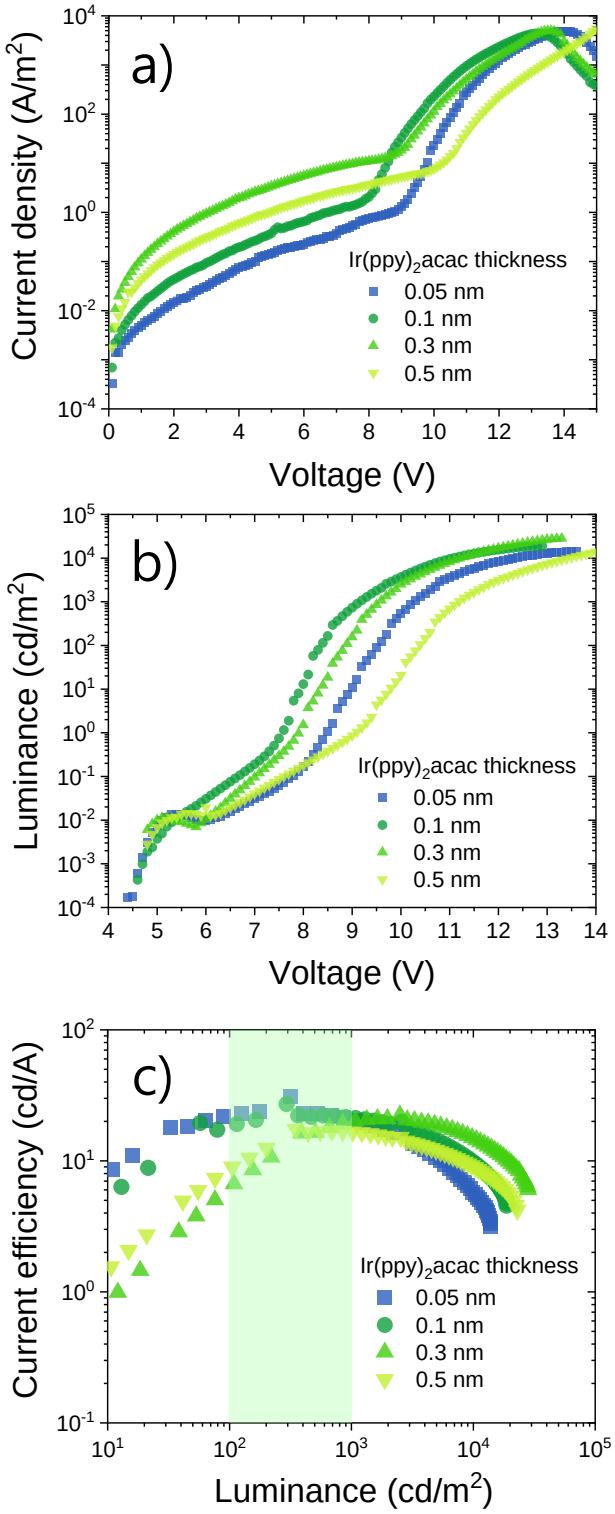

Figure 4.11. Performance parameters of the PUE-LEDs with an m-$CsPbCl_3$ layer thickness of 200 nm and varying thickness of the light emitting $Ir(ppy)_2acac$ layer (as shown in the inset) a) J-V and b) L-V curves c) Current efficiency as a function of Luminance.

A set of various thicknesses are deposited: 0.05 nm, 0.1 nm, 0.3 nm, and 0.5 nm. It should be noted that these thicknesses are the thickness derived from the microbalance crystal sensors and most likely not completely uniform. All the devices show similar trends in the J-V characteristics with a sharp increase near 8 V, while the OLED with 0.5 nm $Ir(ppy)_2acac$ shows the increase only at 10 V. Interestingly the devices with 0.05 nm and 0.1 nm thick iridium complex show similar maximum efficiencies (31 and 27 cd/A) at similar luminance, near 300 cd/m^2, which are display-relevant values. Even with a 0.3 nm thick Iridium complex, the maximum efficiency is still over 20 cd/A.

Hence, there is only a minor influence of the light-emitting layer thickness at least in the range of 0.05 to 0.3 nm (which are all very thin). This means that the process window is rather broad for this emitting layer. In combination with the thick perovskite film, it implies that these PUE-LEDs are promising electroluminescent devices.

We also prepared a more conventional OLED type in which a co-evaporated phosphorescent emitter and host material is used as the emitting to compare the performance with the PUE-LEDs.[78] We adopted this structure with a 200 nm $CsPbCl_3$ perovskite hole transport layer. The details of the OLED stack are schematically depicted in **Figure 4.12a**. The TCTA electron blocking layer had a thickness of 20 nm, the light emitting layer consisting of the Ir-emitter dispersed in TPBI at a concentration of 8 % had a thickness of 10 nm and the electron transporting pure TPBi layer had a thickness of 40 nm.

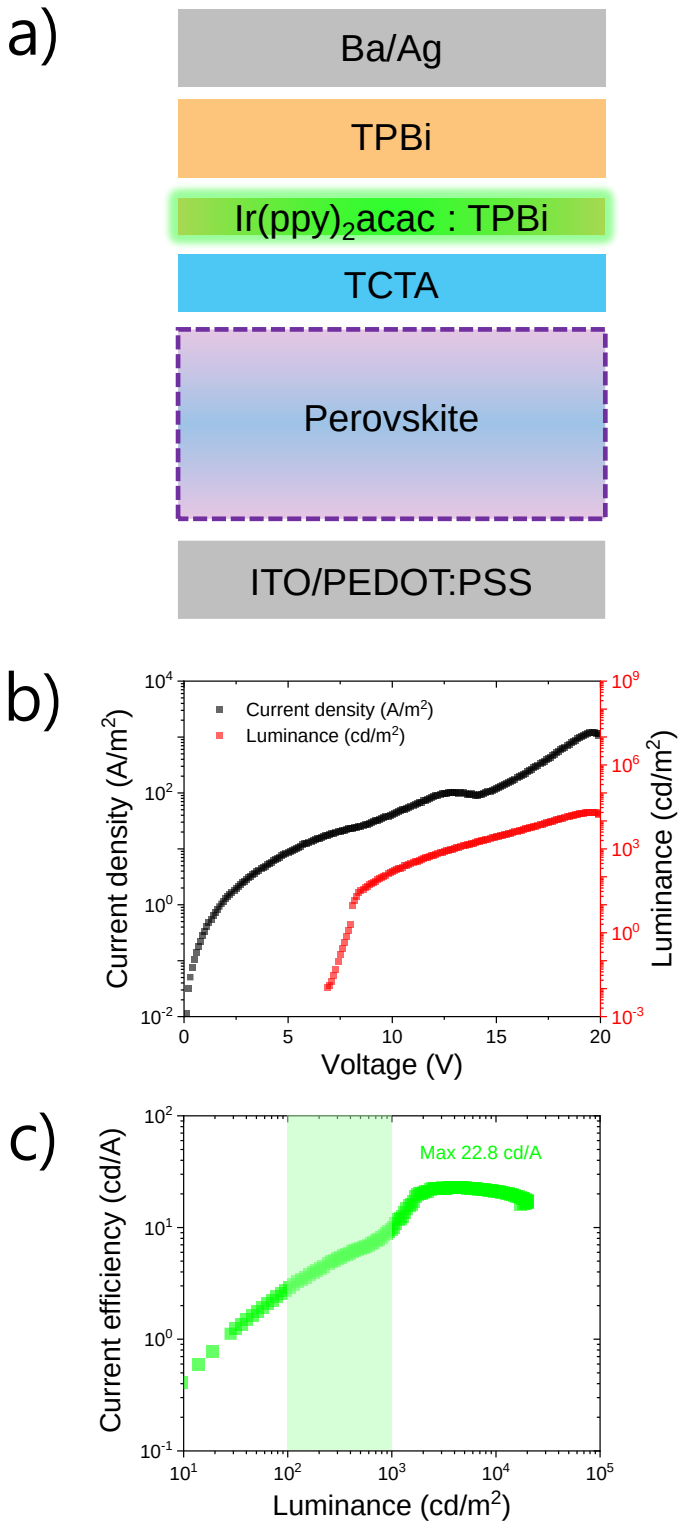

Figure 4.12. a) Schematic illustration of OLEDs with co-evaporated $Ir(ppy)_2acac$ and TPBi, b) J-V-L characteristic of device, and c) Current efficiency as a function of luminance.

As shown in **Figure 4.12b**, the maximum luminance and efficiency of these perovskite containing OLEDs reach over 20000 cd/m^2 and 20 cd/A, respectively. Interestingly, the maximum luminance of the PUE-LEDs was comparable, and the efficiency was even higher (31 cd/A in the case of the 0.05 nm thick UEML) than that of OLED with co-evaporated light emitting layer. Hence, this confirms that the PUE-LEDs are indeed a very promising electroluminescent device type.

4. 3. Conclusions

In this chapter, an attempt was made to demonstrate cost-effective phosphorescent OLEDs consist of evaporated perovskite hole transport layers. It was demonstrated that the photoluminescence of the inorganic $CsPbCl_3$ perovskite is improved by adding an interface layer of CsCl. This passivation layer also improves the OLED performance. A perovskite layer of at least 200 nm is needed to decrease the leakage current of the diodes. Using very thin light-emitting layers consisting of only the emitter molecule we demonstrated for the first time PUE-LEDs that exhibited high luminescence and efficiency values. When comparing the PUE-LED performance with a perovskite-based OLEDs that uses classical host-guest light-emitting layers we observe similar performances. The PUE-LEDs are slightly better and have a less complex preparation methods, which is beneficial for large scale production.

Chapter 5.
General Conclusion

In last decade, metal halide perovskites have attracted huge attention and a remarkable progress has been accomplished owing to efforts from researchers all over the world. In photovoltaic applications, perovskites with narrow band gap could realize solar cells as efficient as silicon based solar cells since perovskites show high charge carrier mobility and especially lead iodide and tin iodide perovskites possess high absorption coefficient in visible region. In case of light-emitting applications, the emission peak can be tuned by halide anion exchange and the width of emission is the narrowest among the emerging materials, organics emitters and inorganic quantum dots. In addition, the low material-cost and processing-cost make this material group attractive, hence, it might be a game changer in semiconductor market. Since the use of display system is getting ubiquitously, the development of cost-effective light emitting system is indispensable.

In chapter 2, a down-conversion light emitter is realized by lead bromide precursor solute and polyethylene glycol solvent by one-pot synthesis. This solution shows 23 % of photoluminescent quantum yield with emission peak at 610 nm, originates from $PbBr_3^-$, which is superior to reported value (0.5 % with acetonitrile). The emission colour is also tunable by introducing alkylammonium halides in dimethyl sulfoxide as solid metal halide perovskites. For instance, introducing 2-folds of tetrabutylammonium bromide results in peak shift to 560 nm, originates from $PbBr_4^{2-}$, (yellowish green), and all chloride solution of tetrabutylammonium chloride has emission peak at 510 nm (bluish green). To achieve white emissions for lighting, equimolecular amount of lead bromide and tetrabutylammonium bromide are dissolved for yellow emission which could be completed with a blue emissive dye, 4,4'-Bis(9-ethyl-3-carbazovinylene)-1,1'-biphenyl (BCzVBi). Corelated colour temperature of two solutions satisfy CIE D55 (5503K, Mid-morning / Mid-afternoon daylight) and CIE D75 (7504K, North sky daylight), respectively. These values are proper to the desktop publishing industry (monitor's colour temperature).

In chapter 3, light-emitting electrochemical cells are developed with a 3D metal halide perovskite material, $CsPbBr_3$, mixed with polyethylene oxide. The perovskite-polymer precursors are dissolved in dimethyl sulfoxide

and spin-coated on a ITO/PEDOT:PSS coated substrate that functions as the anode. The crystallinity of the $CsPbBr_3$:PEO light-emitting layer is enhanced via a vacuum treatment and thermal annealing of the slightly wet coated film. After annealing a metal cathode is deposited on the dried light-emitting layer without inserting an electron transport material. The resulting devices showed good luminance (2200 cd/m^2) and a rather fast turn-on time of 5 min when driven with a constant current (100 A/m^2). This light emitting device consists of cost-effective ionic metal halide perovskite material in polymer electrolyte. Besides the simple structure of this device makes it suitable for low-cost fabrication. Using these perovskite-based LECs a fundamental study on anion interdiffusion at perovskite heterojunction interfaces was performed. For that heterostructures were prepared involving the $CsPbBr_3$:PEO layer and vacuum deposited 3D $CsPbCl_3$ perovskite and 0D Cs_4PbCl_6 perovskite-related material. In the $CsPbBr_3$-$CsPbCl_3$ heterojunctions the emission spectrum shifts, and it emits a cyan-blue colour which is evidence of instant halide mixing taking place in the as-deposited films. On the other hand, there was no significant halide anion intermixing in the $CsPbBr_3$-Cs_4PbCl_6 heterojunction. Hence, it is confirmed that 0D inorganic caesium lead halide compounds only marginally donate halide anions to the adjacent $CsPbBr_3$ layer. Exploiting this point, light-emitting electrochemical cells employing 0D Cs_4PbCl_6 layers are characterized. By sandwiching the $CsPbBr_3$:PEO light-emitting layer in0D Cs_4PbCl_6 layers a two-fold increase in device stability was obtained. This improvement in device operation might arise from the limited and balanced ion movement of the Cs_4PbCl_6 buffer layers.

In chapter 4, a co-evaporated halide perovskite material, $CsPbCl_3$, is used as a hole transport layer in organic light emitting diodes. First, the perovskite film is passivated by depositing a thin film of the precursor salt CsCl at the interfaces. This passivation method increased the photoluminescent of the $CsPbCl_3$ layer 3 times. This modified perovskite hole transport layer is used in phosphorescent organic light emitting diodes comprising ultrathin (sub-nanometre) undoped iridium complex. I refer to these electroluminescent devices as PUE-LEDs (perovskite-ultrathin emitter LEDs). Employing ultrathin emissive layer can reduce the material-cost by almost 70 %. In addition, this makes the fabrication process more facile. However, since such very thin devices are prone to have high leakage currents, I inserted thick perovskite layers to overcome

this issue. As a result, 200 nm thick perovskite hole transport layer with interface passivation and a light-emitting layer of nominally 0.05 nm reach an efficiency of 31 cd/A whereas the efficiency of a co-evaporated counterpart is 20 cd/A.

The work presented in this thesis, present several strategies that can help to decrease the complexity of LED and as such lead to more economic devices. It is shown that metal halide perovskites are promising candidates as down-conversion light emitters, ionic material in light-emitting electrochemical cells, and charge transport material in light emitting diodes. However, the perovskites used in this thesis contain toxic lead, which implies that rigorous encapsulation is needed to prevent leaching of the toxic salts. Additionally, an end-of-life reuse protocol must be put in place. Such a re-use protocol is mandatory for an ever increasing amount of devices. In this light, simplifications as proposed in this thesis by reducing the number of layers in LEDs can help to make the reuse of these materials more sustainable. There are promising developments related to lead-free perovskites which may also be studied in the same way as I did with the lead containing perovskites in this thesis. This can assist in the realization of cost-effective light-emitters and spreading perovskite-based display system all over the world in this Internet-of-Things (IoT) era.

Chapter 6.
Resumen en Castellano

1. Introducción

La sociedad moderna intercambia más del 80% de la información a través de señales visuales y, con el auge del Internet de las Cosas (IoT, por sus siglas en inglés), se prevé que los dispositivos electrónicos vayan a ofrecer una cantidad significativa de información de forma ubicua.[1] Teniendo en cuenta que las pantallas son indispensable para visualizar y procesar una gran cantidad de información, es necesaria una reducción de los costes asociados a los materiales y procesos de fabricación de pantallas. Los diodos emisores de luz (LEDs, por sus siglas en inglés) se utilizan ampliamente como fuentes de luz alternativas a las bombillas incandescentes y los tubos fluorescentes. El mecanismo de funcionamiento de los LEDs se basa en la aplicación de una corriente eléctrica al dispositivo, que genera una emisión de fotones con una energía correspondiente a la banda prohibida del semiconductor elegido. Las ventajas de los LEDs respecto a las fuentes de luz tradicionales son su mayor eficiencia, su mayor vida útil y su tamaño más compacto.[2] Los primeros LEDs comerciales, y de uso aún extendido, se basan en semiconductores inorgánicos, fabricados mediante procesos a alta temperatura y mediante técnicas complejas de deposición. Estos LEDs inorgánicos son fuentes de luz puntuales y rígidas, lo cual dificulta su aplicación en pantallas flexibles o paneles luminiscentes ultrafinos. Más recientemente, se han desarrollado y comercializado LEDs basados en semiconductores orgánicos (OLEDs), que tienen la particularidad de poder utilizarse como superficies emisoras de luz. A pesar de utilizar materiales orgánicos procesables a partir de disolución, los OLEDs comerciales se depositan también mediante técnicas de sublimación en vacío, por lo que el coste de preparación sigue siendo elevado. Los QLEDs son otra alternativa que se basa en el uso de puntos cuánticos como emisores. Estos también pueden procesarse mediante técnicas simples de disolución, pero no son dispositivos electroluminiscentes ya que los puntos cuánticos solo se usan como materiales luminiscentes que tienen que ser excitados con LEDs inorgánicos tradicionales. Entre los criterios de calidad para una pantalla, la anchura a media altura (FWHM, del inglés "*full width at half máximum*") del espectro de emisión es un factor importante ya que determina la gama de colores. Por ejemplo, en el rango de emisión verde, los OLEDs emiten luz con FWHM de 40 nm y

los QLEDs lo hacen con 30 nm. Recientemente, investigadores han desarrollado LEDs basados en perovskitas de haluro de plomo que pueden alcanzar un FHWM de 20 nm.[3] Tras las primeras publicaciones pioneras sobre LEDs basados en puntos cuánticos y capas policristalinas de perovskita en 2014, los LEDs de perovskita (PeLEDs) están siendo ampliamente investigados a nivel global.[4,5]

En 1839, el mineral $CaTiO_3$ fue descubierto en los Montes Urales de Rusia por Gustav Rose y lleva el nombre del mineralogista ruso Lev Perovski. La estructura cristalina de la perovskita fue descrita por primera vez por Victor Goldschmidt en 1926 y publicada en 1945 a partir de datos de difracción de rayos-X en $BaTiO_3$ por Helen Dick Megaw.[6,7] Los óxidos de perovskita tienen una estructura cristalina cúbica o tetragonal que puede describirse por la formula simplificada ABO_3, correspondiente a una red 3D de octaedros BO_6 con el catión A más pequeño ocupando el centro de la celda unitaria y balanceando la carga. La estabilidad de la estructura de perovskita se puede predecir mediante simples consideraciones geométricas, utilizando el factor de tolerancia t, definido por Goldschmidt como se describe a continuación.

$$t = \frac{(R_A + R_O)}{\sqrt{2}(R_B + R_O)}$$

Por ejemplo, con $BaTiO_3$, el radio de Ba, Ti y O podría indicarse como R_A, R_B y R_O respectivamente (ABO_3). Para las perovskitas estables, el factor de tolerancia de Goldschmidt cae en el rango $0.8 \leq t \leq 1.8$ En las perovskitas de halogenuros metálicos, hay aniones de haluro (X = Cl^-, Br^-, I^-) en lugar de oxígeno, por lo que la estructura se reporta como ABX_3. El sitio B está ocupado por un metal divalente (típicamente Pb^{2+} o Sn^{2+}), mientras que A es un catión monovalente del primer o segundo grupo, o un catión orgánico pequeño.[3]

En el caso de las perovskitas de haluros metálicos existen diversos tipos con baja dimensionalidad que pueden clasificarse en dos tipos: i) perovskitas de baja dimensionalidad morfológica, y ii) materiales moleculares de baja dimensionalidad relacionados con la perovskita,

como se muestra en la Figura 1.2.9. Las perovskitas de baja dimensionalidad tienen una fórmula química simplificada de ABX_3, como las perovskitas 3D, pero tienen distintas formas y grosores. Por ejemplo, los puntos cuánticos de perovskita son materiales nanoestructurados con un tamaño inferior al radio de Bohr de los excitones y se definen como perovskitas 0D, mientras que los materiales de tipo 1D o 2D son nanohilos y nanoláminas, respectivamente. Por otra parte, los materiales moleculares de baja dimensionalidad relacionados con la perovskita tienen estructuras cristalinas diferentes de las perovskitas 3D, pero siguen conteniendo las unidades octaédricas de haluro metálico BX_6^{4-}. En 1994, el grupo de Shogo Saito de la Universidad de Kyushu (Japón) usó por primera vez una capa fina de perovskita de haluro metálico 2D en un LED que emitía luz con alta intensidad (más de 10.000 cd/m^2), aunque solo a la temperatura del nitrógeno líquido.[10] Después de este primer ejemplo, los dispositivos optoelectrónicos basados en perovskita no se investigaron durante un tiempo. Fue en 2009, con los primeros ensayos den los que se incorporaba $CH_3NH_3PbI_3$ en células solares sensibilizadas por colorantes realizados por el grupo de Tsutomu Miyasaka en la Universidad de Toin de Yokohama (Japón), cuando empezó el auge actual de las perovskitas. Inicialmente las células solares mostraron una eficiencia de conversión de energía del 3.8%, un valor moderado pero prometedor para un primer ensayo (Figura 1.3).[12] En solamente 3 años los grupos de investigación de la Universidad de Oxford (Reino Unido) y de la Universidad de Sungkyunkwan (República de Corea), dirigidos por Henry Snaith y Nam Gyu Park, respectivamente, desarrollaron células solares de estado sólido con una alta eficiencia de alrededor del 10%.[13,14] En la actualidad, las células solares de perovskita de estado sólido están muy estudiadas por parte de investigadores de todo el mundo y las células solares más eficientes ostentan eficiencias de conversión de energía extremadamente altas, superiores al 25 %, tras tan sólo una década de desarrollo.[15,16] Esta notable mejora de la tecnología fotovoltaica basada en la perovskita de haluro metálico despertó el interés del uso de estos materiales como emisores de luz. En las dos primeras publicaciones de 2014 sobre PeLEDs de películas policristalinas y puntos cuánticos de perovskita, se demostró que estos materiales podían funcionar a temperatura ambiente.[4,5] Para aplicaciones en LEDs las propiedades luminiscentes de las perovskitas pueden modularse fácilmente mediante el intercambio de los aniones haluros, y es posible

obtener una eficiencia cuántica de fotoluminiscencia (PLQY, del inglés "*photoluminescence quantum yield*") elevada mediante la pasivación de defectos, lo que las hace aún más atractivas para esta aplicación.[2,17,18] De acuerdo con las recomendaciones de la ITU y la CIE, los tres picos de emisión primarios para las pantallas y para la colorimetría se centran en 630 nm (rojo), 532 nm (verde) y 467 nm (azul). En el caso de la perovskita de haluro de plomo, la emisión verde sólo puede obtenerse con el anión bromuro, mientras que el rojo y el azul pueden conseguirse con mezclas de yoduro/bromuro y bromuro/cloruro, respectivamente.[19]

La eficiencia de conversión de carga electrónica en luz se describe mediante la eficiencia cuántica externa (EQE, del inglés "*external quantum efficiency*") definida como:[3]

$$EQE\ (\%) = \frac{Fotones\ emitidos}{Portadores\ de\ carga\ inyectados\ en\ la\ película\ emisora} = \eta_{inj} \times \eta_{rad} \times \eta_{out}$$

La eficiencia de inyección (η_{inj}) describe el número de portadores de carga que pasan por los electrodos del dispositivo y que son inyectados en la capa emisora de luz. La eficiencia de recombinación radiativa (η_{rad}) se refiere a la relación entre las cargas (electrones y huecos) que se recombinan resultando en emisión de fotones y el total de las cargas generadas en el dispositivo. Por último, la eficiencia de "*outcoupling*" de la luz (η_{out}) es la cantidad de luz generada en la capa activa que es capaz de salir del dispositivo, y se ve limitada por las pérdidas ópticas debidas a múltiples reflexiones internas, consecuencia de la diferencia de índices de refracción entre las diferentes capas del dispositivo, el sustrato y el aire.

Para describir el rendimiento de los LEDs existen varias figuras de mérito, siendo las más representativas la luminancia, la densidad de corriente y la eficiencia de conversión de corriente:

Luminancia (L): intensidad de luz emitida (expresada en candelas, cd) por unidad de superficie del dispositivo, teniendo en cuenta la curva de sensibilidad del ojo humano. Se expresa en cd/m^2 en el Sistema Internacional de Unidades.

Densidad de corriente (J): Corresponde a la corriente eléctrica por

unidad de superficie del dispositivo. Sus unidades son A/m^2.

Eficiencia de la corriente (CE): Es la relación entre la luminancia y la densidad de corriente correspondiente. Se expresa en cd/A.

En un trabajo reciente del profesor Tae-Woo Lee y sus colaboradores, PeLEDs basados en nanocristales de bromuro de plomo y formamidinio modificados con guanidinio, alcanzaron una CE muy elevada, de 108 cd/A, y una EQE del 23.4%, gracias a la pasivación de los defectos mediante 1,3,5-tris(bromometil)-2,4,6-trietilbenceno. Los mismos dispositivos han podido mejorarse hasta obtener una CE de 205 cd/A y una EQE del 45.5%, mediante el uso de lentes hemisféricas que ayuda a mejorar la eficiencia de *outcoupling*.[18]

Los pares electrón-hueco generados (por excitación óptica o eléctrica) tienden a volver al equilibrio mediante mecanismos de perdida de energía llamados de recombinación, donde un electrón pierde energía y decae desde la banda de conducción a la banda de valencia. En este proceso el electrón aniquila el hueco de la banda de valencia. Existen varios procesos de recombinación importantes para el funcionamiento y la optimización de los dispositivos optoelectrónicos, comúnmente denominados recombinación Shockley-Read-Hall (SRH), recombinación Auger y recombinación radiativa.[34,35]

i. Recombinación Shockley-Read-Hall

La recombinación SRH es una recombinación no radiativa (sin emisión de fotones), originada por defectos en el semiconductor que actúan como centros de recombinación. Los defectos pueden ser estructurales o impurezas del semiconductor, que dan lugar a niveles electrónicos permitidos en la banda prohibida. Estos defectos son capaces de atrapar de manera eficiente un electrón o un hueco, según su cercanía en energía con la banda de conducción o valencia, respectivamente. En el caso de un electrón excitado en la banda de conducción, puede perder energía y ocupar un nivel de defecto o trampa. Desde allí, decaerá a la banda de valencia aniquilando un hueco. En las dos transiciones, la energía del electrón se disipa mediante vibraciones estructurales del material (fonones). Una alta densidad de defectos conlleva un tiempo de vida corto de los portadores de carga, y un bajo rendimiento cuántico de

fotoluminiscencia.

ii. Recombinación radiativa

La recombinación radiativa consiste en la recombinación directa de un electrón de la banda de conducción con un hueco de la banda de valencia, donde la diferencia de energía entre los dos estados se libera en forma de un fotón. Este es el proceso básico de funcionamiento de los LEDs.

iii. Recombinación Auger

Este proceso de recombinación tampoco conlleva la emisión de fotones, y tiene lugar típicamente a elevada densidad de carga. Un electrón excitado en la banda de conducción recombina con un hueco en la banda de valencia, y la energía se transfiere a otro portador (electrón o hueco) dentro de su propia banda. Este electrón (o hueco) cede el exceso de energía y momento mediante fonones, con relajación térmica.

Para contribuir a la tecnología de pantallas e iluminación de próxima generación, es esencial desarrollar LEDs con materiales y procesos de preparación con un coste económico reducido. Los resultados recogidos en esta tesis pretenden contribuir al progreso de la optoelectrónica mediante el desarrollo de perovskitas para dispositivos emisores de luz eficientes y de bajo coste. En los diferentes capítulos de esta tesis se describen y estudian varias aplicaciones de perovskitas en diferentes morfologías o estructuras para fotoluminiscencia y electroluminiscencia. El capítulo 2 se centra en la obtención de soluciones de precursores de perovskita estables y luminiscentes para aplicaciones en fósforos luminescentes para LEDs. El precursor más común de perovskitas para aplicación en LEDs, el $PbBr_2$, es soluble en PEG en fase líquida y forma complejos con fotoluminiscencia (PL) muy eficiente. Con estos dos materiales simples y baratos, se consigue un compuesto luminiscente utilizando una síntesis de un solo paso. La emisión puede cambiarse a verde introduciendo bromuros de alquilamonio, y hasta el azul si se hacen reaccionar con $PbCl_2$. En el capítulo 3, se presenta un dispositivo de tipo LEC basado en un material compuesto de perovskita 3D ($CsPbBr_3$-PEO) procesado desde disolución, donde se omiten además las capas de transporte de carga, lo que reduce el coste global de fabricación. Además,

se coevaporan CsCl y $PbCl_2$ para formar la perovskita 3D $CsPbCl_3$ y el compuesto 0D Cs_4PbCl_6. Con estos materiales, se han estudiado las características de difusión de los aniones haluro en función de la dimensionalidad de los compuestos. Finalmente, en el capítulo 4, se fabrican OLEDs que incluyen capas de transporte de huecos de perovskita de tipo $CsPbCl_3$. En estos OLEDs, los complejos de iridio emisores se evaporan sin matriz en capas extrafinas (de un grosor inferior al nanómetro), reduciendo en gran medida el consumo de material y simplificando el procesado. El uso de capas muy finas reduce la distancia entre el ánodo y el cátodo, aumentando la probabilidad de cortos entre los electrodos. Por ello, se optimiza el grosor de las capas de transporte de huecos de perovskita, disminuyendo la corriente de fuga y obteniendo altas eficiencias de electroluminiscencia.

2. Fósforos luminescentes basados en complejos de $PbBr_2$ luminiscente

2.1. Introducción

Como fue reportado por Dutta y Perkovic en 2002, el $PbBr_2$ disuelto en acetonitrilo (ACN) muestra una señal de PL con un máximo a 610 nm, y un desplazamiento al azul tras la adición de TBABr.[37] A pesar de la baja eficiencia de fotoluminiscencia (PLQY de ~0,5%), este compuesto se ha aplicado a sensores en disolución, y se han investigado las propiedades fotofísicas de los haluros de plomo en varios medios.[38] Sin embargo, la literatura sobre estos materiales es muy limitada y su fotoluminiscencia es baja, como se ha indicado. En este capítulo investigamos específicamente la luminiscencia del $PbBr_2$ en fase líquida en PEGs, que es un polímero muy común y barato en diversas aplicaciones en la industria.[39] Se ha obtenido PLQYs por encima del 20% con una síntesis muy simple. Este hito por si solo ya es un resultado muy prometedor para aplicaciones en sistemas emisores si los comparamos, por ejemplo, con los puntos cuánticos. En el caso de los puntos cuánticos coloidales, normalmente estos se sintetizan, se centrifugan y se vuelven a dispersar en otros disolventes en un proceso complicado que aumenta el coste del producto final. En este capítulo se presentan materiales de bajo coste para sintetizar compuestos altamente fotoluminiscentes de manera simple.

2.2. Metodología

Para la síntesis, se han seleccionado glicoles de polietileno comerciales (cuya estructura molecular se representa en la Figura 2.1.a) con diferentes pesos moleculares, para disolver $PbBr_2$ a la concentración de 62.5 mM. Después de agitar durante una noche a temperatura ambiente, las muestras están listas para ser utilizadas y caracterizadas. Para modificar el color de emisión de la disolución PEG:$PbBr_2$, se introducen bromuros de alquilamonio, TBABr, MABr y BABr (la estructura molecular se representa en la figura 2.1.b-d), previamente disueltos en DMSO. Esta reacción se produce inmediatamente como se muestra en la Figura 2.2. Para investigar las propiedades de luminiscencia de las disoluciones se realizan varias mediciones. Los instrumentos usados se presentan en la Figura 2.3. Las disoluciones se transfieren a una cubeta para medir el espectro de excitación, los espectros estáticos del PL y el tiempo de decaimiento de la PL. Para ello se usa un fluorimetro Hamamatsu Quantaurus-Tau, Edinburgh FLS1000 con lámpara de Xe µF2 y vis-PMT 980 TCSPC). Además, la PLQY de todas las disoluciones se ha medido en una esfera integradora (Hamamatsu C9920-02 con un detector óptico Hamamatsu PMA-11) mediante excitación con una lámpara de xenón y monocromador. Durante las mediciones con esfera integradora, también se han obtenido las coordenadas CIE.

2.3. Resultados y conclusiones

Al disolver $PbBr_2$ en PEG, fue posible obtener un compuesto luminiscente de color naranja con un precio y con materiales muy baratos. Dado que la concentración de esta solución es de tan solo 62.5 mM, el coste total del compuesto se aproxima al precio del PEG, lo que convierte a este sistema luminiscente en un candidato muy interesante también desde un punto de vista económico. El pico de emisión se ajustó con éxito mediante la reacción con una disolución de bromuro de alquilamonio. El pico de PL se desplazó de 610 nm a 560 nm, y este proceso fue más eficiente cuanto más grandes fueron las moléculas de alquilamonio. En particular, con sales de tetrabutilamonio se obtuvo un desplazamiento completo del pico de PL con solo añadirlas en una concentración del doble con respecto al $PbBr_2$. A menor concentración, la disolución emitió en el amarillo con un espectro de PL ancho. Gracias a esta propiedad, se ha podido obtener un compuesto emisor blanco mediante introducción de una pequeña cantidad de colorante orgánico azul, el BCzVBi. El trabajo que se

presenta en este capítulo presenta un método para obtener un fósforo altamente luminiscente y barato.[43] Además, este sistema puede usarse en otras aplicaciones, como en metalogeles multiestímulo y en centelladores para la detección de radiación ionizante con alta resolución espacial.[44,46]

3. Células electroquímicas emisoras de luz con perovskita y heterouniones de perovskita

3.1. Introducción

En 1995, el profesor Alan J. Heeger y sus colaboradores de la Universidad de California en Santa Bárbara reportaron por primera vez células electroquímicas emisoras de luz (LECs, del inglés "*light-emitting electrochemical cells*") también denominadas LEDs de una sola capa.[47] En ese primer trabajo, se colocó entre dos electrodos una capa compuesta por el polímero semiconductor MEH-PPV, un polímero polar (PEO) y la sal $LiCF_3SO_3$. Con esta estructura simple, se obtuvo un voltaje de encendido de tan solo 2.1 V, que es comparable a lo esperando cuando se usan capas adicionales de inyección como el LiF o metales con baja función de trabajo como el Ca y el Ba. El mecanismo de funcionamiento de los LECs se ha descrito generalmente mediante los modelos ED y ECD (Figura 3.1). Ambos modelos coinciden en que la barrera de inyección de electrones y huecos se reduce por la separación de los iones en la capa emisora de luz al aplicar un voltaje. El modelo ED asume que la acumulación de iones conduce a la formación de una doble capa en la interfaz con los electrodos, que da lugar a un campo eléctrico muy intenso que promueve la inyección de carga desde los mismos. En el volumen del material, los aniones y cationes siguen ligados, y la emisión de luz se produce desde la región intrínseca (libre de campo eléctrico) en el volumen del dispositivo. El modelo ECD, en cambio, supone que la acumulación de iones en la interfaz con el ánodo y el cátodo resulta en la formación de regiones dopadas tipo p y n, respectivamente, altamente conductoras. Las regiones dopadas se ensanchan con el tiempo debido al voltaje aplicado, hasta que se forma una unión p-i-n (i = intrínseca, no dopada) entre ellas. El potencial aplicado cae en la región intrínseca, favoreciendo la recombinación electrón-hueco y la emisión de luz. Hasta ahora, los LECs se han

investigado principalmente mediante el uso de polímeros, moléculas pequeñas y complejos iónicos de metales de transición.[49] En 2015, el grupo del profesor Zhibin Yu de la Universidad Estatal de Floria, demostró LECs basados en compuestos perovskita:PEO usando como electrodos nanohilos de Ag y una aleación de indio-galio (In:Ga), una estructura simple muy parecida a la de los LECs.[50–52] Es importante destacar que este dispositivo basado en perovskita:PEO no requiere ningún aditivo iónico para su funcionamiento. Esto se debe probablemente al carácter iónico de la perovskita y podría suponer una nueva estrategia para simplificar el proceso de fabricación de los dispositivos emisores de luz. Posteriormente, el profesor Jason D. Slinker y el profesor Anvar A. Zakhidov, de la Universidad de Texas en Dallas, desarrollaron LECs utilizando una capa activa de tipo $CsPbBr_3$:$LiPF_6$:PEO, una composición más similar a la de los LECs poliméricos.[53] La introducción del $LiPF_6$ pasiva los defectos del $CsPbBr_3$ y ayuda a la inyección de carga, mejorando el rendimiento general del dispositivo. Sin embargo, siguieron utilizando un electrodo de In:Ga líquido, lo que complica una definición precisa del área activa y también limita las aplicaciones del dispositivo. En sus siguientes trabajos, este mismo grupo depositó PEDOT:PSS sobre ITO para mejorar la morfología de la capa activa e introdujo un electrodo sólido LiF/Al estable al aire.[54] El uso de la capa de inyección de electrones de LiF no es propio de un LEC, pero este dispositivo alcanzó una alta luminancia de más de 3000 cd/m^2. Sin embargo, como se muestra en la Figura 3.2, la optimización de la concentración de sal $LiPF_6$ es crucial. Una alta concentración de $LiPF_6$ (2 % y 5 % en peso) conlleva una mayor resistencia eléctrica del dispositivo, probablemente debido a reacciones electroquímicas que ocurren en la capa activa. Además, cabe destacar que, para alcanzar la máxima luminancia, este dispositivo necesita un tiempo de más de 10 horas bajo voltaje. En este capítulo, el objetivo es fabricar LECs con una respuesta rápida basados en perovskita de haluro metálico. Además, dado que el movimiento iónico de la perovskita en el electrolito PEO es un tema novedoso, también se investiga el comportamiento de difusión de iones en la interfaz perovskita-perovskita mediante la fabricación de heterouniones. También se analizan las prestaciones de los dispositivos de perovskita y heterouniones de perovskita fabricados.

3.2. Métodos

La figura 3.3 resume todo el proceso de fabricación de los dispositivos. Se fabrican sobre sustratos comerciales de vidrio recubiertos con ITO, de un tamaño de 3 x 3 cm^2. Las diferentes capas se depositan sobre toda la superficie dejando libre los contactos en los bordes del sustrato. Por ello, en la evaporación en vacío se utiliza una máscara de sombra mientras que en los procesos desde solución se limpian los bordes con disolventes. En primer lugar, el sustrato se limpia con detergente en baño de ultrasonidos. Tras este proceso, se aclara en baño de ultrasonidos primero con agua y luego con isopropanol. El sustrato limpio se trata con ozono en una lámpara UV para activar la superficie y se recubre con PEDOT:PSS en dispersión acuosa (Clevios™ P VP AI 4083; filtrado con filtros de PVDF de 0.45 µm de tamaño de poro) mediante spin-coating (Chemat Technology KW-4ª, Figura 3.4) en aire y se trata térmicamente para eliminar el disolvente residual. A continuación, el sustrato se transfiere a una caja de guantes con atmosfera inerte de N_2. Antes de depositar la perovskita, hay que preparar la disolución de perovskita:PEO y agitarla durante la noche con un agitador magnético a 70 °C. Esta disolución se enfría durante 30 minutos antes de realizar el spin-coating. Luego, las películas de perovskita:PEO se someten a un tratamiento rápido al vacío y a un proceso térmico, tal y como se indica en los trabajos anteriores de Jason D. Slinker que se mencionan en la introducción.[53,54] La proporción en peso de la perovskita y el PEO es de 1.5:1 y no se usan aditivos iónicos. Para los experimentos de interdifusión de aniones, el cloruro de plomo y cesio se deposita por coevaporación en una cámara de vacío (Figura 3.5.; hecha a medida por Thermal Vacuum Projects y con controladores de Cressington Vacuum System) utilizando una presión base inferior a 2 x 10^{-6} mbar. Los dispositivos se terminan con la deposición de electrodos de Ag o Ba/Ag en otro evaporador térmico, utilizando otra máscara de sombra que define el área activa, de 6 mm^2. Para caracterizar las propiedades ópticas, la absorción y el PL de las películas delgadas de perovskita se usa un montaje como el ilustrado en la Figura 3.6. La luz llega a la película a través de una fibra óptica y la señal resultante se lleva al espectrómetro (Avantes, Avaspec2048) con otra fibra óptica. Para las medidas de absorción, se usa una fuente de luz blanca de Xenon, mientras que para las medidas de PL se irradia con luz láser a 375 nm. Para obtener una señal de PL apreciable, la intensidad del láser debe ser lo suficientemente alta (100-300 mW/cm^2). Para no saturar el detector, se usa un filtro de paso alto a 400 nm. Después de la

fabricación del dispositivo, se introduce en un porta muestra para las medidas de J-V-L. Se conectan dos controladores Keithley (Keithley 2400 Source-Meter y un fotodiodo acoplado a un picómetro Keithley 6485, utilizando una cámara Minolta LS100 para calibrar la fotocorriente). La caracterización se lleva a cabo en una caja de guantes con atmosfera de nitrógeno.

3.3. Resultados y conclusiones

En este capítulo se presenta un dispositivo electroluminiscente con una estructura simple y sin aditivos iónicos, ya que su funcionamiento se basa en las propiedades iónicas de las perovskitas de haluro metálico. El dispositivo con estructura ITO/PEDOT:PSS/$CsPbBr_3$:PEO/Ag se ajusta más a la definición de LEC en comparación con otros reportados en la literatura que emplean capas de inyección de carga como el LiF.[54,79–81] Además se ha llevado a cabo un estudio sobre la difusión de aniones haluro entre perovskitas 3D coevaporadas y comparándolas con estructuras similares de tipo 0D, como el Cs_4PbCl_6. Se ha confirmado que el material 0D se caracteriza por una menor difusión de aniones haluro en comparación con la perovskita 3D. Además, el uso de capas finas de Cs_4PbCl_6 0D en la interfaz entre los electrodos y la perovskita emisora, aumenta el rendimiento del dispositivo cuando se aplica una corriente constante (en 100 A/m^2). Las técnicas de fabricación utilizada en este estudio sobre difusión de aniones haluro son aplicables a nivel industrial, pero aumentan la complejidad y así el coste de preparación de los dispositivos. Sin embargo, en un trabajo reciente se han demostrado LECs basados en $CsPbBr_3$:PEO que utilizan capas de nanocristales de Cs_4PbBr_6 0D y presentan una alta luminancia y eficiencia.[81] Por lo tanto, el trabajo presentado en este capítulo puede seguir ofreciendo algunas soluciones para el desarrollo de LECs basados en perovskita de alta eficiencia mediante la incorporación de materiales 0D de tipo Cs_4PbX_6.

4. Diodos orgánicos fosforescentes emisores de luz con capas de transporte de huecos de perovskita inorgánica

4.1. Introducción

La tecnología OLED es una de las más puntera en el mercado de las pantallas y de la iluminación. Los OLEDs pueden utilizarse como

dispositivos electroluminiscente independientes (que emiten en el rojo, verde y azul), o también como retroiluminación de luz azul en pantallas basadas en puntos cuánticos que actúan como fósforos luminiscentes. La electroluminiscencia en semiconductores orgánicos se observó por primera vez en 1965 en cristales de antraceno en los laboratorios del Consejo Nacional de Investigación de Canadá.[66] Helfrich y Schneider obtuvieron y caracterizaron un monocristal de un milímetro de grosor y 1 cm de diámetro. A continuación, conectaron dos tubos de vidrio rellenos de una aleación liquida a la superficie del cristal, y aplicando un potencial eléctrico observaron electroluminiscencia. Sin embargo, este descubrimiento no condujo a ninguna aplicación real debido a la tensión de trabajo extremadamente alta, causada por el grosor del cristal y la alta resistencia de los contactos eléctricos. 22 años después, Tang y Van Slyke de Kodak llevaron a cabo unos experimentos que luego supondrían un gran avance hacia el desarrollo de los OLEDs. Desarrollaron dispositivos de doble capa que consistían ne una unión p-n entre moléculas orgánicas depositadas por evaporación térmica.[67] En particular, depositaron capas de 75 nm de arilamina y de 60 nm de aluminio tris(8-hidroxiquinolinato) (Alq_3) sobre ITO, terminando los dispositivos con una aleación de Mg:Ag. Gracias al uso de capas finas, al eficiente transporte de huecos en la arilamina y al uso de un cátodo con baja función de trabajo (que favorece la inyección de electrones), obtuvieron electroluminiscencia con luminancia de más 1000 cd/m^2 a voltajes inferiores a los 10 V. Posteriormente, el Prof. Richard H. Friend y sus colaboradores demostraron el primer OLED basado en polímeros conjugados (Figura 4.3).[68] La ventaja de estos dispositivos es que los polímeros pueden procesarse en capas delgadas mediante técnica de disolución, con lo que podrían aplicarse a grandes superficies a un coste bajo. La eficacia de estos primeros OLEDs era limitada debido a que usaban emisores orgánicos fluorescentes. Los estados excitados singlete que resultan en fluorescencia representan solo una pequeña fracción (alrededor del 25 %, según la regla de selección de espín) de la población total de estados excitados, siendo el resto los estados triplete, alrededor del 75 %. Como se ilustra en la figura 4.4, la fluorescencia se produce por la relajación desde el primer estado excitado al estado fundamental (S_1 a S_0). Mientras tanto, el estado triplete T_1 se poblará desde el estado excitado por cruce entre sistemas (ISC, de sus siglas en inglés), una transición no radiativa entre dos estados electrónicos con diferente

multiplicidad de espín. Debido a la baja constante de recombinación radiativa de la transición entre T_1 y S_0, la relajación del estado T_1 se produce de forma no radiativa (mediante vibraciones moleculares) a temperatura ambiente. En este proceso, se pierde el 75 % de los excitones del triplete. Sin embargo, los emisores fosforescentes poseen un ion metálico pesado central que induce un fuerte acoplamiento espín-órbita. En este caso, el ISC al estado más bajo en energía T_1 ocurre de manera muy eficiente y la constante de recombinación radiativa de T_1 a S_0 puede llegar a cercana al 100%. Con esta estrategia se podrían convertir todos los excitones de singlete a triplete, y estos últimos relajarse mediante fosforescencia, obteniendo una emisión muy eficiente a temperatura ambiente. El profesor Stephen R. Forrest y sus colaboradores de la Universidad de Princeton, demostraron por primera vez la transferencia electrónica desde estados singlete a estados triplete en OLEDs fosforescentes. Para ello utilizaron un semiconductor orgánico fluorescente dopado con el colorante fosforescente PtOEP, obteniendo eficiencias cuánticas internas (IQEs) de hasta el 23%.[69] Posteriormente, el mismo equipo de investigación llevó la IQE hasta casi el 100%, utilizando un complejo de iridio, $Ir(ppy)_2acac$ (que tiene un PLQY cercano a 1), diluyéndolo en una matriz orgánica para evitar el TTA.[70] 18 años después, el primer autor de ese trabajo, el Prof. Chihaya Adachi, ha desarrollado OLEDs usando capas muy gruesas (> 1 μm) de perovskita de haluro metálico para el transporte de huecos y electrones. El uso de capas gruesas a ambos lados de la capa emisora disminuye la probabilidad de cortos electrónicos, y hace que el dispositivo se pueda fabricar en condiciones menos estrictas, en comparación a los OLEDs tradicionales.[72,73] Los autores investigaron OLEDs con una capa emisora fluorescente de Alq_3 y capas de transporte de perovskita $CH_3NH_3PbCl_3$, así como OLEDs fosforescentes más eficientes. En este trabajo se consiguió una elevada EQE, superior al 20%, que podría incluso mejorarse mediante el uso de sustratos que mejoren la eficiencia de *outcoupling*. Sin embargo, el proceso de deposición de la capa activa se basa en la coevaporación al vacío de 3 fuentes, lo que aumenta la complejidad y el coste del proceso. Además, los compuestos fosforescentes, como los complejos de iridio, cuestan miles de euros por gramo. Recientemente, se han desarrollado OLEDs con capas emisoras ultrafinas (UEML), que podrían suponer ser una opción para resolver el problema de los costes.[74] Por ejemplo, el profesor Man-Keung Fung, de

la Universidad de Soochow, desarrolló OLEDs con una eficiencia razonable usando UEML de 0.3 nm de grosor.[75] Los materiales fosforescentes se intercalan entre una capa de transporte de huecos (TCTA) y una capa de transporte de electrones (TmPyPb), como se muestra en la figura 4.6. Los autores afirman que el uso de capas ultrafinas de complejos de iridio resultaría en un abaratamiento del 70% en el coste del material. Además, al no utilizar la coevaporación, se simplifican los procesos de optimización y fabricación. En este capítulo se fabrican OLEDs fosforescentes basados en complejos de iridio de manera convencional y también empleando UEML. Además, se emplean capas de transporte de carga gruesas basadas en perovskita ($CsPbCl_3$) estudiando el efecto del grosor en las prestaciones globales del dispositivo.

4.3. Resultados y conclusiones

En este capítulo, se ha realizado un estudio para fabricar OLEDs fosforescentes compuestos por capas de transporte de huecos de perovskita depositadas por evaporación. En primer lugar, se investigan las propiedades de PL de la perovskita inorgánica $CsPbCl_3$ y el rendimiento de los OLEDs resultantes, estudiando el efecto de una capa fina de CsCl como pasivación interfacial. Además, se fabrican OLEDs con UEML y se caracterizan para evaluar el rendimiento en comparación con OLEDs convencionales. Con una capa activa de tan solo 0.5 nm de grosor, se ha observado que la eficiencia del dispositivo supera a la de los OLEDs con diseño convencional, y su eficiencia máxima se ha producido con una luminancia útil para aplicaciones en pantallas, de entre 100 cd/m^2 y 1000 cd/m^2. Además hemos observado que el uso de capas gruesas de perovskita para el trasporte de carga permite minimizar la corriente de fuga.

5. Conclusión general

En la última década, las perovskitas de haluro metálico han despertado mucho interés y se han logrado notables avances en su desarrollo gracias a los esfuerzos de investigadores de todo el mundo. Las perovskitas con una banda prohibida estrecha se han aplicado en células solares que han resultado ser tan eficientes como las basadas en el silicio, gracias a su alta movilidad de carga y alto coeficiente de absorción. En el caso de las

aplicaciones en luminiscencia, el pico de emisión puede ajustarse mediante el intercambio de los aniones de haluro, y la anchura del pico es la más estrecha observada entre los materiales emergentes, tales como los emisores orgánicos y los puntos cuánticos inorgánicos. Además, el bajo coste de los precursores y la simplicidad de los procesos de síntesis hace que las perovskitas sean materiales muy atractivos para el mercado de los semiconductores. Dado que el uso de sistemas de visualización (como las pantallas móviles) se está volviendo ubicuo, es indispensable el desarrollo de sistemas emisores de luz con un coste reducido. En el capítulo 2, se desarrolla un fósforo luminiscente mediante una síntesis de un solo paso, mezclando bromuro de plomo con polietilenglicol. Esta solución muestra un pico de emisión a 610 nm, característico de la especie $PbBr_3^-$, con un rendimiento cuántico de fotoluminiscencia del 23%, muy superior a valores reportados anteriormente (0.5%). El color de emisión se puede modular introduciendo haluros de alquilamonio en DMSO, de manera análoga a la luminiscencia de perovskitas de haluro metálico en estado sólido. Por ejemplo, la introducción de un exceso de bromuro de tetrabutilamonio da lugar a un desplazamiento del pico a 560 nm (verde amarillento), originado por el $PbBr_4^{2-}$, y la sustitución con cloruro de tetrabutilamonio resulta en una emisión a 510 nm (verde azulado). Para conseguir luminiscencia blanca útil en aplicaciones de iluminación, se mezclan en proporciones equimolares bromuro de plomo y bromuro de tetrabutilamonio, obteniendo emisión amarilla, y se añade un colorante orgánico azul, el BCzVBi. La temperatura de color de las disoluciones satisface las normas CIE D55 (5503 K, luz diurna de media mañana/media tarde) y CIE D75 (7504 K, luz diurna del cielo del norte), respectivamente. Estos valores son aptos para pantallas de móviles y ordenadores. En el capítulo 3, se desarrollan unas células electroquímicas emisoras de luz, también llamadas diodos emisores de luz de una sola capa, con un material de perovskita de haluro metálico 3D de $CsPbBr_3$ mezclado con óxido de polietileno. Los precursores de la perovskita-polímero se disuelven en DMSO para su procesado por *spin-coating* sobre el ánodo de ITO/PEDOT:PSS. La capa activa se somete a un tratamiento de vacío y recocido térmico, y el cátodo metálico se deposita sobre ella sin utilizar capas de transporte de electrones. Los dispositivos resultantes muestran una luminancia comparable a la de un trabajo anterior, también basado en $CsPbBr_3$:PEO, mientras que el

tiempo de encendido es de solo 5 minutos, mucho más rápido que en el ejemplo anterior donde los dispositivos se encendían después de varias horas. El material emisor de luz es económicamente viable, ya que consiste en una perovskita binaria simple mezclada con un polímero producido a escala industrial. Además, la estructura de este dispositivo es muy sencilla, pudiéndose fabricar mediante técnicas de coste reducido. Se llevó a cabo también un estudio fundamental sobre la difusión de aniones en la interfaz de la perovskita emisora $CsPbBr_3$:PEO con una perovskita 3D coevaporada $CsPbCl_3$ y con el compuesto 0D Cs_4PbCl_6. La heterounión $CsPbBr_3$-$CsPbCl_3$ muestra luminiscencia cian-azul, que indica una mezcla instantánea de haluros. Por otro lado, no se observó desplazamiento del pico de emisión en la heterounión $CsPbBr_3$-Cs_4PbCl_6. Por lo tanto, se confirma que los compuestos inorgánicos de haluro de plomo de tipo 0D tienen menor movilidad iónica en comparación con las perovskitas análogas de tipo 3D. Aprovechando esta propiedad, se han caracterizado células electroquímicas emisoras de luz que emplean capas interfaciales del compuesto 0D Cs_4PbCl_6. En estos dispositivos hemos observado una mejora sustancial en la estabilidad de la emisión a lo largo del tiempo. Esta mejora en el funcionamiento del dispositivo se debe probablemente a la menor movilidad iónica del Cs_4PbCl_6 en la interfaz con el electrodo metálico. La metodología aplicada en este trabajo se basa en la evaporación térmica en vacío, sin embargo es posible aplicar capas finas de los materiales 0D también mediante procesos de disolución, usando los correspondientes nanocristales coloidales. En el capítulo 5, se utiliza la perovskita de cloruro de plomo y cesio, $CsPbCl_3$, como capa de transporte de huecos en OLEDs. La perovskita se deposita por coevaporación, y se recubre con una capa fina de CsCl que pasiva los defectos superficiales y mejora la inyección de carga. Esta capa de transporte de huecos de perovskita se utiliza en OLEDs fosforescentes donde la capa emisora consiste en un complejo de iridio no dopado ultrafino (< 1 nm). El empleo de capas emisoras ultrafinas puede ahorrar el coste del material en casi un 70%, facilitando además el proceso de fabricación. Sin embargo, los dispositivos muy finos tienden a mostrar una alta corriente de fuga, por lo tanto el uso de capas de transporte gruesas es deseable. Por ello, se introduce una capa de transporte de huecos de perovskita de 200 nm de espesor, logrando una eficiencia máxima de 31 cd/A, superior a los dispositivos de referencia que tienen una eficiencia del 20 cd/A.

El trabajo presentado en esta tesis incluye varias estrategias que pueden ayudar a reducir los costes en dispositivos electroluminiscentes. Se ha demostrado que las perovskitas de haluro metálico son candidatas prometedoras para fósforos luminiscentes, semiconductores iónicos en células electroquímicas emisoras de luz, y también como materiales de transporte de carga en diodos emisores de luz. Sin embargo, las perovskitas utilizadas en esta tesis contienen plomo, un metal altamente tóxico. Es de esperar que el desarrollo de perovskitas basadas en otro metales pueda ayudar a la realización de materiales luminiscentes de baja toxicidad y bajo coste, que puedan implementarse a nivel global en nuevos sistemas de visualización e iluminación.

Chapter 7.
Appendix

7.1. Bibliography

(1) Lee, S.-J.; Choi, J. W.; Kumar, S.; Lee, C.-L.; Lee, J.-S. Preparation of Perovskite-Embedded Monodisperse Copolymer Particles and Their Application for High Purity down-Conversion LEDs. *Mater. Horizons* **2018**, *5* (6), 1120–1129. https://doi.org/10.1039/C8MH00619A.

(2) Fakharuddin, A.; Gangishetty, M. K.; Abdi-Jalebi, M.; Chin, S.-H.; bin Mohd Yusoff, A. R.; Congreve, D. N.; Tress, W.; Deschler, F.; Vasilopoulou, M.; Bolink, H. J. Perovskite Light-Emitting Diodes. *Nat. Electron.* **2022**, *5* (4), 203–216. https://doi.org/10.1038/s41928-022-00745-7.

(3) Young-Hoon, K.; Himchan, C.; Tae-Woo, L. Metal Halide Perovskite Light Emitters. *Proc. Natl. Acad. Sci.* **2016**, *113* (42), 11694–11702. https://doi.org/10.1073/pnas.1607471113.

(4) Schmidt, L. C.; Pertegás, A.; González-Carrero, S.; Malinkiewicz, O.; Agouram, S.; Mínguez Espallargas, G.; Bolink, H. J.; Galian, R. E.; Pérez-Prieto, J. Nontemplate Synthesis of CH3NH3PbBr3 Perovskite Nanoparticles. *J. Am. Chem. Soc.* **2014**, *136* (3), 850–853. https://doi.org/10.1021/ja4109209.

(5) Tan, Z.-K.; Moghaddam, R. S.; Lai, M. L.; Docampo, P.; Higler, R.; Deschler, F.; Price, M.; Sadhanala, A.; Pazos, L. M.; Credgington, D.; Hanusch, F.; Bein, T.; Snaith, H. J.; Friend, R. H. Bright Light-Emitting Diodes Based on Organometal Halide Perovskite. *Nat. Nanotechnol.* **2014**, *9* (9), 687–692. https://doi.org/10.1038/nnano.2014.149.

(6) Goldschmidt, V. M. Die Gesetze Der Krystallochemie. *Naturwissenschaften* **1926**, *14* (21), 477–485. https://doi.org/10.1007/BF01507527.

(7) Crystal Structure of Barium Titanate. *Nature* **1945**, *155* (3938), 484–485. https://doi.org/10.1038/155484b0.

(8) Travis, W.; Glover, E. N. K.; Bronstein, H.; Scanlon, D. O.; Palgrave, R. G. On the Application of the Tolerance Factor to Inorganic and Hybrid Halide Perovskites: A Revised System.

Chem. Sci. **2016**, *7* (7), 4548–4556. https://doi.org/10.1039/c5sc04845a.

(9) Zhou, C.; Lin, H.; He, Q.; Xu, L.; Worku, M.; Chaaban, M.; Lee, S.; Shi, X.; Du, M. H.; Ma, B. Low Dimensional Metal Halide Perovskites and Hybrids. *Mater. Sci. Eng. R Reports* **2019**, *137* (October 2018), 38–65. https://doi.org/10.1016/j.mser.2018.12.001.

(10) Era, M.; Morimoto, S.; Tsutsui, T.; Saito, S. Organic-inorganic Heterostructure Electroluminescent Device Using a Layered Perovskite Semiconductor (C6H5C2H4NH3)2PbI4. *Appl. Phys. Lett.* **1994**, *65* (6), 676–678. https://doi.org/10.1063/1.112265.

(11) Chondroudis, K.; Mitzi, D. B. Electroluminescence from an Organic-Inorganic Perovskite Incorporating a Quaterthiophene Dye within Lead Halide Perovskite Layers. *Chem. Mater.* **1999**, *11* (11), 3028–3030. https://doi.org/10.1021/cm990561t.

(12) Kojima, A.; Teshima, K.; Shirai, Y.; Miyasaka, T. Organometal Halide Perovskites as Visible-Light Sensitizers for Photovoltaic Cells. *J. Am. Chem. Soc.* **2009**, *131* (17), 6050–6051. https://doi.org/10.1021/ja809598r.

(13) Kim, H. S.; Lee, C. R.; Im, J. H.; Lee, K. B.; Moehl, T.; Marchioro, A.; Moon, S. J.; Humphry-Baker, R.; Yum, J. H.; Moser, J. E.; Grätzel, M.; Park, N. G. Lead Iodide Perovskite Sensitized All-Solid-State Submicron Thin Film Mesoscopic Solar Cell with Efficiency Exceeding 9%. *Sci. Rep.* **2012**, *2*, 1–7. https://doi.org/10.1038/srep00591.

(14) M., L. M.; Joël, T.; Tsutomu, M.; N., M. T.; J., S. H. Efficient Hybrid Solar Cells Based on Meso-Superstructured Organometal Halide Perovskites. *Science (80-.).* **2012**, *338* (6107), 643–647. https://doi.org/10.1126/science.1228604.

(15) Grätzel, M. The Rise of Highly Efficient and Stable Perovskite Solar Cells. *Acc. Chem. Res.* **2017**, *50* (3), 487–491. https://doi.org/10.1021/acs.accounts.6b00492.

(16) Yoo, J. J.; Seo, G.; Chua, M. R.; Park, T. G.; Lu, Y.; Rotermund, F.; Kim, Y. K.; Moon, C. S.; Jeon, N. J.; Correa-Baena, J. P.; Bulović, V.; Shin, S. S.; Bawendi, M. G.; Seo, J. Efficient Perovskite Solar Cells via Improved Carrier Management. *Nature* **2021**, *590* (7847), 587–593. https://doi.org/10.1038/s41586-021-03285-w.

(17) Xu, W.; Hu, Q.; Bai, S.; Bao, C.; Miao, Y.; Yuan, Z.; Borzda, T.; Barker, A. J.; Tyukalova, E.; Hu, Z.; Kawecki, M.; Wang, H.; Yan, Z.; Liu, X.; Shi, X.; Uvdal, K.; Fahlman, M.; Zhang, W.; Duchamp, M.; Liu, J.-M.; Petrozza, A.; Wang, J.; Liu, L.-M.; Huang, W.; Gao, F. Rational Molecular Passivation for High-Performance Perovskite Light-Emitting Diodes. *Nat. Photonics* **2019**, *13* (6), 418–424. https://doi.org/10.1038/s41566-019-0390-x.

(18) Kim, Y. H.; Kim, S.; Kakekhani, A.; Park, J.; Park, J.; Lee, Y. H.; Xu, H.; Nagane, S.; Wexler, R. B.; Kim, D. H.; Jo, S. H.; Martínez-Sarti, L.; Tan, P.; Sadhanala, A.; Park, G. S.; Kim, Y. W.; Hu, B.; Bolink, H. J.; Yoo, S.; Friend, R. H.; Rappe, A. M.; Lee, T. W. Comprehensive Defect Suppression in Perovskite Nanocrystals for High-Efficiency Light-Emitting Diodes. *Nat. Photonics* **2021**, *15* (2), 148–155. https://doi.org/10.1038/s41566-020-00732-4.

(19) Protesescu, L.; Yakunin, S.; Bodnarchuk, M. I.; Krieg, F.; Caputo, R.; Hendon, C. H.; Yang, R. X.; Walsh, A.; Kovalenko, M. V. Nanocrystals of Caesium Lead Halide Perovskites (CsPbX3, X = Cl, Br, and I): Novel Optoelectronic Materials Showing Bright Emission with Wide Color Gamut. *Nano Lett.* **2015**, *15* (6), 3692–3696. https://doi.org/10.1021/nl5048779.

(20) Ma, D.; Lin, K.; Dong, Y.; Choubisa, H.; Proppe, A. H.; Wu, D.; Wang, Y. K.; Chen, B.; Li, P.; Fan, J. Z.; Yuan, F.; Johnston, A.; Liu, Y.; Kang, Y.; Lu, Z. H.; Wei, Z.; Sargent, E. H. Distribution Control Enables Efficient Reduced-Dimensional Perovskite LEDs. *Nature* **2021**, *599* (7886), 594–598. https://doi.org/10.1038/s41586-021-03997-z.

(21) Jeon, N. J.; Noh, J. H.; Kim, Y. C.; Yang, W. S.; Ryu, S.; Seok, S. Il. Solvent Engineering for High-Performance Inorganic–Organic Hybrid Perovskite Solar Cells. *Nat. Mater.* **2014**, *13* (9), 897–903. https://doi.org/10.1038/nmat4014.

(22) Li, X.; Bi, D.; Yi, C.; Décoppet, J. D.; Luo, J.; Zakeeruddin, S. M.; Hagfeldt, A.; Grätzel, M. A Vacuum Flash-Assisted Solution Process for High-Efficiency Large-Area Perovskite Solar Cells. *Science (80-.).* **2016**, *353* (6294), 58–62. https://doi.org/10.1126/science.aaf8060.

(23) Ávila, J.; Momblona, C.; Boix, P. P.; Sessolo, M.; Bolink, H. J. Vapor-Deposited Perovskites: The Route to High-Performance Solar Cell Production? *Joule* **2017**, *1* (3), 431–442.

https://doi.org/10.1016/j.joule.2017.07.014.

(24) Gil-Escrig, L.; Roß, M.; Sutter, J.; Al-Ashouri, A.; Becker, C.; Albrecht, S. Fully Vacuum-Processed Perovskite Solar Cells on Pyramidal Microtextures. *Sol. RRL* **2021**, *5* (1), 1–9. https://doi.org/10.1002/solr.202000553.

(25) Liu, M.; Johnston, M. B.; Snaith, H. J. Efficient Planar Heterojunction Perovskite Solar Cells by Vapour Deposition. *Nature* **2013**, *501* (7467), 395–398. https://doi.org/10.1038/nature12509.

(26) Li, H.; Zhou, J.; Tan, L.; Li, M.; Jiang, C.; Wang, S.; Zhao, X.; Liu, Y.; Zhang, Y.; Ye, Y.; Tress, W.; Yi, C. Sequential Vacuum-Evaporated Perovskite Solar Cells with More than 24% Efficiency. *Sci. Adv.* **2022**, *8* (28), 1–9. https://doi.org/10.1126/sciadv.abo7422.

(27) El Ajjouri, Y.; Palazon, F.; Sessolo, M.; Bolink, H. J. Single-Source Vacuum Deposition of Mechanosynthesized Inorganic Halide Perovskites. *Chem. Mater.* **2018**, *30* (21), 7423–7427. https://doi.org/10.1021/acs.chemmater.8b03352.

(28) Palazon, F.; El Ajjouri, Y.; Bolink, H. J. Making by Grinding: Mechanochemistry Boosts the Development of Halide Perovskites and Other Multinary Metal Halides. *Adv. Energy Mater.* **2020**, *10* (13), 1–13. https://doi.org/10.1002/aenm.201902499.

(29) Palazon, F.; El Ajjouri, Y.; Sebastia-Luna, P.; Lauciello, S.; Manna, L.; Bolink, H. J. Mechanochemical Synthesis of Inorganic Halide Perovskites: Evolution of Phase-Purity, Morphology, and Photoluminescence. *J. Mater. Chem. C* **2019**, *7* (37), 11406–11410. https://doi.org/10.1039/c9tc03778k.

(30) Lee, K. J.; Turedi, B.; Sinatra, L.; Zhumekenov, A. A.; Maity, P.; Dursun, I.; Naphade, R.; Merdad, N.; Alsalloum, A.; Oh, S.; Wehbe, N.; Hedhili, M. N.; Kang, C. H.; Subedi, R. C.; Cho, N.; Kim, J. S.; Ooi, B. S.; Mohammed, O. F.; Bakr, O. M. Perovskite-Based Artificial Multiple Quantum Wells. *Nano Lett.* **2019**, *19* (6), 3535–3542. https://doi.org/10.1021/acs.nanolett.9b00384.

(31) Lee, K. J.; Merdad, N. A.; Maity, P.; El-Demellawi, J. K.; Lui, Z.; Sinatra, L.; Zhumekenov, A. A.; Hedhili, M. N.; Min, J.-W.; Min, J.-H.; Gutiérrez-Arzaluz, L.; Anjum, D. H.; Wei, N.; Ooi, B. S.; Alshareef, H. N.; Mohammed, O. F.; Bakr, O. M. Engineering Band-Type Alignment in CsPbBr3 Perovskite-Based Artificial Multiple Quantum Wells. *Adv. Mater.* **2021**, *33* (17), 2005166.

https://doi.org/https://doi.org/10.1002/adma.202005166.

(32) Longo, G.; Gil-Escrig, L.; Degen, M. J.; Sessolo, M.; Bolink, H. J. Perovskite Solar Cells Prepared by Flash Evaporation. *Chem. Commun.* **2015**, *51* (34), 7376–7378. https://doi.org/10.1039/c5cc01103e.

(33) Lee, W.; Lee, J.; Lee, H. D.; Kim, J.; Ahn, H.; Kim, Y.; Yoo, D.; Lee, J.; Lee, T. W.; Kang, K.; Lee, T. Controllable Deposition of Organic Metal Halide Perovskite Films with Wafer-Scale Uniformity by Single Source Flash Evaporation. *Sci. Rep.* **2020**, *10* (1), 1–10. https://doi.org/10.1038/s41598-020-75764-5.

(34) Stranks, S. D.; Burlakov, V. M.; Leijtens, T.; Ball, J. M.; Goriely, A.; Snaith, H. J. Recombination Kinetics in Organic-Inorganic Perovskites: Excitons, Free Charge, and Subgap States. *Phys. Rev. Appl.* **2014**, *2* (3), 34007. https://doi.org/10.1103/PhysRevApplied.2.034007.

(35) Satpathy, R.; Pamuru, V. *Making of Crystalline Silicon Solar Cells*; 2021. https://doi.org/10.1016/b978-0-12-817626-9.00004-6.

(36) Kim, G.-W.; Petrozza, A. Defect Tolerance and Intolerance in Metal-Halide Perovskites. *Adv. Energy Mater.* **2020**, *10* (37), 2001959. https://doi.org/https://doi.org/10.1002/aenm.202001959.

(37) Dutta, S. K.; Perkovic, M. W. Lead as Its Own Luminescent Sensor. *Inorg. Chem.* **2002**, *41* (26), 6938–6940. https://doi.org/10.1021/ic0260724.

(38) Li, S. H.; Chen, F. R.; Zhou, Y. F.; Xu, J. G. Pb4Br113- Cluster as a Fluorescent Indicator for Micro Water Content in Aprotic Organic Solvents. *Analyst* **2009**, *134* (3), 443–446. https://doi.org/10.1039/b817787b.

(39) Chen, J.; Spear, S. K.; Huddleston, J. G.; Rogers, R. D. Polyethylene Glycol and Solutions of Polyethylene Glycol as Green Reaction Media. *Green Chem.* **2005**, *7* (2), 64–82. https://doi.org/10.1039/b413546f.

(40) Oldenburg, K.; Vogler, A. Electronic Spectra and Photochemistry of Tin(II), Lead(II), Antimony(III), and Bismuth(III) Bromide Complexes in Solution. **1993**, *48* (11), 1519–1523. https://doi.org/doi:10.1515/znb-1993-1109.

(41) Yoon, S. J.; Stamplecoskie, K. G.; Kamat, P. V. How Lead Halide

Complex Chemistry Dictates the Composition of Mixed Halide Perovskites. *J. Phys. Chem. Lett.* **2016**, *7* (7), 1368–1373. https://doi.org/10.1021/acs.jpclett.6b00433.

(42) Ray, A.; Maggioni, D.; Baranov, D.; Dang, Z.; Prato, M.; Akkerman, Q. A.; Goldoni, L.; Caneva, E.; Manna, L.; Abdelhady, A. L. Green-Emitting Powders of Zero-Dimensional Cs4PbBr6: Delineating the Intricacies of the Synthesis and the Origin of Photoluminescence. *Chem. Mater.* **2019**, *31* (18), 7761–7769. https://doi.org/10.1021/acs.chemmater.9b02944.

(43) Chin, S. H.; Choi, J. W.; Hu, Z.; Mardegan, L.; Sessolo, M.; Bolink, H. J. Tunable Luminescent Lead Bromide Complexes. *J. Mater. Chem. C* **2020**, *8* (45), 15996–16000. https://doi.org/10.1039/d0tc04057f.

(44) Chen, P.; Li, Q.; Grindy, S.; Holten-Andersen, N. White-Light-Emitting Lanthanide Metallogels with Tunable Luminescence and Reversible Stimuli-Responsive Properties. *J. Am. Chem. Soc.* **2015**, *137* (36), 11590–11593. https://doi.org/10.1021/jacs.5b07394.

(45) McCamy, C. S. Correlated Color Temperature as an Explicit Function of Chromaticity Coordinates. *Color Res. Appl.* **1992**, *17* (2), 142–144. https://doi.org/https://doi.org/10.1002/col.5080170211.

(46) Morad, V.; McCall, K. M.; Sakhatskyi, K.; Lehmann, E.; Walfort, B.; Losko, A. S.; Trtik, P.; Strobl, M.; Yakunin, S.; Kovalenko, M. V. Luminescent Lead Halide Ionic Liquids for High-Spatial-Resolution Fast Neutron Imaging. *ACS Photonics* **2021**, *8* (11), 3357–3364. https://doi.org/10.1021/acsphotonics.1c01348.

(47) Qibing Pei, Gang Yu, Chi Zhang, Yang Yang, A. J. H. Polymer Light-Emitting. *Science (80-.).* **1995**, *269* (5227), 1086–1088.

(48) Van Reenen, S.; Matyba, P.; Dzwilewski, A.; Janssen, R. A. J.; Edman, L.; Kemerink, M. A Unifying Model for the Operation of Light-Emitting Electrochemical Cells. *J. Am. Chem. Soc.* **2010**, *132* (39), 13776–13781. https://doi.org/10.1021/ja1045555.

(49) Costa, R. D.; Ortí, E.; Bolink, H. J.; Monti, F.; Accorsi, G.; Armaroli, N. Luminescent Ionic Transition-Metal Complexes for Light-Emitting Electrochemical Cells. *Angew. Chemie - Int. Ed.* **2012**, *51* (33), 8178–8211. https://doi.org/10.1002/anie.201201471.

(50) Li, J.; Bade, S. G. R.; Shan, X.; Yu, Z. Single-Layer Light-Emitting Diodes Using Organometal Halide Perovskite/Poly(Ethylene Oxide) Composite Thin Films. *Adv. Mater.* **2015**, *27* (35), 5196–5202. https://doi.org/10.1002/adma.201502490.

(51) Bade, S. G. R.; Li, J.; Shan, X.; Ling, Y.; Tian, Y.; Dilbeck, T.; Besara, T.; Geske, T.; Gao, H.; Ma, B.; Hanson, K.; Siegrist, T.; Xu, C.; Yu, Z. Fully Printed Halide Perovskite Light-Emitting Diodes with Silver Nanowire Electrodes. *ACS Nano* **2016**, *10* (2), 1795–1801. https://doi.org/10.1021/acsnano.5b07506.

(52) Chou, S.-Y.; Ma, R.; Li, Y.; Zhao, F.; Tong, K.; Yu, Z.; Pei, Q. Transparent Perovskite Light-Emitting Touch-Responsive Device. *ACS Nano* **2017**, *11* (11), 11368–11375. https://doi.org/10.1021/acsnano.7b05935.

(53) Alahbakhshi, M.; Mishra, A.; Haroldson, R.; Ishteev, A.; Moon, J.; Gu, Q.; Slinker, J. D.; Zakhidov, A. A. Bright and Effectual Perovskite Light-Emitting Electrochemical Cells Leveraging Ionic Additives. *ACS Energy Lett.* **2019**, *4* (12), 2922–2928. https://doi.org/10.1021/acsenergylett.9b01925.

(54) Mishra, A.; Alahbakhshi, M.; Haroldson, R.; Bastatas, L. D.; Gu, Q.; Zakhidov, A. A.; Slinker, J. D. Enhanced Operational Stability of Perovskite Light-Emitting Electrochemical Cells Leveraging Ionic Additives. *Adv. Opt. Mater.* **2020**, *8* (13), 1–11. https://doi.org/10.1002/adom.202000226.

(55) Boyd, C. C.; Cheacharoen, R.; Leijtens, T.; McGehee, M. D. Understanding Degradation Mechanisms and Improving Stability of Perovskite Photovoltaics. *Chem. Rev.* **2019**, *119* (5), 3418–3451. https://doi.org/10.1021/acs.chemrev.8b00336.

(56) Aygüler, M. F.; Weber, M. D.; Puscher, B. M. D.; Medina, D. D.; Docampo, P.; Costa, R. D. Light-Emitting Electrochemical Cells Based on Hybrid Lead Halide Perovskite Nanoparticles. *J. Phys. Chem. C* **2015**, *119* (21), 12047–12054. https://doi.org/10.1021/acs.jpcc.5b02959.

(57) Aygüler, M. F.; Puscher, B. M. D.; Tong, Y.; Bein, T.; Urban, A. S.; Costa, R. D.; Docampo, P. Light-Emitting Electrochemical Cells Based on Inorganic Metal Halide Perovskite Nanocrystals. *J. Phys. D. Appl. Phys.* **2018**, *51* (33). https://doi.org/10.1088/1361-6463/aad203.

(58) Yin, J.; Brédas, J. L.; Bakr, O. M.; Mohammed, O. F. Boosting Self-Trapped Emissions in Zero-Dimensional Perovskite Heterostructures. *Chem. Mater.* **2020**, *32* (12), 5036–5043. https://doi.org/10.1021/acs.chemmater.0c00658.

(59) Thumu, U.; Piotrowski, M.; Owens-Baird, B.; Kolen'ko, Y. V. Zero-Dimensional Caesium Lead Halide Perovskites: Phase Transformations, Hybrid Structures, and Applications. *J. Solid State Chem.* **2019**, *271* (January), 361–377. https://doi.org/10.1016/j.jssc.2019.01.005.

(60) Shen, Z.; Song, P.; Qiao, B.; Cao, J.; Bai, Q.; Song, D.; Xu, Z.; Zhao, S.; Zhang, G.; Wu, Y. Impeding Anion Exchange to Improve Composition Stability of CsPbX 3 (X = Cl, Br) Nanocrystals through Facilely Fabricated Cs4Pb X 6 Shell. *Chinese Phys. B* **2019**, *28* (8), 4–8. https://doi.org/10.1088/1674-1056/28/8/086102.

(61) Karlsson, M.; Yi, Z.; Reichert, S.; Luo, X.; Lin, W.; Zhang, Z.; Bao, C.; Zhang, R.; Bai, S.; Zheng, G.; Teng, P.; Duan, L.; Lu, Y.; Zheng, K.; Pullerits, T.; Deibel, C.; Xu, W.; Friend, R.; Gao, F. Mixed Halide Perovskites for Spectrally Stable and High-Efficiency Blue Light-Emitting Diodes. *Nat. Commun.* **2021**, *12* (1), 1–10. https://doi.org/10.1038/s41467-020-20582-6.

(62) Chin, S. H.; Choi, J. W.; Woo, H. C.; Kim, J. H.; Lee, H. S.; Lee, C. L. Realizing a Highly Luminescent Perovskite Thin Film by Controlling the Grain Size and Crystallinity through Solvent Vapour Annealing. *Nanoscale* **2019**, *11* (13), 5861–5867. https://doi.org/10.1039/C8NR09947B.

(63) Liashenko, T. G.; Pushkarev, A. P.; Naujokaitis, A.; Pakštas, V.; Franckevičius, M.; Zakhidov, A. A.; Makarov, S. V. Suppression of Electric Field-Induced Segregation in Sky-Blue Perovskite Light-Emitting Electrochemical Cells. *Nanomaterials* **2020**, *10* (10), 1–13. https://doi.org/10.3390/nano10101937.

(64) Ren, Z.; Xiao, X.; Ma, R.; Lin, H.; Wang, K.; Sun, X. W.; Choy, W. C. H. Hole Transport Bilayer Structure for Quasi-2D Perovskite Based Blue Light-Emitting Diodes with High Brightness and Good Spectral Stability. *Adv. Funct. Mater.* **2019**, *29* (43). https://doi.org/10.1002/adfm.201905339.

(65) Qian, X.-Y.; Tang, Y.-Y.; Zhou, W.; Shen, Y.; Guo, M.-L.; Li, Y.-Q.; Tang, J.-X. Strategies to Improve Luminescence Efficiency and

Stability of Blue Perovskite Light-Emitting Devices. *Small Sci.* **2021**, *1* (8), 2000048. https://doi.org/10.1002/smsc.202000048.

(66) Helfrich, W.; Schneider, W. G. Recombination Radiation in Anthracene Crystals. *Phys. Rev. Lett.* **1965**, *14* (7), 229–231. https://doi.org/10.1103/PhysRevLett.14.229.

(67) Tang, C. W.; Vanslyke, S. A. Organic Electroluminescent Diodes. *Appl. Phys. Lett.* **1987**, *51* (12), 913–915. https://doi.org/10.1063/1.98799.

(68) Burroughes, J. H.; Bradley, D. D. C.; Brown, A. R.; Marks, R. N.; Mackay, K.; Friend, R. H.; Burns, P. L.; Holmes, A. B. Light-Emitting Diodes Based on Conjugated Polymers. *Nature* **1990**, *347* (6293), 539–541. https://doi.org/10.1038/347539a0.

(69) Baldo, M. A.; an dY. You, D. F. O.; Shoustikov, A.; Sibley, S.; Thompson, M. E.; Forrest, S. R. Highly Efficient Phosphorescent Emission from Organic Electroluminescent Devices. *Nature* **1998**, *395* (September), 151.

(70) Adachi, C.; Baldo, M. A.; Thompson, M. E.; Forrest, S. R. Nearly 100% Internal Phosphorescence Efficiency in an Organic Light Emitting Device. *J. Appl. Phys.* **2001**, *90* (10), 5048–5051. https://doi.org/10.1063/1.1409582.

(71) Matsushima, T.; Bencheikh, F.; Komino, T.; Leyden, M. R.; Sandanayaka, A. S. D.; Qin, C.; Adachi, C. High Performance from Extraordinarily Thick Organic Light-Emitting Diodes. *Nature* **2019**, *572* (7770), 502–506. https://doi.org/10.1038/s41586-019-1435-5.

(72) Ok, K. H.; Kim, J.; Park, S. R.; Kim, Y.; Lee, C. J.; Hong, S. J.; Kwak, M. G.; Kim, N.; Han, C. J.; Kim, J. W. Ultra-Thin and Smooth Transparent Electrode for Flexible and Leakage-Free Organic Light-Emitting Diodes. *Sci. Rep.* **2015**, *5*, 1–8. https://doi.org/10.1038/srep09464.

(73) Tak, Y.-H.; Kim, K.-B.; Park, H.-G.; Lee, K.-H.; Lee, J.-R. Criteria for ITO (Indium–Tin-Oxide) Thin Film as the Bottom Electrode of an Organic Light Emitting Diode. *Thin Solid Films* **2002**, *411* (1), 12–16. https://doi.org/https://doi.org/10.1016/S0040-6090(02)00165-7.

(74) Miao, Y.; Yin, M. Recent Progress on Organic Light-Emitting Diodes with Phosphorescent Ultrathin (<1nm) Light-Emitting Layers. *iScience* **2022**, *25* (2), 103804.

https://doi.org/https://doi.org/10.1016/j.isci.2022.103804.

(75) Wu, S.; Li, S.; Sun, Q.; Huang, C.; Fung, M. K. Highly Efficient White Organic Light-Emitting Diodes with Ultrathin Emissive Layers and a Spacer-Free Structure. *Sci. Rep.* **2016**, *6* (April), 4–11. https://doi.org/10.1038/srep25821.

(76) Ganose, A. M.; Scanlon, D. O.; Walsh, A.; Hoye, R. L. Z. The Defect Challenge of Wide-Bandgap Semi- Conductors for Photovoltaics and Beyond. *Nat. Commun.* **2022**, *13*, 4715. https://doi.org/10.1038/s41467-022-32131-4.

(77) Liao, Y.; Tian, N.; Wang, J.; Yao, D.; Zheng, G.; Zhou, B.; Yang, Y.; Long, F. Performance Enhancement of Evaporated CsPbI2Br Perovskite Solar Cells with a CuSCN Hole Transport Layer via a Caesium Bromide Buffer Layer. *ACS Appl. Energy Mater.* **2022**. https://doi.org/10.1021/acsaem.2c01155.

(78) Bangsund, J. S.; Van Sambeek, J. R.; Concannon, N. M.; Holmes, R. J. Sub-Turn-on Exciton Quenching Due to Molecular Orientation and Polarization in Organic Light-Emitting Devices. *Sci. Adv.* **2020**, *6* (32), 1–11. https://doi.org/10.1126/sciadv.abb2659.

(79) Mishra, A.; Alahbakhshi, M.; Haroldson, R.; Gu, Q.; Zakhidov, A. A.; Slinker, J. D. Pure Blue Electroluminescence by Differentiated Ion Motion in a Single Layer Perovskite Device. https://doi.org/10.1002/adfm.202102006.

(80) Mishra, A.; Alahbakhshi, M.; Gu, Q.; Zakhidov, A. A.; Slinker, J. D. Leveraging a Stable Perovskite Composite to Satisfy Blue Electroluminescence Standards. *ACS Mater. Lett.* **2021**, *3* (9), 1357–1362. https://doi.org/10.1021/acsmaterialslett.1c00404.

(81) Mishra, A.; Bose, R.; Zheng, Y.; Xu, W.; McMullen, R.; Mehta, A. B.; Kim, M. J.; Hsu, J. W. P.; Malko, A. V.; Slinker, J. D. Stable and Bright Electroluminescent Devices Utilizing Emissive 0D Perovskite Nanocrystals Incorporated in a 3D CsPbBr3 Matrix. *Adv. Mater.* **2022**, *34* (31), 1–11. https://doi.org/10.1002/adma.202203226.

7.2. List of Abbreviations

ACN	Acetonitrile
Alq_3	Tris(8-hydroxyquinolinato) aluminium
AQ1250	Poly(thiophene-3-[2[(2-methoxyethoxy) ethoxy]-2,5-diyl)
BABr	Butylammonium bromide
BCzVBi	4,4'-Bis(9-ethyl-3-carbazovinylene)-1,1'-biphenyl
CCT	Correlated color temperature
CE	Current efficiency
CIE	Commission on illumination (Commission Internationale de l'éclairage)
DFT	Density functional theory
DMF	Dimethyl formamide
DMSO	Dimethyl sulfoxide
ECD	Electrochemical doping
ED	Electrodynamical
EDL	Electric double layers
EL	Electroluminescence
EQE	External Quantum Efficiency
FWHM	Full width at half maximum
GBL	γ-butyrolactone
IoT	Internet of things
IPA	Isopropyl alcohol
$Ir(ppy)_2acac$	Bis(2-phenylpyridine) iridium (III) acetylacetonate
ISC	Intersystem crossing
ITU	International telecommunication union
J	Current density
L	Luminance
LEC	Light-emitting electrochemical cell
LED	Light-emitting diode
MABr	Methylammonium bromide
m-$CsPbCl_3$	Modified $CsPbCl_3$ (interface passivated by CsCl)
MEH-PPV	Poly[2-methoxy-5-(2-ethylhexyloxy)-1,4-phenylenevinylene]
η_{inj}	Injection efficiency
η_{out}	Light outcoupling efficiency
η_{rad}	Radiative recombination efficiency

OLED	Organic light-emitting diode
OXD-7	1,3-bis[2-(4-tert-butylphenyl)-1,3,4-oxadiazo-5-yl] benzene
PEDOT:PSS	Poly(3,4-ethylenedioxythiophene) polystyrene sulfonate
PEG	Poly-ethylene glycol
PeLED	Perovskite light emitting diode
PEO	Poly-ethylene oxide
PL	Photoluminescence
PLE	Photoluminescence excitation
PLQY	Photoluminescent quantum yield
PPV	Poly (p-phenylene vinylene)
PtOEP	2,3,7,8,12,13,17,18-octaethyl-21H,23H-porphine platinum (II)
PUE-LEDs	Perovskite-ultrathin emitter LEDs
QLED	Quantum dot light-emitting diode
SRH	Shockley-Read-Hall recombination
SVA	Solvent vapour annealing
TAZ	3-phenyl-4(1′-naphthyl)-5-phenyl-1,2,4-triazole
TBABr	Tetrabutylammonium bromide
TCSPC	Time-corelated single photon counting
TCTA	Tris(4-carbazoyl-9-ylphenyl) amine
TmPyPb	1,3,5-Tri(m-pyridin-3-ylphenyl) benzene
TPBi	2,2',2''-(1,3,5-Benzinetriyl)-tris(1-phenyl-1-H-benzimidazole)
TTA	Triplet-triplet annihilation
UEML	Ultrathin emissive layer
V_{bi}	Built-in potential

7.3. List of Figures and Tables

solution injection, c) after 3 seconds, and d) after 6 seconds.

Figure 2.3. Measurement setups for a. PL spectra and decay time measurement, b. PLE spectra, and c. PLQY.

Figure 2.4. a) Normalized PLE and PL spectra of lead bromide-PEG solution. b) PEG-molecular weight dependency on PL decay time.

Table 2.1. Photoluminescent characteristics of lead bromide in different polyethylene glycols.

Figure 2.5. a) PL spectra of TBABr, MABr, and BABr added lead bromide solution and b) normalized spectra.

Figure 2.6. DFT simulation results on interaction distance in lead bromide solutions with alkylammonium bromide ligands.

Figure 2.7. PL stability of $PbBr_3^-$ and $PbBr_4^{2-}$.

Figure 2.8. Photoluminescent spectra of lead chloride + TBACl and lead bromide + TBABr (TBAX is 2-fold to lead halide).

Figure 2.9. a) Luminescent metallogels under UV irradiation. b) PL spectra of blue-emitting BCzVBi dye and yellow-emissive solution. c) PL spectrum and d) CIE-coordinates of white and yellow-emissive solution and BCzVBi.

Figure 2.10. a) PL spectra of 3 white emitters. b) PL spectra of 2 yellow emitters.

Figure 4.2. p-n junction OLED comprising Alq_3 (n-type, emitter) and diamine (p-type).

Figure 4.3. Synthesis of PPV.

Figure 4.4. Schematic illustration of recombination process in fluorescent and phosphorescent emissions.

Figure 4.5. a) Efficiency of phosphorescent OLEDs with perovskite transport layers as a function of current density. b) flat band diagram of device.

Figure 4.6. a) Flat band diagram and b) current efficiency as a function luminance of OLEDs comprising UEMLs.

Figure 4.7. PL spectra of 30 nm $CsPbCl_3$ with and without CsCl passivation.

Figure 4.8. Fabrication process of phosphorescent OLEDs with perovskite hole transport layer.

Figure 4.9. a) J-V curves and b) L-V curves. c) Current efficiency as a function of Luminance.

Figure 4.10. a) J-V and b) L-V curves of OLEDs comprising 30 nm and 200 nm thick perovskite hole transport layers. c) Current efficiency as a function of Luminance.

Figure 4.11. a) J-V and b) L-V curves of OLEDs comprising 0.05 nm, 0.1 nm, 0.3 nm, and 0.5 nm thick $Ir(ppy)_2acac$. c) Current efficiency as a function of luminance.

Figure 4.12. a) Schematic illustration of OLEDs with co-evaporated $Ir(ppy)_2acac$ and TPBi, b) J-V-L characteristic of device, and c) Current efficiency as a function of luminance.

7.4. List of Publications

1. “Temperature-Dependent Photoluminescence of $CH_3NH_3PbBr_3$ Perovskite Quantum Dots and Bulk Counterparts” - Hee Chul Woo *et al., J. Phys. Chem. Lett.,* 2018, 9, 4066–4074 (Co-Author)

2. “Realizing a Highly Luminescent Perovskite Thin Film by Controlling Grain Size and Crystallinity through Solvent Vapour Annealing” – **Sang-Hyun Chin** *et al., Nanoscale,* 2019, 11, 5861-5867. (1st Author)

3. “Tunable Luminescent Lead Bromide Complex” – **Sang-Hyun Chin** *et al., J. Mater. Chem. C*, 2020, 8, 15996-16000. (1st Author)

4. “Binding Sites, Vibrations and Spin-Lattice Relaxation Times in Europium (II)-Based Metallofullerene Spin Qubits” - Ziqi Hu *et al., Chem. Eur. J.,* 2021, 27, 13242. (Co-Author)

5. “Perovskite Light Emitting Diodes” - Azhar Fakharuddin *et al., Nat. Electron.*, 2022, 5, 203–216. (Co-Author)

6. “Dimensionality Controls Anion Intermixing in Electroluminescent Perovskite Heterojunctions” – **Sang-Hyun Chin** *et al., ACS Photonics*, 2022, 9, 2483–2488. (1st Author)

7.5. Acknowledgements

The work presented in this book contains part of the results collected through three and half years of research at the Institute of Molecular Science (Instituto de Ciencia Molecular, ICMol) in University for Valencia. I feel that writing these 2 pages is a good chance to shout out my people whom I appreciate.

Firstly, I would like to thank my thesis advisor and group leader Prof. Henk J. Bolink for giving me a chance to conduct a thesis in this team even if I am quite ignorant in evaporated perovskite solar cell field. I am sure that running this big research group must be exhausting and tight but your permission on new research and advice for me was fast and real. Also, I appreciated advice from another thesis advisor Dr. Michele Sessolo. We could share and discuss brand new research papers on light emitters with perovskites and organic materials. The tips on research and publication are juicy as well as your advice on wine. I promise that I will try Barolo someday. I hope to keep up our collaboration with my two thesis advisors even after my thesis.

I am genuinely grateful to my teammates. Thanks to our great technician, Jorge F, I could fabricate publishable devices on time. Sometimes it is unbelievable that you fix evaporators and other setups that fast. Thanks to Ana, Laura, and Lidon, I could learn our instruments quite properly. I appreciate the measurements and discussions with Lorenzo who was only friend working on light emitting devices. And Abhi, thank you for your comments on device fabrication and interesting comments on new research papers. Even without it, you are always an inspirational dancer, traveller, and fisher. Also, my ball-milling brother Bas, I always appreciate your speed on drinking with Dutch spirit. And Isidora, thank you for organizing many parties. It is a pity that Porque lo digo yo is closed now but you deserve some commission from them. Always Bas and me made fun of you that you talk too much but I didn´t mean it. (Or did I?) Also, I would like to acknowledge our real physicist, Chris. I have never worked on TRPL and photo-physics after my master, so it was grateful to catch this up thanks to you. Finally, our fellows and an assistant professor, Cris, Kassio, Fede, and Dani, please guide our junior students to right way in

research and party as always! And my favourite communist Ziqi, thank you for organizing the feasts with Christian, Aman, Victor, Azeem, and Matteo. Go ICMol!

Thanks to Dr. Annamaria Petrozza, I could enjoy research during my stay in IIT Politecnico di Milano. I appreciate warm hospitality even during a winter of Milano. I still remember Risotto a la Milanese from that lunch in Porta Garibaldi organized by Dr. Daniele Cortecchia. I hope Sara grows up healthy and happy with you and Lidi. I am also thankful to Ada, Jack, Jesus, Giulia, Elaine, Felix, Samuele, Isabella, Antonella, and Peter for showing me the lab work. And thanks to an explanation from Andrea, now I can distinguish Pizza and Focaccia.

For the last, of course, I would like to express my thankful heart to my family for the undying trust and support even when I do not visit Korea for you so many times. And I would like to dedicate the honour on my lifetime achievements to my family.

This thesis has been revised thanks to the referees listed below.

Prof. Mohammad Khaja Nazeeruddin, EPFL, Switzerland

Prof. Enrique Ortí Guillén, Universidad de Valencia, Spain

Prof. Senku Tanaka, Kindai University, Japan

Dr. Juan F. Galisteo López, ICMS-CSIC, Spain

Dr. Annamaria Petrozza, IIT, Italy

and Dr. Raquel E. Galian, Universidad de Valencia, Spain